Pattern Dynamics in Systems of Self-Propelling Particles
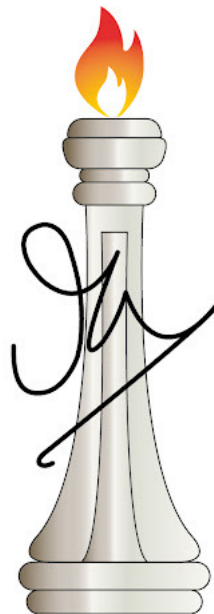
A Thesis

Submitted for the Degree of

DOCTOR OF PHILOSOPHY

in the Faculty of Science

by

Arabinda Bera

JNCASR

THEORETICAL SCIENCES UNIT

JAWAHARLAL NEHRU CENTRE FOR ADVANCED SCIENTIFIC RESEARCH

(A Deemed University)

Bangalore − 560 064

November 2022

To my parents

DECLARATION

I hereby declare that the matter embodied in the thesis entitled "**Pattern Dynamics in Systems of Self-Propelling Particles**" is the result of investigations carried out by me at the Theoretical Sciences Unit, Jawaharlal Nehru Centre for Advanced Scientific Research, Bangalore, India under the supervision of **Prof. Subir K. Das**, and that it has not been submitted elsewhere for the award of any degree or diploma.
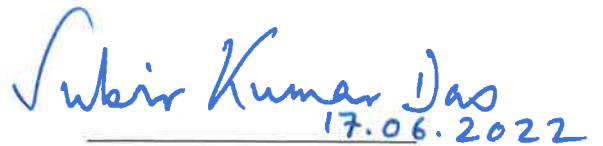
In keeping with the general practice in reporting scientific observations, due acknowledgment has been made whenever the work described is based on the findings of other investigators.

Arabinda Bera

Arabinda Bera

CERTIFICATE

I hereby certify that the matter embodied in this thesis entitled "**Pattern Dynamics in Systems of Self-Propelling Particles**" has been carried out by **Arabinda Bera** at the Theoretical Sciences Unit, Jawaharlal Nehru Centre for Advanced Scientific Research, Bangalore, India under my supervision and that it has not been submitted elsewhere for the award of any degree or diploma.

Subir Kumar Das

17.06.2022

Prof. Subir K. Das

(Research Supervisor)

Acknowledgements

Synopsis

Active matter systems are made of self-propelling particles. These systems are known to exhibit interesting nonequilibrium phase transitions. This thesis deals with structure and dynamics associated with phase transitions in a few model active matter systems.

Chapter 1 introduces phase transitions and active matter systems in a general context. Various models and simulation techniques that are relevant for the studies in subsequent chapters are discussed. Methods of analyses are also outlined.

Chapter 2 contains results from the studies of growth of fractal clusters in two different models of active matter systems. In one of the models the particles align their velocities following the well-known Vicsek rule. The other model contains active Brownian particles as constituents. Each of these systems exhibits vapor-"solid" transition at the considered low temperature. We have performed molecular dynamics (MD) simulations using Langevin thermostat. We have chosen a low density of particles in space dimension $d = 2$ such that the morphology consists of disconnected "solid" clusters in the vapor background. We have identified the mechanisms of growth of these clusters and corresponding growth laws for both types of systems. These are explained via appropriate theoretical consideration.

In **Chapter 3** we study the dynamics of ordering in the velocity field in two-dimensional systems of Vicsek-like active particles. We analyze the structure and growth in line with that in the XY model that is frequently used in studies of ordering dynamics in magnetic systems. It is observed that the growth in the system occurs via annihilation of vortex and anti-vortex pairs. We aim at quantification of such structure and dynamics.

Chapter 4 contains a study of clustering dynamics in systems of Vicsek-like active particles that are embedded in an explicit solvent bath in $d = 3$. We have performed a hybrid MD and Multi-Particle Collision Dynamics study to understand the role of hydrodynamics in the growth of clusters of the active particles. These results are compared with the corresponding passive case. Results from each of these cases are examined

against those when the dynamics of solvent particles do not satisfy the hydrodynamic requirements.

In **Chapter 5** we have studied the structure and dynamics in mixtures of active colloids and passive polymers that are confined inside spherical cavities with repulsive wall. We have performed MD simulations to quantify the miscibility gap in such finite systems. Inside the coexistence region, we probe the dynamics of colloids and polymers in steady states. We consider compositions for which one has partially wet situation, mimicking approximately a neutral wall, in the fully passive scenario. The introduction of the Vicsek-like velocity-aligning activity to the colloids changes the wetting picture. For a reasonably high strength of activity, the polymer-rich domain takes the distinct shape of an ellipsoid, around the long axis of which the colloid-rich domain attains a macroscopic rotation. We study dynamics and scaling related to such steady state structure.

In **Chapter 6**, we investigate the phase-separation dynamics in a mixture of active and passive particles on spherical and flat surfaces. Our objective is to probe the morphological and dynamical differences between the two cases. There exists alignment interaction among the active particles.

Publications

1. Subhajit Paul, Arabinda Bera, and Subir K. Das, How do clusters in phase-separating active matter systems grow? A study for Vicsek activity in systems undergoing vapor-solid transition, Soft Matter **17**, 645 (2021).

2. Arabinda Bera , Soudamini Sahoo, Snigdha Thakur, and Subir K. Das, Active particles in explicit solvent: Dynamics of clustering for alignment interaction, Phys. Rev. E **105**, 014606 (2022).

3. Arabinda Bera, Kurt Binder, Sergei A Egorov, and Subir K. Das, Macroscopic rotation of active colloids in a colloid-polymer mixture confined inside a spherical cavity, arXiv preprint arXiv:2112.00500.

4. Arabinda Bera and Subir K. Das, Dynamics of velocity ordering during coarsening in an active matter system (to be submitted).

5. Arabinda Bera and Subir K. Das, Comparative study of demixing transition in a binary mixture of active and passive particles on a spherical surface and a flat plane (Manuscript under preparation).

6. Sutapa Roy, Arabinda Bera, Suman Majumder, and Subir K. Das, Aging phenomena during phase separation in fluids: decay of autocorrelation for vapor-liquid transitions, Soft Matter **15**, 4743 (2019) [work not included in the thesis].

Table of contents

List of figures

Chapter 1

Introduction

1.1 Phase Transition

Phase transition is a change of phase of a system via the tuning of thermodynamic variables such as pressure and temperature. The occurrence of phase transitions is common in nature, over wide ranges of length and time scales [1–10]. Well known examples are paramagnetic to ferromagnetic transition in magnetic systems, vapor-liquid transitions in water, etc. In Fig. 1.1(a) we have shown a schematic phase diagram of a chemical substance in the pressure (P) and temperature (T) plane. Here different phases, viz., solid, liquid and gaseous states, are shown. Two different phases coexist with each other in equilibrium along the coexistence curves that are shown in solid lines. The merging point of these curves is known as the triple point (T_t, P_t). The vapor-liquid coexistence curve terminates at the critical point (ρ_c, T_c) and at this point a second order or continuous phase transition occurs. Quantities like susceptibility, specific heat and correlation length show divergences at this point. These interesting features near T_c are referred to as the critical phenomena [5–10]. The vapor-liquid coexistence is shown schematically in temperature versus density (ρ) plane in Fig. 1.1(b).

Phase transition processes are non-equilibrium in nature. Following a quench inside the coexistence region, from a high temperature homogeneous phase, a system approaches new equilibrium via the formation and growth of domains of particle-rich phases. One such phase-separation process has been shown in Fig. 1.1(b). During this non-equilibrium process the average length of domains, ℓ, typically grows with time (t) in power-law fashion [1–3, 9], i.e.,

$$\ell \sim t^\alpha. \tag{1.1}$$

The growth exponent α depends on many factors like order-parameter conservation, hydrodynamic environment and type of interactions. The morphology and dynamics of growth strongly depend also on the region of quench in the phase plane. We have shown evolution snapshots in Fig. 1.2 for two densities $\rho = 0.05$ and 0.35, from molecular dynamics (MD) simulations of systems containing single component Lennard-Jones (LJ) particles in space dimension $d = 2$. For the quench with very low overall particle density, morphology consisting of disconnected clusters forms and grows [2–5, 11, 12], as shown in Fig. 1.2(a). For a quench close to the critical density (ρ_c), the phase separation process is known as spinodal decomposition [2–5]. In this case *nearly* bicontinuous morphology is formed that we have shown in Fig. 1.2(b). The morphology also depends on temperatures of quench, like in low temperature and overall low density fractal-like disconnected structure forms during evolution [13]. In this thesis, we have worked with both disconnected cluster morphology and bicontinuous morphology in different environments and for varying nature of particles.
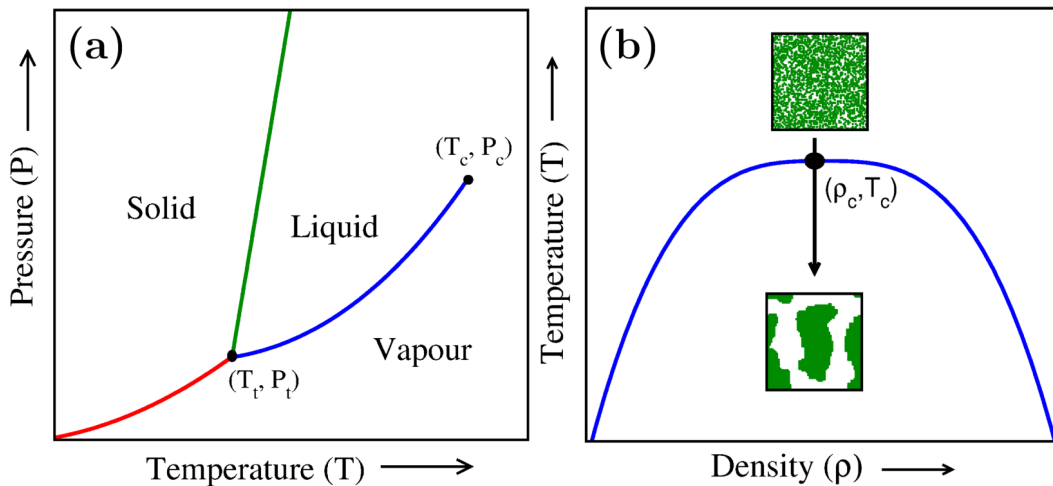
Figure 1.1: (a) A schematic phase diagram of a chemical substance in T-P plane. We show the triple point (T_t, P_t) and the critical point (T_c, P_c) by filled circles. (b) Vapor-liquid coexistence curve for the same is shown in density (ρ) versus temperature (T) plane. The snapshots demonstrate the process of a vapor-liquid transition.

1.2   Active Matter Systems

Active matter systems, consisting of self-propelling agents, are observed in nature in a wide span of scale [14–34]. Typical examples are mammal herds [14], flock of birds [15, 16],

(a) Nucleation and Growth   **(b)** Spinodal Decomposition

$t = 10^3$ $t = 10^4$ $t = 10^2$ $t = 10^3$
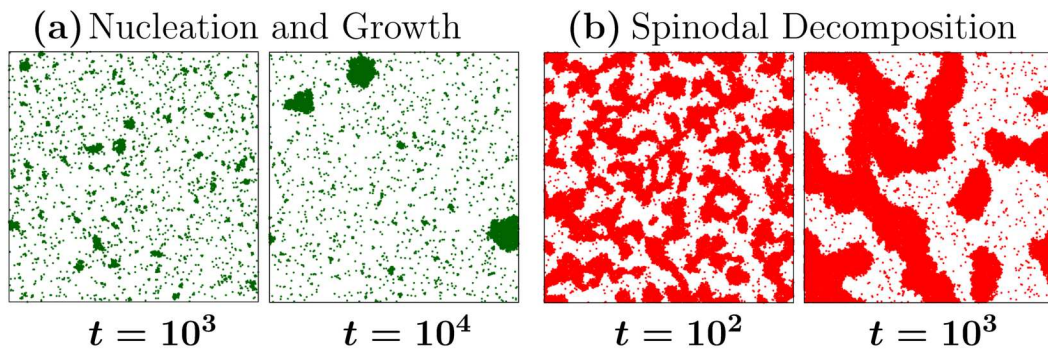
Figure 1.2: (a) Evolution of a single component 2D LJ system, with overall density of particles $\rho = 0.05$, is demonstrated for a quench of a random initial configuration to $T = 0.35$. Nucleation and growth of droplets are seen. (b) Same as (a) but here we have $\rho = 0.35$. Spinodal decomposition of particles can be appreciated. These results are obtained for $L = 256$, with Nosé-Hoover thermostat.

Figure 1.3: Flocking in a collection of birds. Picture courtesy: Sumukh Anil Purohit.

colony of ants [17], bacterial suspensions [18, 19], sperm cells [20], molecular motors [21], etc. Energy consumption by these active elements, drawing it from surrounding environment, drives these systems away from equilibrium. Collective motion in these systems, arising from the coherent movements of the particles, is widely studied [14–34]. The pattern formation, growth, correlations exhibited by active particles may significantly differ from passive systems. In Fig. 1.3 we have shown flocking of birds as an example of structure formation in active matter system.

There exist a large number of theoretical models to understand natural and experimental observations in such systems. Active matter systems need not be made of living entities. For example, there exist systems consisting of polar granular rods [35],

photoactivated colloidal particles [36], etc. There are different types of self-propulsion or motility. The active matter systems are classified accordingly. Usually, the nature of self-propulsion falls into two primary categories: non-aligning and aligning. Non-aligning interactions are independent of the direction of motion of the particles, while aligning interactions are concerning parallelization of the directions of motion of particles. Active Brownian, run-and-tumble dynamics of particles are examples of non-aligning type and coherent motion in a flock of birds, and herds of mammals are typical physical examples of systems having aligning active interactions. One of the simplest models with alignment interactions was introduced by Vicsek and coworkers [26]. In our thesis, we will mainly focus on Vicsek-like aligning active particles. Below we discuss these two types of systems in some detail.

1.2.1 Active Brownian Particles

These particles can move in random directions depending upon their translational and rotational diffusion coefficients. Typical active Brownian particles (ABP) can interact via short-range inter-particle repulsive potential. One may, of course, include long range interactions. This will enable investigations of different critical and coarsening universality classes as in passive systems [37, 38]. To the best of our knowledge, such studies, however, are not yet undertaken in the literature. Phase-separation here is driven by the overall particle density/packing fraction and self-propulsion velocity. This is known as "motility-induced" phase separation (MIPS) [28]. Depending on the packing fractions, diffusion constant and self-propulsion velocity these systems exhibit different kinds of phase behaviors. Various phenomena in such systems have received importance in the context of phase transition or clustering dynamics [28–34]. In the later part of this chapter we will provide further details on such systems.

1.2.2 Vicsek Model

The Vicsek model (VM) of active matter is one of the simplest models that exhibits phase transition from random velocity orientations to coherent motion [26]. Starting with random initial positions and random directions of velocities, having uniform magnitude, say, in a two-dimensional plane, the model prescribes evolution to a steady state via the dynamical rule where each particle at every instant of time tries to align its direction of velocity in the average direction of its neighbors. This kind of local alignment induces growth and ordering in the overall system. The equations describing the rule(s) are

written as [26]

$$\vec{r}_i(t + \Delta t) = \vec{r}_i(t) + \vec{v}_i \Delta t, \tag{1.2}$$

$$\theta_i(t + \Delta t) = \langle \theta_i(t) \rangle_r + \Delta\theta. \tag{1.3}$$

Note that the velocity of the ith particle is $\vec{v}_i = (v_0 \cos\theta_i, v_0 \sin\theta_i)$ and the magnitude of the velocity of each particle is v_0. Here $\langle \theta_i(t) \rangle_r$ represents the average direction of the velocities of all the particles (including the ith one) situated within a distance r from particle i and $\Delta\theta$ is a random noise taken from a uniform distribution in the interval $[-\eta/2, \eta/2]$. This noise plays a role similar to what temperature does in the phase separation of many passive systems. Note that in this model there is no inter-particle passive interaction. This model exhibits a continuous phase transition from disordered motion to ordered motion with the change of particle density ρ and noise strength η. Interesting phenomena of flocking are observed when ρ is large and η is small, exhibiting ordered motion on a macroscopic scale within which the flock of the particles move in the same spontaneously selected direction.

1.3 Langevin Dynamics for Active Particles

Typical motion of particles can be described by a stochastic differential equation. The interplay between a constant drag force, acting against the direction of velocity, and a random noise often satisfy 'fluctuation-dissipation' theorem and keeps the temperature T of the system constant. This stochastic motion can be studied via the Langevin equation [39–41]

$$m\ddot{\vec{r}}_i = -\vec{\nabla} u_i - \gamma m \dot{\vec{r}}_i + \vec{F}_i^r(t) + \vec{f}_i. \tag{1.4}$$

Here u_i is the potential due to the inter-particle passive interaction and m is the mass of each of the particles. The coefficient γ in the drag term is related to the random force $\vec{F}_i^r(t)$ via the standard fluctuation-dissipation relation at thermal energy $k_B T$ (k_B being Boltzmann constant). The Cartesian components of the random force $\vec{F}_i^r$ satisfy the relations [39–41]

$$\langle F_i^{r,\mu}(t) \rangle = 0, \quad \mu \equiv x, y, z \tag{1.5}$$

and

$$\langle F_i^{r,\mu}(t) F_j^{r,\nu}(t') \rangle = 2m\gamma k_B T \delta_{ij} \delta_{\mu\nu} \delta(t - t'). \tag{1.6}$$

Due to the self-propelling nature of the particles in active matter systems an active force $\vec{f}_i$ is included in Eq. (1.4). Thus, $\vec{f}_i = 0$ represents the motion of passive Brownian

particles, while non-zero values of $\vec{f_i}$ result in energy drive in the system due to this active force.

The motions of aligning active particles can be studied via the numerical integration [39–41] of the Eq. 1.4. For the Vicsek-like alignment rule in self-propulsion, the active force term can be written as $\vec{f_i} = f_A \hat{n}_i$, where $\hat{n}_i = \frac{\sum_j \vec{v}_j}{|\sum_j \vec{v}_j|}$ [42, 43]. Here $\vec{v}_j$ is the velocity of particle j that falls inside the neighborhood/interacting radius defined by the distance r_v from particle i and f_A is the strength of the activity. The implementation of this active force $\vec{f_i}$ can enhance the effective temperature of the system to a higher value, which is shown in phase separation in a mixture of active colloids and passive polymers [42]. However, the implementation can be done in such a way that this active force is responsible only for the directional alignment of particles [43]. A large value of f_A is equivalent to a low noise-strength η in the pure Vicsek model. For systems having additional passive interactions, the updates may deviate from the original Vicsek case. In that case, special care needs to be taken so that this force leads only to a change in direction of velocity [43].

For various situations the over-damped limit is considered, i.e., strong drag force leads to the constant velocity of particles. Then Eq. (1.4) can be written as [29–33]

$$\dot{\vec{r}}_i = \beta' D_t [-\vec{\nabla} u_i + f_p \hat{p}_i] + \sqrt{2D_t} \vec{\Lambda}_i^t, \tag{1.7}$$

where $\beta' = 1/k_B T$ and D_t is the translational diffusion constant. Here the active force $\vec{f_i} = f_p \hat{p}_i$, where $\hat{p}_i$ is the self-propelling direction and f_p is the magnitude of propulsion force. The friction coefficient γ is related to the translational diffusion constant D_t as $D_t = 1/m\beta'\gamma$.

The dynamics of the system depends on the nature of the self-propelling direction $\hat{p}_i$. For the active Brownian particles, the self-propelling directions of particles decorrelates with the rotational diffusion. The dynamical equation for the self-propelling direction can be written as [29]

$$\dot{\hat{p}}_i = \sqrt{2D_r}(\hat{p}_i \times \vec{\Lambda}_i^r), \tag{1.8}$$

where D_r is the rotational diffusivity. In the above, each of $\vec{\Lambda}_i^t$ and $\vec{\Lambda}_i^r$ are Gaussian random noise of unit-variance having Cartesian components Λ_i^μ, that satisfy

$$\langle \Lambda_i^\mu(\vec{r}, t) \Lambda_j^\nu(\vec{r'}, t') \rangle = \delta_{ij} \delta_{\mu\nu} \delta(\vec{r} - \vec{r'}) \delta(t - t'). \tag{1.9}$$

For the motion of particles on a two-dimensional plane, the self-propulsion direction can be represented by a scalar variable θ_i, the angle between the self-propulsion direction and the $x-$axis, i.e., $\hat{p}_i = (\cos\theta_i, \sin\theta_i)$. Thus, for $d = 2$, Eq. (1.8) has a form [29–33]

$$\dot{\theta}_i = \sqrt{2D_r}\Lambda_i^r, \tag{1.10}$$

Λ_i^r being a scalar Gaussian noise. Despite having non-aligning nature of self-propulsion these systems exhibit robust phase-separation depending on the parameters like self-propulsion speed, packing fraction, transnational and rotational diffusivities and passive interactions.

For aligning active particles in $d = 2$, one can introduce an alignment term in Eq. (1.10). Then Eq. (1.10) can be written as [44, 45]

$$\dot{\theta}_i = \frac{K}{S_v}\sum_{j \in \mathbb{S}}\sin(\theta_j - \theta_i) + \sqrt{2D_r}\Lambda_i^r. \tag{1.11}$$

Here K is the coupling strength and S_v $(= \pi r_v^2)$ is the area of the interacting region $\mathbb{S}$, i.e., r_v is the maximum distance within which two particles can interact. This interaction is Vicek-like in nature, where the coupling strength K determines the strength of velocity alignment between particles. The characteristic time scale [45] associated with the directional alignment is $\tau_k = \frac{\pi r_v^2}{K}$, while that for the rotational diffusion $\tau_r = \frac{1}{D_r}$. This ferromagnetic-like coupling is similar to the synchronization of phase oscillators in Kuramoto model [46] and XY model [47, 48] in $d = 2$. We have considered this interaction for a phase-separating binary mixture of active and passive particles.

1.4   Entropy Driven Phase Separation

Phase separations in many systems occur via the change of the internal energy of the system. Examples are nucleation of water molecules in the environment, paramagnetic to ferromagnetic transition in magnetic systems, etc. Phase transition can also occur by purely change in the entropy of a system. Such phase transitions are referred to as being "entropy driven" [49]. Examples are the freezing transition in hard sphere systems [50], an isotropic-nematic transition in $(d = 3)$ systems containing thin hard rods [51], phase separation in a polymer-colloid mixture [52–54], etc. For one of our studies on active matter we have considered a colloid-polymer mixture as the passive backbone where the
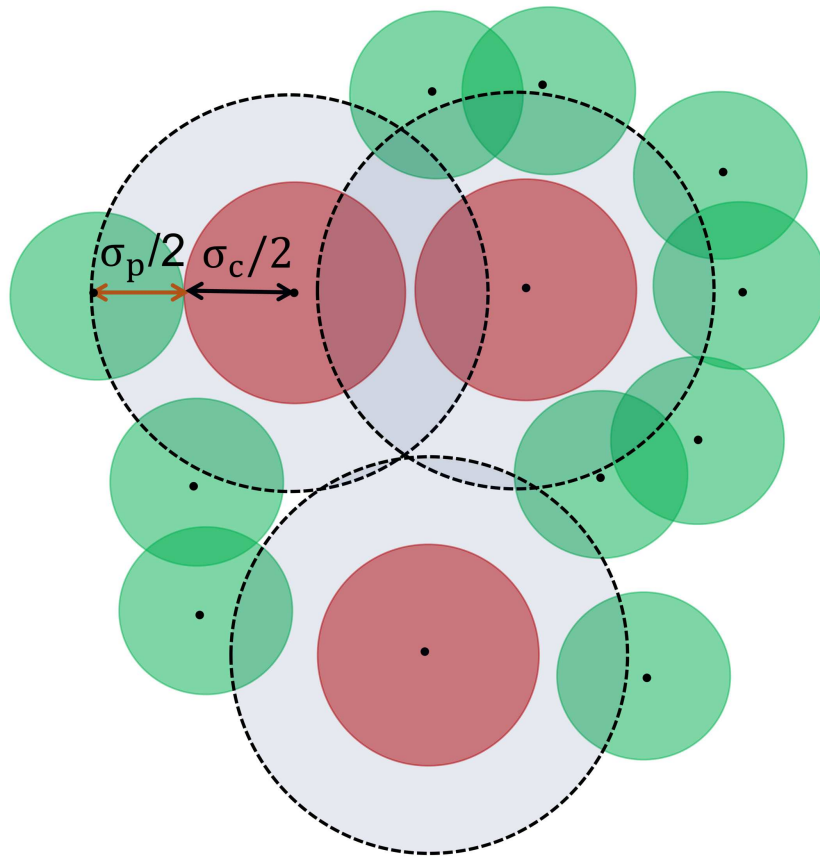
Figure 1.4: A schematic picture illustrating the depletion interaction is presented here. Inside the depletion zone (light-blue shaded region inside the dotted circle) of each colloid (red) there will be no center of mass of the soft polymer coil. When the centers of two colloids come closer than twice the size of a depletion zone there is overlap of the depletion zones. This results in extra free volume for the polymers and raises the entropy in the system. The induction of the net effective attraction between colloids as a result of this is known as the "depletion attraction".

interactions are variants of the well-known Asakura Oosawa (AO) model [52, 53]. Below we discuss this in detail.

1.4.1   Asakura-Oosawa Model

The colloids (c) here are considered as hard spheres having diameter σ_c and the polymers (p) are treated as ideal soft spheres with diameter σ_p. Thus, the polymers overlap with each other without any energy cost, i.e., the interaction potential among polymers is

$$U_{pp}(r) = 0. \tag{1.12}$$

Colloids being hard spheres strictly prohibit overlap either with another colloid or any polymer. The pair interactions for colloid-colloid (U_{cc}) and colloid-polymer (U_{cp}) are given by [52–54]

$$U_{cc}(r \leq \sigma_c) = \infty; \quad U_{cc}(r > \sigma_c) = 0, \tag{1.13}$$

$$U_{cp}(r \leq (\sigma_c + \sigma_p)/2) = \infty; \quad U_{cp}(r > (\sigma_c + \sigma_p)/2) = 0. \tag{1.14}$$

Due to the hard-core repulsion with polymers, each colloidal particle will form a depletion zone within which no polymer can exist. The depletion zones of two colloids overlap when the distance between them becomes less than $(\sigma_c + \sigma_p)$, creating an excess free volume for polymers. This leads to the increase of transnational entropy in the systems. Essentially the polymer concentrations in the system cause an effective attraction among colloids and is known as the depletion effect. A schematic diagram is shown in Fig. 1.4 to explain the depletion. Thus, the phase separation in this system is purely "entropy driven". The size ratio (q_s) between polymer and colloid, i.e., $q_s = \sigma_p/\sigma_c$ controls the nature of the phase-separation [52–54]. The phase behaviors are studied in the plane of colloid packing fraction η_c and polymer packing fraction η_p, defined as

$$\eta_c = (\pi\sigma_c^3/6)\rho_c, \qquad \eta_p = (\pi\sigma_p^3/6)\rho_p. \tag{1.15}$$

The particle density is given by $\rho_b = N_b/V$, $[b = (c, p)]$. Here N_b is the total number of particles of type b within the system of volume V. A liquid-liquid phase separation with a polymer-rich phase and a colloid-rich phase occurs for a large size ratio q_s. This model captures the fundamental features of the phase behavior of a polymer-colloid mixture observed in experiments [55, 56].

1.4.2 Modified AO Model for Molecular Dynamics Simulation

The thesis contains a study of phase behavior of a colloid-polymer mixture under confinement, using molecular dynamics simulations, when colloids are made active [42]. However, the above mentioned original model is not advantageous for molecular dynamics simulations. Thus, we have used a modified version [57] where perfectly hard-core and ideal soft-sphere interactions have been replaced by more suitable potentials. E.g., the Weeks-Chandler-Andersen (WCA) potentials have been used to describe the hard-core repulsion for colloid-colloid and colloid-polymer pairs. On the other hand, a soft repulsive potential has been used to describe polymer-polymer interactions. In this modified version the phase behaviors depend weakly on the temperature [57]. We have used the above mentioned Langevin thermostat for this study. The details of the interactions have been discussed in Chapter 5.

1.5 Mechanisms of Growth in a Few Coarsening Systems

1.5.1 Particle Diffusion

The power-law growth of the characteristic length, ℓ, of a phase-separating super-saturated solid solution was proposed by Lifshitz and Slyozov (LS) [58]. For off-critical binary alloys, i.e., alloys in which one of the components, say, A, is of negligible fraction, the evolution occurs via the nucleation and growth of clusters of the minority component. The chemical potential, μ, on the surface dividing the A-rich and B-rich domains scales as σ/ℓ, where σ is the surface tension. The concentration current, arising due to chemical potential gradient between two phases, is given by [59] $D|\vec{\nabla}\mu| \sim D\sigma/\ell^2$, D being a diffusion constant. The interfacial velocity of a domain is governed by this [2, 3, 58, 59], i.e.,

$$\frac{d\ell}{dt} \sim \frac{D\sigma}{\ell^2}.$$ (1.16)

This leads to the power-law growth of the characteristic length $\ell(t) \sim (D\sigma t)^{1/3}$ and is referred to as the Liftshitz-Slyozov (LS) law of growth. This growth applies to spinodal decomposition as well.

1.5.2 Diffusive Coalescence of Clusters

For low density of particles in a single component system, undergoing vapor-liquid transition, or an off-critical composition in a liquid-liquid transition, the growth may primarily occur via the coalescence of droplets. When these droplets move diffusively then the rate of change of droplet density can be written as [11, 12, 60, 61]

$$\frac{dn}{dt} = -D\ell n^2. \tag{1.17}$$

Here D is the droplet diffusion constant and ℓ is the average size of the droplets. The Stokes-Einstein-Sutherland [62] relation provides a constant value for $D\ell$. From the conservation of total mass of the particles, one gets $n \sim 1/\ell^d$. Incorporating these facts in Eq. (1.17) one can write

$$\frac{d\ell}{dt} \sim \frac{1}{\ell^{d-1}}, \tag{1.18}$$

that provides $\ell \sim t^{1/d}$. Here the growth is dependent on the space dimension d. Such a mechanism was proposed by Binder and Stauffer [11].

1.5.3 Ballistic Aggregation of Clusters

The growth mechanism in this case occurs via the collision among ballistically moving clusters. The dynamical equation for binary collisions in this case can be written as [63–66]

$$\frac{\mathrm{d}n}{\mathrm{d}t} = -\sigma_{\mathrm{coll}} \times \langle v_{\mathrm{rel}} \rangle \times n^2, \tag{1.19}$$

where σ_{coll} is the collision cross-section and is related to the space dimension d as

$$\sigma_{\mathrm{coll}} \sim R_g^{d-1}, \tag{1.20}$$

R_g being the average radius of gyration of clusters. Typically R_g shows a power-law behavior with the average mass of the clusters M, i.e.,

$$M \sim R_g^{d_f}, \tag{1.21}$$

where d_f is the fractal-dimension of the clusters. When motion of the clusters is uncorrelated [63], the mean relative velocity $\langle v_{\mathrm{rel}} \rangle$ can be replaced by the root-mean-

squared velocity v_{rms}. Generally, v_{rms} depends on M as [63, 67]

$$v_{\text{rms}} \sim M^z. \tag{1.22}$$

The conservation of mass implies $n \propto 1/M$. During phase separation, the average mass, M, of domains or clusters typically grows [2] with time (t) as

$$M \sim t^\beta. \tag{1.23}$$

Using Eq. (1.19), (1.20), (1.21), (1.22) and (1.23) one obtains [13, 68]

$$\beta = \frac{d_f}{d_f(1-z) - (d-1)}. \tag{1.24}$$

When the system does not exhibit fractal morphology, i.e, $d_f \approx d$, then one has $\beta = d/(1-dz)$.

1.6 Morphology and Characterization of Growth

1.6.1 Correlation Function and Scaling

The morphology of various phase-separating systems is generally captured by the two-point equal time correlation function, $C(r,t)$, that is defined as [2, 3]

$$C(r,t) = \langle \phi(\vec{r},t)\phi(\vec{0},t) \rangle - \langle \phi(\vec{r},t) \rangle \langle \phi(\vec{0},t) \rangle. \tag{1.25}$$

Here $\phi(\vec{r},t)$ is a time-dependent local order parameter and $\langle ... \rangle$ represents statistical average. In simple situations, the morphology of the domains remains the same with time apart from the change in the length scale. This is referred to as self-similarity and there exists scaling [2, 3] of $C(r,t)$ in such situations, viz.,

$$C(r,t) \equiv \tilde{C}(r/\ell(t)). \tag{1.26}$$

The order parameter can be a vector instead of a scalar variable, e.g., spin variables in XY model [47, 48].

Analytical form of the correlations of an n-component vector order parameter ($\vec{\phi}$), in connection with ferromagnetic ordering, was obtained by Bray, Puri and Toyoki (BPT)
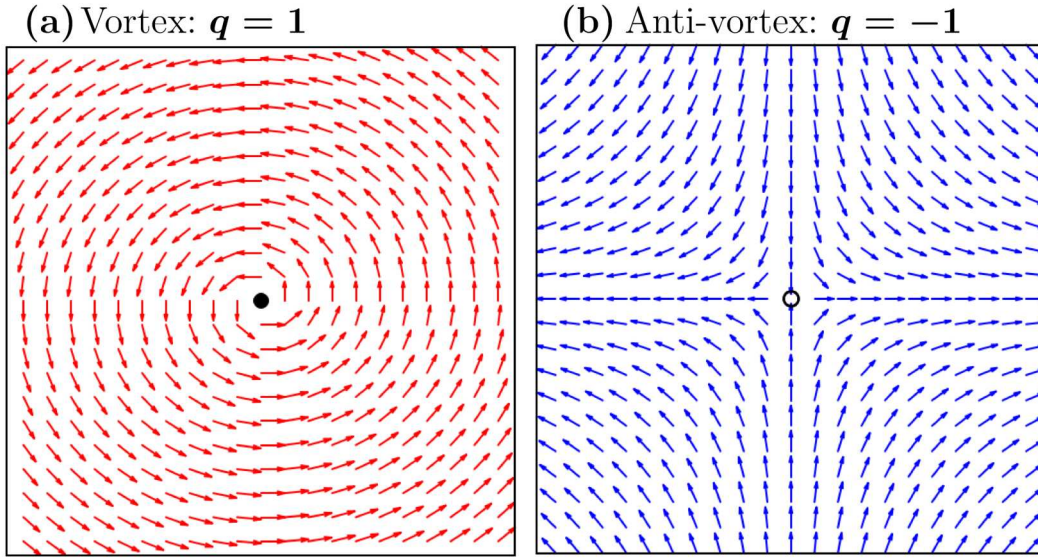
Figure 1.5: Vector fields corresponding to typical (a) vortex and (b) anti-vortex structures for $d = 2$ and $n = 2$. The location of defect cores with topological charge $q = +1$ (-1) is shown by filled circle (empty circle).

[69, 70]. This is given by

$$C_{\vec{\phi}}(r,t) = \frac{n\gamma}{2\pi} \left[\mathbf{B}\left(\frac{n+1}{2}, \frac{1}{2} \right) \right]^2 \mathbf{F}\left(\frac{1}{2}, \frac{1}{2}; \frac{n+2}{2}; \gamma^2 \right), \qquad (1.27)$$

where $\mathbf{B}(x,y)$ $\left[= \Gamma(x)\Gamma(y)/\Gamma(x+y) \right]$ is the beta function $[\Gamma(a)$: gamma function], $\mathbf{F}(a,b;c;z^2)$ is a hypergeometric function [71] and γ is related to the characteristic length scale $\ell(t)$ as $\gamma = \exp\{ -r^2/2\ell(t)^2 \}$. For a scalar order parameter $(n = 1)$, the limiting case is the Ohta-Jasnow-Kawasaki (OJK) function [72], given by

$$C(r,t) = \frac{2}{\pi} \sin^{-1} \gamma. \qquad (1.28)$$

For non-conserved Ising model [3, 73] during evolution from paramagnetic to ferromagnetic phase, the correlation function satisfies this OJK form [2, 3, 74].

1.6.2 Topological Defects

Defects are commonly observed during growth for both scalar and vector fields. For a n-component order-parameter $\vec{\phi}$ in d-dimensional space, $\vec{\phi}$ vanishes at the defect core that resides in a surface of dimension $d - n$. There exists topological defects only when $n \leq d$. For scalar fields $(n = 1)$ these defects are domain walls that separate domains

of two different phases [2]. Few topological defects in vector fields are 'vortices' ($d = 2$, $n = 2$); 'strings' ($d = 3$, $n = 2$); 'hedgehogs' or 'monopoles' ($d = 3$, $n = 3$), etc. In space dimension two and vector order-parameter ($d = 2$, $n = 2$), vortex and anti-vortex have different topological charges [2, 47, 48], estimated as

$$q = \frac{1}{2\pi} \oint \vec{\nabla}\theta \cdot \vec{d\ell}, \tag{1.29}$$

where θ is the continuous phase angle corresponding to the vector field and the integral is carried over the closed path around the defect core. The topological charge $q = +1$ (-1) corresponds to a vortex (anti-vortex). The vector fields for typical vortex and anti-vortex are presented in Fig. 1.5(a) and (b). The defect cores are marked in filled circle for $q = +1$ and empty circle for $q = -1$.

1.7 Simulation Methods

The thesis contains simulation studies of passive and active particles in bulk as well as in presence of walls. For this purpose, we have used molecular dynamics (MD) and hybrid-MD simulations. Below we discuss the methods.

1.7.1 Molecular Dynamics

Molecular dynamics (MD) is an useful technique in the domain of condensed matter physics [39, 40]. There one generally solves the Newton's equations

$$\dot{\vec{r}}_i = \frac{\vec{p}_i}{m_i}, \tag{1.30}$$

$$\dot{\vec{p}}_i = \vec{F}_i, \tag{1.31}$$

where $\vec{F}_i$ is the force acting on particle i. The contributions to the force field can arise from various interactions in the systems, e.g., interparticle potential, random noise, external driving force, self-propulsion, etc. The interparticle force is calculated as $\vec{F}_i^{\text{in}} = -\vec{\nabla}u_i$, where u_i is the inter-particle pair potential. One of the most time consuming parts of MD simulation is the calculation of force. For short-range interactions there exist various efficient methods [39, 40], e.g., constructions of Verlet list and cell list. To obtain the update equations for positions and velocities of the particles, there are several integration algorithms [39, 40] for solving Eq. (1.30) and Eq. (1.31), e.g., Euler, Varlet, Leap-frog

and velocity-Verlet. For the simulation in canonical ensemble one needs to keep the temperature of the system to an assigned value. Few useful thermostats for this purpose are Nosé-Hoover [75, 76], Lowe-Andersen [77], dissipative particle dynamics [78], velocity rescaling [39] and Langevin[39–41].

1.7.2 Multi-Particle Collision Dynamics

Previously mentioned Langevin thermostat is stochastic in nature and does not preserve hydrodynamic laws. Many studies describing the motion of active particles have neglected the effects of hydrodynamic interactions. However, active particles are commonly seen in fluid/aqueous environments: typical examples are marine mammals in ocean, bacteria and sperm cells in the human body [79]. The environment/solvent in which the active particles are immersed can play a significant role in the structure and dynamics of the systems. Although the length and time scales of dynamics of typical active particles and that of the solvent particles may differ by several orders of magnitude, leading to computational difficulty, there exist coarse-grained models for solvent which can preserve the hydrodynamic laws in the systems. Few such methods are the Lattice-Boltzmann (LB) method [80–82], dissipative particle dynamics (DPD) [83–85] and multi-particle collision dynamics (MPCD) [86, 87]. Here we will discuss only MPCD which we have used for our simulations.

In MPCD a collection of actual solvent molecules are represented by a point particle. A typical MPCD [86, 87] consists of two steps, as described below.

I. **Streaming Step:**

Here all solvent particles move freely in the system over a time interval τ, i.e., until they undergo collision event. The position of the ith solvent particle, thus, having velocity $\vec{v}_i$, is updated as [86, 87]

$$\vec{r}_i(t + \tau) = \vec{r}_i(t) + \tau \vec{v}_i(t). \tag{1.32}$$

II. **Collision Step:**

The solvent particles periodically undergo collisions, resulting in local momentum exchange among themselves at intervals τ. The system is divided into cubic collision cells of side a and all solvent particles within the same cell interchange linear momentum. This is achieved [86, 87] via the rotation of the relative velocities of the particles with respect

to the center of mass velocity of the cell by an angle γ around a randomly chosen axis $\hat{n}$. The velocity of ith solvent particle after undergoing a collision is updated as [86, 87]

$$\vec{v}_i(t+\tau) = \vec{v}_{\text{cm}}(t) + \mathbb{R}(\hat{n},\gamma)(\vec{v}_i(t) - \vec{v}_{\text{cm}}(t)) \tag{1.33}$$

Here $\vec{v}_{\text{cm}}$ is the center of mass velocity of the cell containing the ith particle, defined as $\vec{v}_{\text{cm}}(t) = \frac{1}{N_s}\sum_{j=1}^{N_s}\vec{v}_j(t)$, N_s being the number of solvent particles in the corresponding cell. $\mathbb{R}$ is a rotation matrix, constructed in such a way that the hydrodynamic requirements are satisfied.

One can construct [86] the rotation matrix $\mathbb{R}$, from the formulation of the rotation of a vector $\vec{A}$ about an axis $\hat{n}$ by an angle γ in space dimension $d = 3$. As shown in Fig. 1.6 one can write the final vector $\vec{A}_f$ as

$$\vec{A}_f = \vec{A}_\parallel + \vec{B}, \tag{1.34}$$

where $\vec{A}_\parallel$ and $\vec{A}_\perp$ are the parallel and perpendicular components of $\vec{A}$ with respect to $\hat{n}$, respectively, viz., $\vec{A}_\parallel = \hat{n}(\hat{n}\cdot\vec{A})$ and $\vec{A}_\perp = \vec{A} - \vec{A}_\parallel$. Here $\vec{B} = \vec{A}_\perp\cos\gamma + (\vec{A}_\perp\times\hat{n})\sin\gamma$ (see Fig. 1.6). Now $\vec{A}_f$ can be written as

$$\begin{aligned}
\vec{A}_f &= \vec{A}_\parallel + (\vec{A} - \vec{A}_\parallel)\cos\gamma - \hat{n}\times(\vec{A} - \vec{A}_\parallel)\sin\gamma \\
&= \vec{A}_\parallel + [\vec{A} - \hat{n}(\hat{n}\cdot\vec{A})]\cos\gamma - (\hat{n}\times\vec{A})\sin\gamma \\
&= \hat{n}(\hat{n}\cdot\vec{A}) + (\mathbb{I} - \hat{n}\hat{n})\cdot\vec{A}\cos\gamma - (\hat{n}\times\vec{A})\sin\gamma.
\end{aligned} \tag{1.35}$$

Here $\mathbb{I}$ is the identity matrix.

Now if we replace $\vec{A}$ by $(\vec{v}_i(t)-\vec{v}_{\text{cm}}(t))$ and $\vec{A}_f$ by $(\vec{v}_i(t+\tau)-\vec{v}_{\text{cm}}(t))$ $[\vec{v}_{\text{cm}}(t+\tau) = \vec{v}_{\text{cm}}(t)$, due to the local conservation of momentum in each cell] in Eq. (1.35), then Eq. (1.33) can be rewritten as [86]

$$\begin{aligned}
\vec{v}_i(t+\tau) = {}&\vec{v}_{\text{cm}}(t) + \hat{n}[(\vec{v}_i(t) - \vec{v}_{\text{cm}}(t))\cdot\hat{n}] \\
&- \hat{n}\times(\vec{v}_i(t) - \vec{v}_{\text{cm}}(t))\sin\gamma + (\mathbb{I} - \hat{n}\hat{n})\cdot(\vec{v}_i(t) - \vec{v}_{\text{cm}}(t))\cos\gamma.
\end{aligned} \tag{1.36}$$

In MPC the rotation angle γ is fixed throughout the simulation but the directions of the rotation axis $\hat{n}$ are different for each cell and also different for every collision step. This implies that the collisions in different cells are independent of each other.
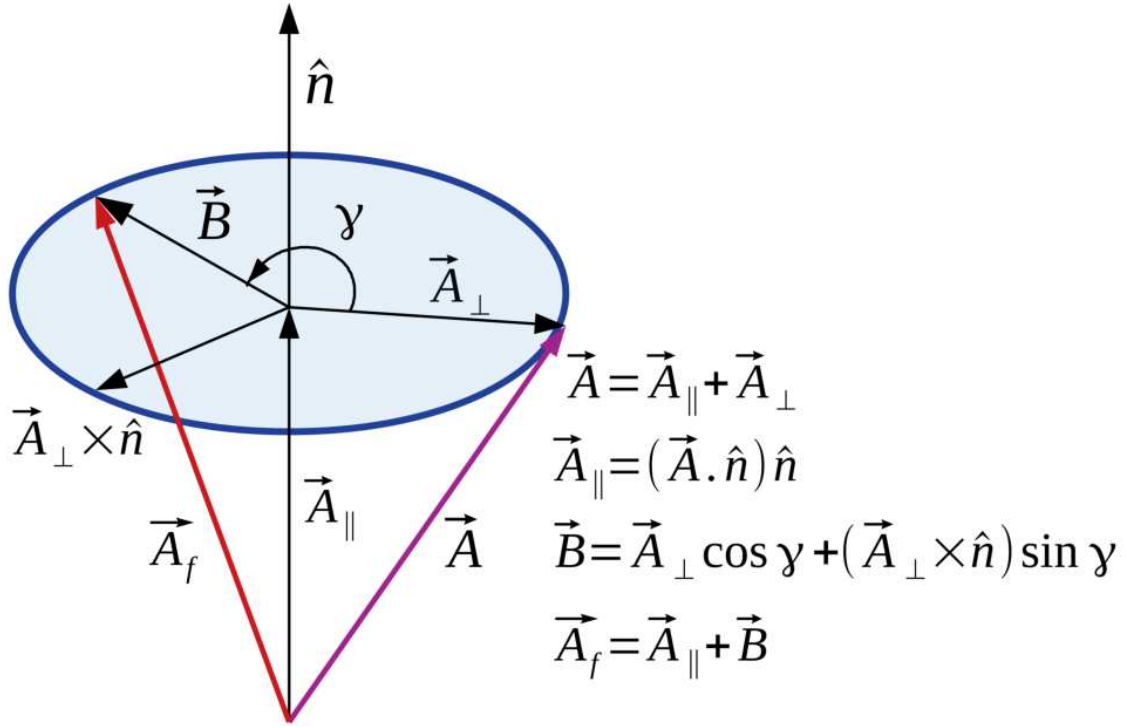
Figure 1.6: Rotation of a vector $\vec{A}$ around a unit vector $\hat{n}$ with an angle γ. $\vec{A}_{\parallel}$ and $\vec{A}_{\perp}$ are the parallel and perpendicular components of $\vec{A}$, respectively, with respect to the direction $\hat{n}$. The final vector after the rotation is $\vec{A}_f$. This demonstration is useful to appreciate Eq. (1.36).

Galilean Invariance

The degree of coarse graining of the system is measured by the cell size a for multi-particle collision for a given average solvent density n_s ($= N/V$, N and V being total number of solvent particles and the volume of the box, respectively). At a temperature T, the mean thermal speed of the solvent particles is $\bar{v} \sim \sqrt{k_B T/m}$. The average (streaming) distance traveled by the solvent particles in the time interval (τ) between two MPC steps is $\lambda = \bar{v}\tau$, called the mean free path. Typically, the streaming distance of most of the particles have to be of the order of the cell length, i.e., $a \approx \lambda$. This ensures that different sets of solvent particles will undergo collisions in different MPC steps, eventually destroying the correlation among collision events. This is known as "Galilean Invariance", an essential criterion for the MPCD [86, 87].

In many applications the above criterion may not be possible to satisfy, for example, the systems at very low temperatures. In these situations, the mean free path λ is very small and this will lead to a strong correlation among collision events. A combination of

grid shifting and multi-particle collisions were introduced by Ihle and Kroll [88, 89] to deal with the small free path limit, i.e., $\lambda << a$. Before each MPC step, the positions of all particles in the system are randomly translated with a vector having components taken from a uniform distribution within the interval $[-a/2, a/2]$. This is known as grid shifting and is demonstrated in Fig. 1.7. After the collision, the original positions of the particles are restored. This random shifting helps avoid the frequent occurrence of collision events among the same set of particles in a cell due to a small mean free path and restores the "Galilean Invariance".
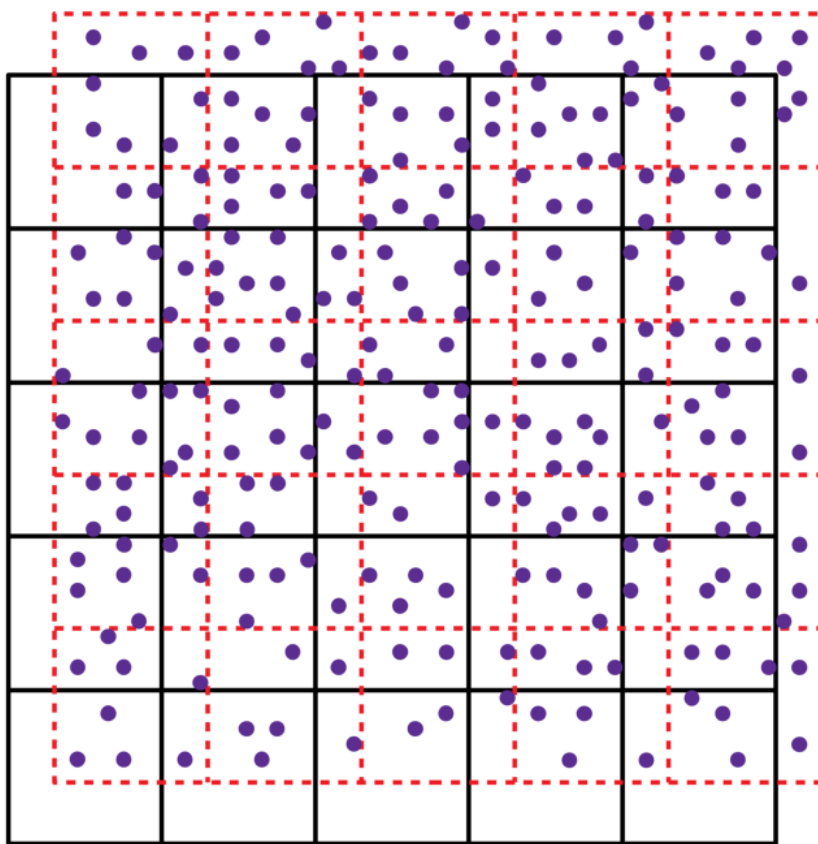
Figure 1.7: A schematic diagram showing grid shifting in the system. The particles are transferred from the original grid (solid lines) to a shifted grid (dashed lines) in x and y directions before multi-particle collision event. The circles represent point-like solvent particles.

1.7.3 Hybrid MD-MPC Dynamics

The motion of a particle is influenced by the background medium. Often there exists strong coupling between solute and solvent particles. The relevant time and length

scales of solute and solvent particles can hugely differ from each other. To capture hydrodynamic effects in such systems a hybrid MD-MPCD technique [86, 87] has been useful. In this method all particles (solute and solvent) undergo position and velocity updates due to the inter-particle forces present in the system. The interactions among solvent particles are taken care of only via multiparticle collisions. For an assembly of active particles in a solvent medium, in addition, we have used the velocity-Verlet MD algorithm [39]. The update equations, for the ith solute or solvent particle, are given by

$$\vec{r_i}(t + \Delta t) = \vec{r_i}(t) + \vec{v_i}\Delta t + \frac{\vec{f_i}(t)}{2m_i}\Delta t^2, \tag{1.37}$$

$$\vec{v_i}(t + \Delta t) = \vec{v_i}(t) + \frac{1}{2m_i}[\vec{f_i}(t) + \vec{f_i}(t + \Delta t)]\Delta t. \tag{1.38}$$

After a certain time interval τ, only solvent particles undergo multiparticle collision steps. As discussed earlier, here the system is divided into cubical cells of size a. After undergoing multi-particle collision, the velocity of kth solvent particle is updated as [86, 87]

$$\vec{v}_{s,k} = \vec{v}_{s,\text{cm}} + \mathbb{R}(\gamma)\delta\vec{v}. \tag{1.39}$$

Here $\mathbb{R}$ is a rotation matrix and $\delta\vec{v} = \vec{v}_{s,k} - \vec{v}_{s,\text{cm}}$, $\vec{v}_{s,\text{cm}}$ being the centre of mass velocity of the cell that contains k^{th} solvent particle. As discussed earlier, this step conserves the mass, momentum and energy. The transport properties of the solvent have bearing cell size a, the average number of particles in a cell n_s, rotation angle γ, etc. Appropriate choices of these parameters are essential to design and study the systems of interest.

1.8 A Few Structural Aspects

1.8.1 Gyration Tensor

To go deeper into the structural features of an object, one can calculate the radius of gyration tensor **Q** with components [90, 91]

$$Q_{kl} = \frac{1}{N}\sum_{i=1}^{N}(x_i^k - x_{\text{cm}}^k)(x_i^l - x_{\text{cm}}^l); \quad k, l = 1, ..., d, \tag{1.40}$$

where $\vec{r_i} = (x_i^1, ..., x_i^d)$ is the position of the ith particle in space dimension d and N is the total number of particles that form the object or system. A component of the center

of mass position $\vec{r}_{\mathrm{cm}}$ is calculated as [90, 91]

$$x_{\mathrm{cm}}^k = \frac{1}{N} \sum_{i=1}^{N} x_i^k. \tag{1.41}$$

To characterize the shape of the cluster of the particles it is beneficial to express $\mathbf{Q}$ in the principal axis system and work with the eigenvalues λ_k ($k = 1, ..., d$). The λ_ks of the gyration tensor describe the compactness of the cluster. An invariant of $\mathbf{Q}$ is the squared radius of gyration [90, 91]

$$R_g^2 = \frac{1}{N} \sum_{i=1}^{N} (\vec{r}_i - \vec{r}_{\mathrm{cm}})^2 = \sum_{k=1}^{d} Q_{kk} = \mathrm{Tr}\ \mathbf{Q}, \tag{1.42}$$

which quantifies the average distribution of particles relative to the center of mass of the cluster. The asphericity of the configuration is quantified by the quantity A_d, given by [90, 91]

$$A_d = \frac{d}{d-1} \frac{\mathrm{Tr}\ \hat{\mathbf{Q}}^2}{\mathrm{Tr}\ \mathbf{Q}^2} = \frac{1}{d(d-1)} \sum_{k=1}^{d} \frac{(\lambda_k - \bar{\lambda})^2}{\bar{\lambda}^2}, \tag{1.43}$$

where $\hat{\mathbf{Q}} = \mathbf{Q} - \bar{\lambda}\mathbf{I}$, $\mathbf{I}$ being the identity tensor and $\bar{\lambda}$ ($= \mathrm{Tr}\ \mathbf{Q}/d$) is the average eigenvalue of $\mathbf{Q}$. The eigenvalues are generally sorted in descending order, e.g., in $d = 3$, $\lambda_1 \geq \lambda_2 \geq \lambda_3$. The quantity A_3 (A_d; $d = 3$) equals zero for a spherical configuration, since, for this symmetry, all eigenvalues are equal, i.e., $\lambda_k = \bar{\lambda}$, for all k. It reaches maximum value 'unity' for a rod-like configuration: in this case $\lambda_1 \neq 0$, $\lambda_2 = \lambda_3 = 0$. This relative shape anisotropy parameter converges to the value of $1/4$ for planar symmetric objects for which $\lambda_1 = \lambda_2 \neq 0$ and $\lambda_3 = 0$.

Another quantity, called prolateness S, in $d = 3$, is defined as [90, 91]

$$S = 27 \frac{\det \hat{\mathbf{Q}}}{(\mathrm{Tr}\ \mathbf{Q})^3} = \frac{\prod_{k=1}^{3}(\lambda_k - \bar{\lambda})}{\bar{\lambda}^3}. \tag{1.44}$$

If the structure is absolute prolate, i.e., rod-like ($\lambda_1 \neq 0$, $\lambda_2 = \lambda_3 = 0$), then S equals two. For absolute oblate, i.e., disk-like structure ($\lambda_1 = \lambda_2$, $\lambda_3 = 0$), one has $S = -1/4$. Typically S is greater than zero for prolate conformation ($\lambda_1 \gg \lambda_2 \approx \lambda_3$) and is less than zero for oblate ones ($\lambda_1 \approx \lambda_2 \gg \lambda_3$), while magnitude measures the extent of oblate or prolateness.

1.8.2   Rotation in Three Dimensions

When asymmetric objects rotate, for certain averaging purpose it is essential to transform the associated coordinate system. We have used the rotation of a vector/coordinate system in $d = 3$ via the standard Euler angles (ψ_1, ψ_2, ψ_3). We followed x-convention of the rotation of the coordinate system [92]. At first x and y axes have been rotated by an angle ψ_1 clockwise about z-axis and the resultant coordinate system is denoted by (x', y', z'). Then the system is further rotated about x'-axis, counterclockwise, by an angle ψ_2, the resultant coordinate system becoming (x'', y'', z''). Finally x'' and y'' axes are rotated counterclockwise by an angle ψ_3 about the z''-axis. A vector $\vec{r}$ will transform to $\vec{r'}$ with respect to the new coordinate system [92], as

$$\vec{r'} = A\vec{r} \qquad (1.45)$$

where A is the rotation matrix [40, 92], written as

$$A = \begin{pmatrix} c_0^2 + c_1^2 - c_2^2 - c_3^2 & 2(c_1 c_2 + c_0 c_3) & 2(c_1 c_3 - c_0 c_2) \\ 2(c_1 c_2 - c_0 c_3) & c_0^2 - c_1^2 + c_2^2 - c_3^2 & 2(c_2 c_3 + c_0 c_1) \\ 2(c_1 c_3 + c_0 c_2) & 2(c_2 c_3 - c_0 c_1) & c_0^2 - c_1^2 - c_2^2 + c_3^2 \end{pmatrix}, \qquad (1.46)$$

with the quaternions written as $c_0 = \cos\left(\frac{\psi_2}{2}\right)\cos\left(\frac{\psi_1+\psi_3}{2}\right)$; $c_1 = \sin\left(\frac{\psi_2}{2}\right)\cos\left(\frac{\psi_1-\psi_3}{2}\right)$; $c_2 = \sin\left(\frac{\psi_2}{2}\right)\sin\left(\frac{\psi_1-\psi_3}{2}\right)$ and $c_3 = \cos\left(\frac{\psi_2}{2}\right)\sin\left(\frac{\psi_1+\psi_3}{2}\right)$. These were introduced to avoid certain singularities in the dynamics when expressed in standard fashion [40].

We have chosen (ψ_1, ψ_2, ψ_3) appropriately, for various analysis. When there is a need to transform the coordinate system in such a way that the z-axis of the new coordinate system should coincide with any unit vector $\hat{n} \equiv (n_x, n_y, n_z)$ of the present coordinate system, one may adopt the choice $\psi_1 = \cos^{-1}\left(\frac{n_y}{\sqrt{n_x{}^2+n_y{}^2}}\right)$, $\psi_2 = \cos^{-1}(n_z)$ and $\psi_3 = -\psi_1$, implying $c_0 = \cos\left(\frac{\psi_2}{2}\right)$, $c_1 = \sin\left(\frac{\psi_2}{2}\right)\cos(\psi_1)$, $c_2 = \sin\left(\frac{\psi_2}{2}\right)\sin(\psi_1)$ and $c_3 = 0$, among many others.

1.9   A Brief Statement on the Problems Addressed in the Thesis

We have investigated various aspects of the structure and dynamics of active matter systems. In chapters 2 and 3, we have considered Vicsek-like aligning active particles and active Brownian particles in $d = 2$. We have quantified the growth in the density and

velocity fields of these systems. In chapter 4 we investigate the role of hydrodynamics in clustering dynamics in systems of Vicsek-like active particles embedded in solvent in $d = 3$. In chapter 5, we consider a mixture of active colloids and passive polymers inside a spherical cavity and quantified the phase behavior and dynamics of the system. Chapter 6 contains a comparative study of another mixture of active and passive particles that are constrained to move on a spherical surface and a flat plane.

Bibliography

[1] K. Binder, *in Phase Transformation of Materials*, edited by R. W. Cahn, P. Haasen, and E. J. Kramer (VCH, Weinheim, 1991), Vol. 5, p. 405.

[2] A. J. Bray, Adv. Phys. **51**, 481 (2002).

[3] S. Puri and V. Wadhawan (eds.), *Kinetics of Phase transitions* (CRC Press, Boca Raton, 2009).

[4] R. A. L. Jones, *Soft Condensed Matter* (Oxford University Press, Oxford, 2008).

[5] A. Onuki, *Phase Transition Dynamics* (Cambridge University Press, Cambridge, 2002).

[6] H. E. Stanley, *Introduction to Phase Transitions and Critical Phenomena* (Oxford University Press, Oxford, 1971).

[7] M. E. Fisher, *in Critical Phenomena*, edited by M. S. Green (Academic, London, 1971) p1.

[8] K. Kawasaki, *in Phase Transition and Critical Phenomena*, edited by C. Domd and M.S. Green (Academic, New York, 1972), Vol. 2, p.443.

[9] P. C. Hohenberg and B. I. Halperin, Rev. Mod. Phys. **49**, 435 (1977).

[10] V. Privman, P. C. Hohenberg, and A. Aharony, *in Phase Transitions and Critical Phenomena*, edited by C. Domb and J. L. Lebowitz (Academic Press, New York, 1991), Vol. 14, Chap. I.

[11] K. Binder and D. Stauffer, Phys. Rev. Lett. **33**, 1006 (1974).

[12] S. Roy and S. K. Das, Phys. Rev. E **85**, 050602(R) (2012).

[13] J. Midya and S. K. Das, Phys. Rev. Lett. **118**, 165701 (2017).

[14] J. K. Parrish and W. M. Hamner, *Animal Groups in Three Dimensions* (Cambridge University Press, Cambridge, U.K., 1997).

[15] M. Ballerini, N. Cabibbo, R. Candelier, A. Cavagna, E. Cisbani, I. Giardina, V. Lecomte, A. Orlandi, G. Parisi, A. Procaccini, M. Viale, and V. Zdravkovic, Proc. Natl. Acad. Sci. U. S. A. **105**, 1232 (2008).

[16] M. Nagy, Z. Ákos, D. Biro, and T. Vicsek, Nature **464**, 890 (2010).

[17] O. Feinerman, I. Pinkoviezky, A. Gelblum, E. Fonio, and N. S. Gov, Nature Physics **14**, 683 (2018).

[18] C. Dombrowski, L. Cisneros, S. Chatkaew, R. E. Goldstein, and J. O. Kessler, Phys. Rev. Lett. **93**, 098103 (2004).

[19] H. P. Zhang, A. Béer, E.-L. Florin and H. L. Swinney, Proc. Natl. Acad. Sci. USA **107**, 13626 (2010).

[20] S. F. Schoeller, W. V. Holt, and E. E. Keaveny, Cells. Phil. Trans. R. Soc. B **375**, 20190384 (2020).

[21] M. Scholz, K. L. Weirich, M. L. Gardel, and A. R. Dinner, Soft Matter **16**, 2135 (2020).

[22] G. Gompper et. al., J. Phys.: Condens. Matter **32**,193001 (2020).

[23] M. C. Marchetti, J. F. Joanny, S. Ramaswamy, T. B. Liverpool, J. Prost, M. Rao, and R. A. Simha, Rev. Mod. Phys. **85**, 1143 (2013).

[24] S. Ramaswamy, Annu. Rev. Condens. Matter Phys. **1**, 323 (2010).

[25] G. Grégoire and H. Chaté, Phys. Rev. Lett. **92**, 025702 (2004).

[26] T. Vicsek, A. Czirôk, E. Ben-Jacob, I. Cohen, and O. Schochet, Phys. Rev. Lett., **75**, 1226 (1995).

[27] T. Vicsek and A. Zafeiris, Phys. Rep. **517**, 71 (2012).

[28] M. E. Cates and J. Tailleur, Annu. Rev. Condens. Matter Phys. **6**, 219 (2015).

[29] J. Stenhammar, D. Marenduzzo, R. J. Allen, and M. E. Cates, Soft Matter **10**, 1489 (2014).

[30] J. Bialké, T. Speck, and H. Löwen, Phys. Rev. Lett. **108**, 168301 (2012).

[31] Y. Fily and M. C. Marchetti, Phys. Rev. Lett. **108**, 235702 (2012).

[32] P. Digregorio, D. Levis, A. Suma, L. F. Cugliandolo, G. Gonnella, and I. Pagonabarraga, Phys. Rev. Lett. **121**, 098003 (2018).

[33] C. B. Caporusso, P. Digregorio, D. Levis, L. F. Cugliandolo, and G. Gonnella, Phys. Rev. Lett. **125**, 178004 (2020).

[34] L. Caprini, U. Marini Bettolo Marconi, and A. Puglisi, Phys. Rev. Lett. **124**, 078001 (2020).

[35] A. Kudrolli, G. Lumay, D. Volfson, and L. S. Tsimring, Phys. Rev. Lett. **100**, 058001 (2008).

[36] J. Palacci, S. Sacanna, A. P. Steinberg, D. J. Pine, and P. M. Chaikin, Science, **339**, 936 (2013).

[37] P.-H. Chavanis, Physica A **390**, 1546 (2011).

[38] A. Campa, T. Dauxois, and S. Ruffo, Phys. Rep. **480**, 57 (2009).

[39] D. Frenkel and B. Smit, *Understanding Molecular Simulations: From Algorithms to Applications* (Academic Press, San Diego, California, 2002).

[40] M. P. Allen and D. J. Tildesley, *Computer Simulations of Liquids* (Clarendon, Oxford, 1987).

[41] T. Schlick, *Molecular Modeling and Simulation: An Interdisciplinary Guide* (Springer, New York, 2010).

[42] S. K. Das, S. A. Egorov, B. Trefz, P. Virnau, and K. Binder, Phys. Rev. Lett. **112**, 198301 (2014).

[43] S. K. Das, J. Chem. Phys. **146**, 044902 (2017).

[44] F. D. C. Farrell, M. C. Marchetti, D. Marenduzzo, and J. Tailleur, Phys. Rev. Lett. **108**, 248101 (2012).

[45] A. Martin-Gomez, D. Levis, A. Diaz-Guilera, and I. Pagonabarraga, Soft Matter **14**, 2610 (2018).

[46] J. A. Acebrón, L. L. Bonilla, C. J. Pérez-Vicente, F. Ritort, and R. Spigler, Rev. Mod. Phys. **77**, 137 (2005).

[47] J. M. Kosterlitz and D. J. Thouless, J. Phys. C: Solid State Phys. **6**, 1181 (1973).

[48] J. M. Kosterlitz, J. Phys. C: Solid State Phys. **7**, 1046 (1974).

[49] D. Frenkel, Physica A **263**, 26 (1999).

[50] A. Buhot and W. Krauth, Phys. Rev. Lett. **80**, 3787 (1998).

[51] L. Onsager, Prop. NY. Acad. Sci. **51**, 627 (1949).

[52] S. Asakura and F. Oosawa, J. Chem. Phys. **22**, 1255 (1954).

[53] S. Asakura and F. Oosawa, J. Pol. Sci. **33**, 183 (1958).

[54] A. Vrij. Pure Appl. Chem. **48**, 471 (1976).

[55] S. M. Ilett, A. Orrock, W. C. K. Poon, and P. N. Pusey, Phys. Rev. E **51**, 1344 (1995).

[56] W. C. K. Poon, J. Phys.: Condens. Matter **14**, R859 (2002).

[57] J. Zausch, P. Virnau, K. Binder, J. Horbach, and R. L. C. Vink, J. Chem. Phys. **130**, 064906 (2009).

[58] I. M. Lifshitz and V. V. Slyozov, J. Phys. Chem. Solids **19**, 35 (1961).

[59] D. A. Huse, Phys. Rev. B **34**, 7845 (1986).

[60] H. Tanaka, J. Chem. Phys. **105**, 10099 (1996).

[61] E. D. Siggia, Phys. Rev. A **20**, 595 (1979).

[62] S. K. Das, J. V. Sengers, and M. E. Fisher, J. Chem. Phys. **127**, 144506 (2007).

[63] G. F. Carnevale, Y. Pomeau, and W. R. Young, Phys. Rev. Lett. **64**, 2913 (1990).

[64] E. Trizac and P. L. Krapivsky, Phys. Rev. Lett. **91**, 218302 (2003).

[65] E. Trizac and J.-P. Hansen, J. Stat. Phys. **82**, 1345 (1996).

[66] N. Brilliantov, P. L. Krapivsky, A. Bodrova, F. Spahn, H. Hayakawa, V. Stadnichuk, and J. Schmidt, Proc. Natl. Acad. Sci. USA **112**, 9536 (2015).

[67] J.-P. Hansen and I. R. McDonald, *Theory of Simple Liquids* (Academic Press, London, 2008).

[68] S. Paul and S. K. Das, Europhys. Lett. **108**, 66001 (2014).

[69] A. J. Bray and S. Puri, Phys. Rev. Lett. **67**, 2670 (1991).

[70] H. Toyoki, Mod. Phys. Lett. B **7**, 397 (1993).

[71] *Definite Integrals of Special Functions*, Editor(s): D. Zwillinger, V. Moll, I. S. Gradshteyn, I. M. Ryzhik, *Table of Integrals, Series, and Products* (Eighth Edition), Academic Press, 2014, Pages 776-865.

[72] T. Ohta, D. Jasnow, and K. Kawasaki, Phys. Rev. Lett. **49**, 1223 (1982).

[73] D. P. Landau and K. Binder, *A Guide to Monte Carlo Simulations in Statistical Physics* (Cambridge University Press, Cambridge, 2009).

[74] N. Vadakkayil, S. Chakraborty, and S. K. Das, J. Chem. Phys. **150**, 054702 (2019).

[75] S. Nosé, J. Chem. Phys. **81**, 511 (1984).

[76] W. G. Hoover, Phys. Rev. A **31**, 1695 (1985).

[77] E. A. Koopman and C. P. Lowe, J. Chem. Phys. **124**, 204103 (2006).

[78] S. D. Stoyanov and R. D. Groot, J. Chem. Phys. **122**, 114112 (2005).

[79] E. Gillies, R. Cannon, R. Green, and A. Pacey, J. Fluid Mech. **625**, 445 (2009).

[80] G. R. McNamara and G. Zanetti, Phys. Rev. Lett. **61**, 2332 (1988).

[81] X. Shan and H. Chen, Phys. Rev. E **47**, 1815 (1993).

[82] X. He and L.-S. Luo, Phys. Rev. E **56**, 6811 (1997).

[83] P. J. Hoogerbrugge and J. M. V. A. Koelman, Europhys. Lett. **19**, 155 (1992).

[84] P. Espanol, Phys. Rev. E **52**, 1734 (1995).

[85] P. Espanol and P. B. Warren, Europhys. Lett. **30**, 191 (1995).

[86] R. Kapral, Adv. Chem. Phys. **140**, 89 (2008).

[87] G. Gompper, T. Ihle, D. M. Kroll, and R. G. Winkler, Adv. Polym. Sci. **221**, 1 (2008).

[88] T. Ihle and D. M. Kroll, Phys. Rev. E **63**, 020201(R) (2001).

[89] T. Ihle and D. M. Kroll, Phys. Rev. E **67**, 066705 (2003).

[90] K. Šolc and W. H. Stockmayer, J. Chem. Phys. **54**, 2756 (1971).

[91] H. Arkin and W. Janke, J. Chem. Phys. **138**, 054904 (2013).

[92] H. Goldstein, *Classical Mechanics* (Addison-Wesley, 1951).

Chapter 2

Nucleation and Growth in Assemblies of Active Brownian and Vicsek-like Particles

2.1 Introduction

There has been significant progress in the understanding of structure and dynamics, in both equilibrium and nonequilibrium contexts, in passive systems exhibiting phase transitions [1–14]. In the non-equilibrium domain much effort has been devoted to quantify the dynamics of growth and investigation of associated scaling. In recent times, there has been a growing interest in studies of phase-separation in active matter systems [15–43]. These systems contain particles that self-propel by converting energy into mechanical work [15–43]. Such systems are always far from equilibrium and their corresponding steady states can be considered as equilibrium in passive systems [16, 21]. Phase separation in these systems can be robust that can be appreciated from the flocking of birds, for example. The latter and cluster formation in many similar systems display fascinating pattern formation not only in density field but also in the velocity field [16–24]. There have been elegant efforts in developing theories, replicating experimental pictures and thus, to understand the nature of interactions among active particles and the corresponding phase-separation dynamics [15–43].

Depending on the nature of self-propulsion these systems exhibit different kinds of behaviour. To capture the dynamics in a system, such as a flock of birds, one simple model was introduced by Vicsek et. al., where the velocity direction of a particle tends

to be aligned with the average direction of motion of its neighbours [34]. This model exhibits flocking with high particle density and low noise strength. For one part of the study, in this chapter, we have considered this alignment interaction in space dimension $d = 2$ and investigated the dynamics of cluster growth during vapor-'solid' transitions. For the other part, we consider systems containing active Brownian particles (ABP) [17, 22–24, 40, 41].

In systems of active Brownian particles there exist no alignment interactions. These particles change their directions depending on the rotational diffusion constant D_r. There also exists translational diffusion of particles. These systems also undergo phase-separation with vapor-like phases (particle-poor) and liquid-like (particle-rich) phases even in absence of any attractive potential. This phase separation is primarily driven by the packing fractions and Péclet number [17, 22–24, 40, 41]. This is known as motility induced phase separation (MIPS) [17]. In our systems of low density of particles that we consider, however, there will be no prominent phase separation unless there is an attractive interparticle passive interaction. The latter will lead to phase separation even when there is no self-propulsion [11, 12, 14]. Here we investigate how the self-propulsion influences this phase separation. The objective is stated below.

In this work, we have investigated the structure and dynamics during a vapor-'solid' phase transitions. There the morphology consists of well-separated clusters of "solid" phases, with short-range order, having fractal nature. This passive picture we influence via the addition of two different types of activity that are described above. Corresponding quantitative results are discussed.

2.2 Model and Methods

Passive interactions among active particles are taken as [44–46]

$$u(r) = U(r) - U(r_c) - (r - r_c)\left(\frac{dU}{dr}\right)_{r=r_c},$$ (2.1)

where

$$U(r) = 4\epsilon\left[\left(\frac{\sigma}{r}\right)^{12} - \left(\frac{\sigma}{r}\right)^{6}\right]$$ (2.2)

is the standard Lennard-Jones (LJ) pair potential. Here ϵ is the strength of the interaction. The cut-off distance r_c is taken to be 2.5σ, σ being the particle diameter.

Two different kinds of active particles are considered, viz., Vicsek-like aligning active particles and active Brownian particles. We have placed these particles inside two dimensional ($d = 2$) square boxes having periodic boundary conditions (PBC) in both directions. The number density of particles in the system is $\rho = N/L^2$. We have studied low density systems ($\rho = 0.05$) at a very low temperature $T = 0.1\epsilon/k_B$ (k_B is the Boltzmann constant). Further details are given below.

2.2.1 Systems of Vicsek-like particles

For Vicsek-like aligning active particles we have performed molecular dynamics (MD) simulations by numerically solving the Langevin equation [44],

$$m\ddot{\vec{r}}_i = -\nabla u_i - \gamma m\dot{\vec{r}}_i + \sqrt{2\gamma k_B T m}\vec{\eta}_i(t) + \vec{f}_i, \tag{2.3}$$

via the Verlet velocity algorithm [44, 45]. In Eq. (2.3) m and γ are the mass of each particle and the damping coefficient, respectively. The random noise $\vec{\eta}_i$ satisfies [46]

$$\left\langle \eta_i^\mu(t)\eta_j^\nu(t') \right\rangle = \delta_{\mu\nu}\delta_{ij}\delta(t - t'), \tag{2.4}$$

where t and t' stand for two different times; η_i^μ and η_j^ν are the μ and ν Cartesian components, corresponding to the ith and j^{th} particles, respectively; and T is the quenched temperature of the system.

The active force $\vec{f}_i$ has been incorporated via a local velocity alignment rule, mimicking Vicsek [34] interaction. For particle i, it acts along the average direction of motion of its neighbors [38]:

$$\hat{n}_i = \frac{\sum_j \vec{v}_j}{|\sum_j \vec{v}_j|}. \tag{2.5}$$

The summation above is carried over all the neighbors of particle i, situated within the distance r_c. This active interaction is incorporated in such a way that it only causes the rotation of the velocity field. Since the force $\vec{f}_i$ acts along $\hat{n}_i$, we have

$$\vec{f}_i = f_A\hat{n}_i, \tag{2.6}$$

f_A being the strength of the alignment interaction [38]. The value $f_A = 0$ corresponds to the passive system.

The units of mass, length and time are m, σ and t_0 ($= \sqrt{m\sigma^2/\epsilon}$), respectively. We set m, σ, ϵ, k_B and γ to unity. We used the MD integration time step $\Delta t = 0.01t_0$. All the

results in this case are for $L = 1024$ and presented after averaging over 50 independent initial configurations.

2.2.2 Systems consisting of active Brownian particles

In this case we have considered the standard model for active Brownian particles. The dynamical equations for this case are given by [41, 42]

$$\dot{\vec{r}}_i = \beta' D_t [-\vec{\nabla} u_i + f_p \hat{p}_i] + \sqrt{2D_t}\vec{\Lambda}_i^t, \tag{2.7}$$

and

$$\dot{\theta}_i = \sqrt{2D_r}\Lambda_i^r. \tag{2.8}$$

Here $\vec{r}_i$ is the position of the ith particle, u_i is the passive LJ energy, f_p is the strength of the self-propulsion force having direction $\hat{p}_i \equiv (\cos\theta_i, \sin\theta_i)$ and β' $(= 1/k_B T)$ is the inverse kinetic energy. Here D_t and D_r are the translational and rotational diffusion constants of the particles, respectively, and these are dependent on each other by the relation $D_r = D_t/3\sigma^2$ [41]. Here Λ_i^r and the components of $\vec{\Lambda}_i^t$ are the zero-mean and unit-variance delta-correlated random noise.

We have considered, as stated above, the overall particle density $\rho = 0.05$ and the background temperature $T = 0.1$. We are interested in studying the disconnected cluster morphology. For this purpose we have considered such a low density of particles. In this case we set $L = 512$. We solve the Eqs. (2.7) and (2.8) by the method of finite differences, that is known as Euler–Maruyama scheme [42, 47], with time step $\Delta t = 10^{-3}$. We have presented the results for $D_t = 0.1$ and few different f_p values, viz., $f_p = 0$, 0.5 and 1.

2.3   Results

As stated above, we are interested in studying the growth dynamics for disconnected cluster morphology. To achieve that consideration of low density of particles is important. Here we have used $\rho = 0.05$, as mentioned already. We will first present results for the Vicsek-like active particles and then for active Brownian particles.

2.3.1   Vicsek-like Active Particles

The evolution snapshots following quenches of homogeneous systems to a low temperature, viz., $T = 0.1$, are shown for different values of f_A in Fig. 2.1. We observe the formation

of fractal structure at late-time. Also, one gets the impression that growth occurs faster for a stronger value of f_A. While we will investigate this feature later, in Fig. 2.2(a) we have shown a 36×36 part, from inside a fractal cluster, for $f_A = 1$ at $t = 10^4$. Crystalline arrangement of particles is visible. A parameter related to the hexagonal order ($\vec{\psi}_6^k$) corresponding to the kth particle in this case can be defined as [48–50]
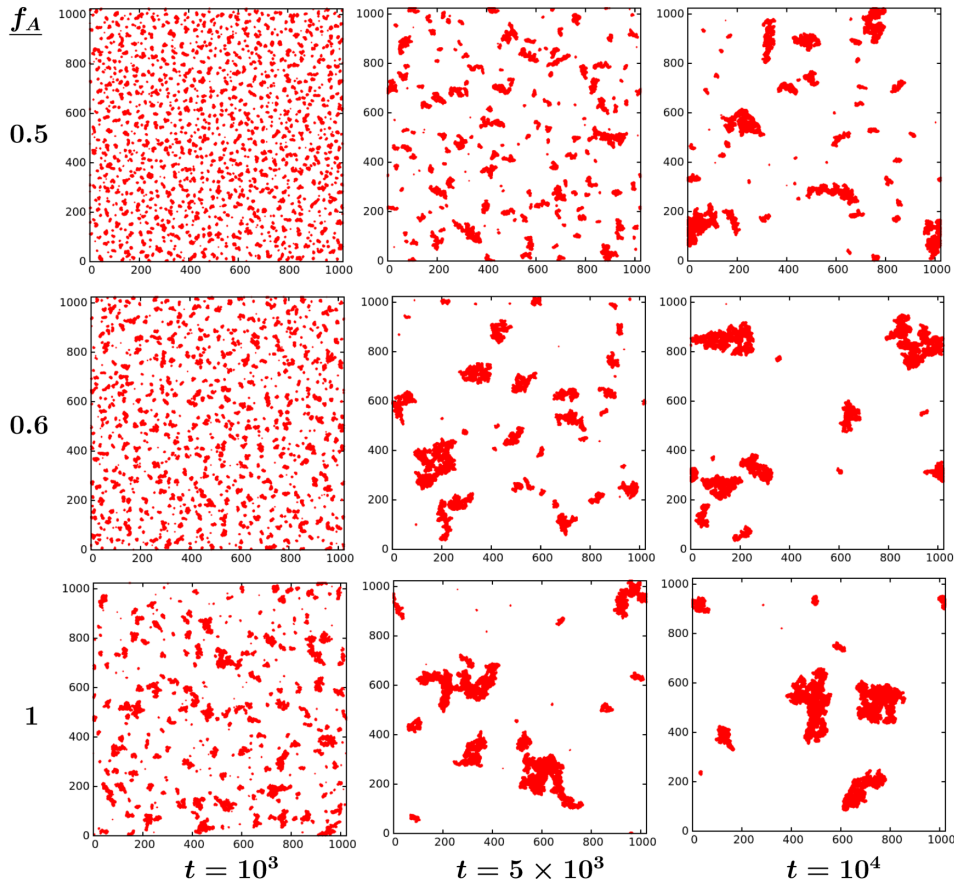
Figure 2.1: Snapshots, obtained during evolution following quenches of homogeneous systems, with $\rho = 0.05$, to $T = 0.1$, are shown for different activity strength f_A. In each of the cases frames from three different times are included. These results are for Vicsek-like particles.

$$\vec{\psi}_6^k = \sum_{j=1}^{n_v} \frac{l_j}{l} \exp(6i\phi_{kj}), \tag{2.9}$$

where ϕ_{kj} is the angle between the kth particle and its jth Voronoi neighbor, l_j is the length of the voronoi edge corresponding to the jth neighbor and $l = \sum_{j=1}^{n_v} l_i$; n_v being the total number of Voronoi topological neighbors of particle k. In Fig. 2.2(b) we show
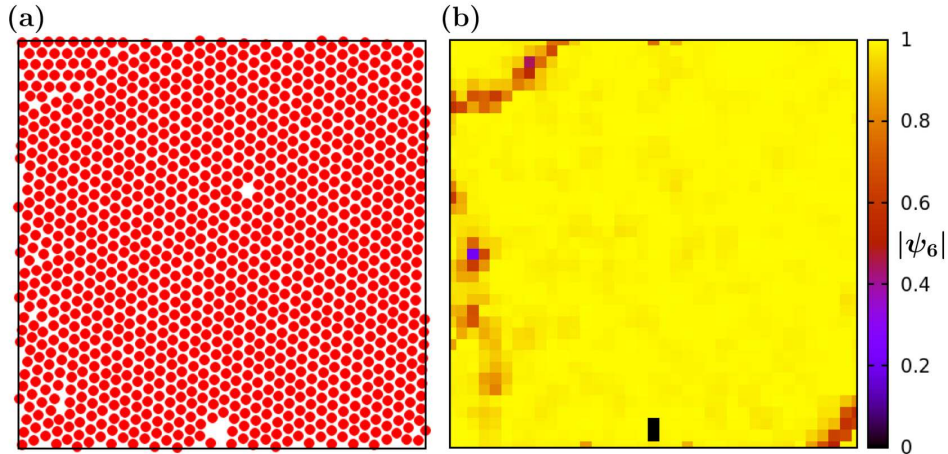
Figure 2.2: (a) A portion of the system in Fig. 2.1 is shown from $t = 10^4$, for $f_A = 1$. (b) Hexatic order-parameter $|\psi_6|$ for the configuration in (a) is shown. Note that the size of the portion here is 36×36.

ψ_6 $(=|\vec{\psi}_6^k|)$ for the particles shown in Fig. 2.2(a). The high value of ψ_6 (see the color coding) indicates the 'solid' phase of particles in the background of vapor phase.

The formation of fractal clusters in this case can be for various reasons [14]. The inherent tendency of the clusters during the evolution process is to minimize the interfacial free energy. This should lead to the formation of circular boundaries of clusters in $d = 2$. However, when there exists a 'solid'-like arrangement of particles inside clusters, the relaxation process regarding the rearrangement of particles inside a cluster can be significantly slower than that of growth. However, the introduction of activity reduces the fractal character compared to the pure passive case (the results for the pure passive case are not presented here). We will investigate the mechanism of growth in the latter part of the Chapter.

To quantify the dynamics of growth we have identified all the clusters at different times and calculated the mass as the number of particles in each of them. The average mass, M, has been obtained from the first moment of the mass distribution function [11, 12]. In Fig. 2.3 we show the variation of M with time, on a log-log scale, for different alignment strengths f_A. For the considered values of f_A, the asymptotic behavior of growth is similar. However, for a lower value of f_A, the appearance of the asymptotic power-law growth gets delayed. The late-time growth exponent, β, is approximately 1.8, which is, as mentioned, the same for all the considered values of f_A.

To quantify the fractal nature of the clusters, as well as to understand the growth, we calculate, among other quantities, the fractal dimension d_f of the clusters for different f_A.

Typically the average mass M is related to the average radius of gyration R_g as [51, 52]

$$M \sim R_g^{d_f}. \tag{2.10}$$
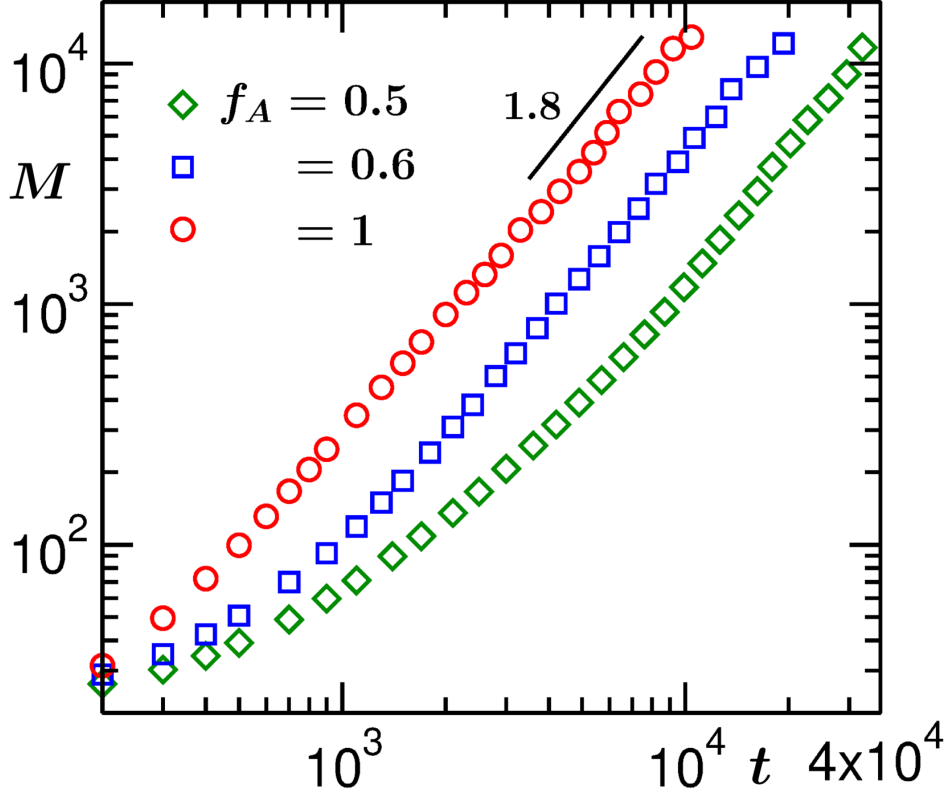
Figure 2.3: Average mass (M) is plotted versus time (t), on a log-log scale. Data for three values of f_A are shown. The consistency of the data sets at late times with the solid line is indicative of power-law growth with mentioned exponent. These results are for Vicsek-like particles.

For a cluster, the radius of gyration (R_g^c) is calculated as [53]

$$R_g^c = \left[\frac{1}{N_c} \sum_{i=1}^{N_c} (\vec{r}_i - \vec{r}_{cm})^2 \right]^{1/2}. \tag{2.11}$$

where the sum is carried over all the particles (N_c) within the cluster and $\vec{r}_{cm}$ is the position of the center of mass of the cluster, i.e.,

$$\vec{r}_{cm} = \frac{1}{N_c} \sum_{i=1}^{N_c} \vec{r}_i. \tag{2.12}$$
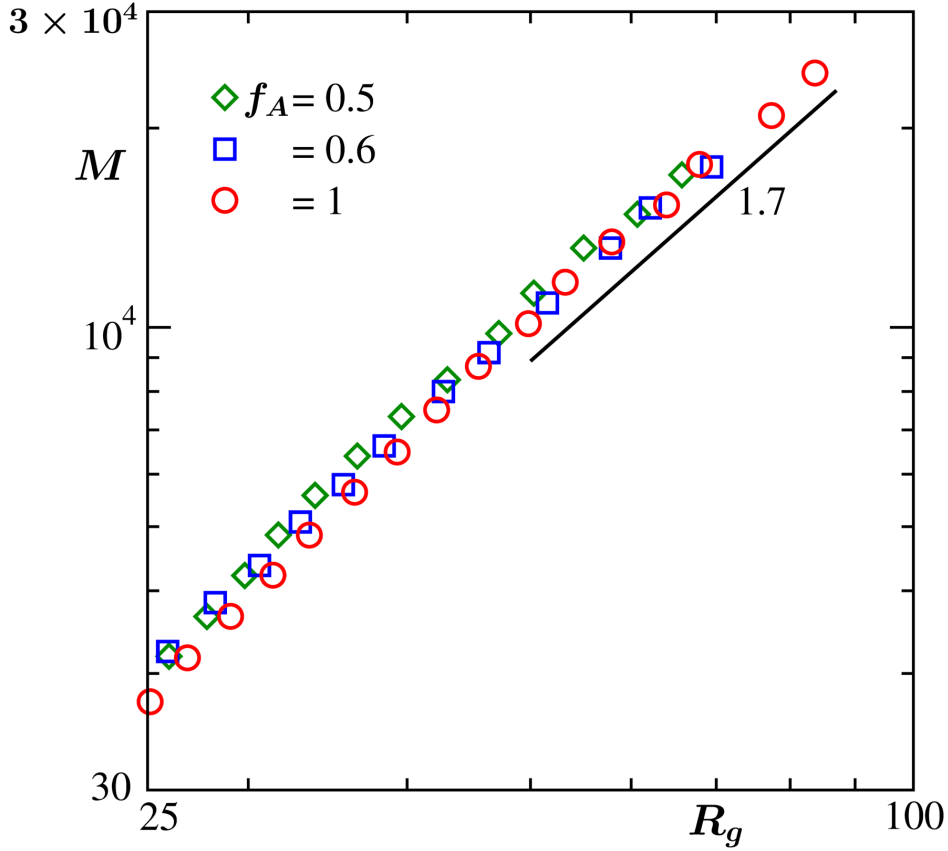
Figure 2.4: Plots of average mass (M) versus radius of gyration (R_g) are shown for different values of f_A, on a log-log scale. The black solid line represents a power-law with exponent $d_f = 1.7$. These data sets are for the Vicsek-like particles.

The average radius of gyration R_g then is calculated from the first moment of the distribution of R_g^c. In Fig. 2.4 we have presented R_g versus M plots, on a log-log scale, for different values of f_A. For large R_g, the appearance is linear, confirming the power-law behavior in Eq. 2.10. It seems, there is no strong dependence of d_f on f_A.

Due to the coherent movement of the particles, the solid clusters of particles are expected to have some directional mobility. The growth here mainly occurs via certain cluster coalescence mechanisms. When these clusters exhibit diffusive motion, the growth of clusters can be explained via the Binder and Stauffer (BS) diffusive coalescence mechanism [6–8]. The value of the exponent in this case is $\beta = 1$ in $d = 2$. For this case, a dynamical equation can be written as [8]

$$\frac{dn}{dt} = -Cn^2, \qquad (2.13)$$
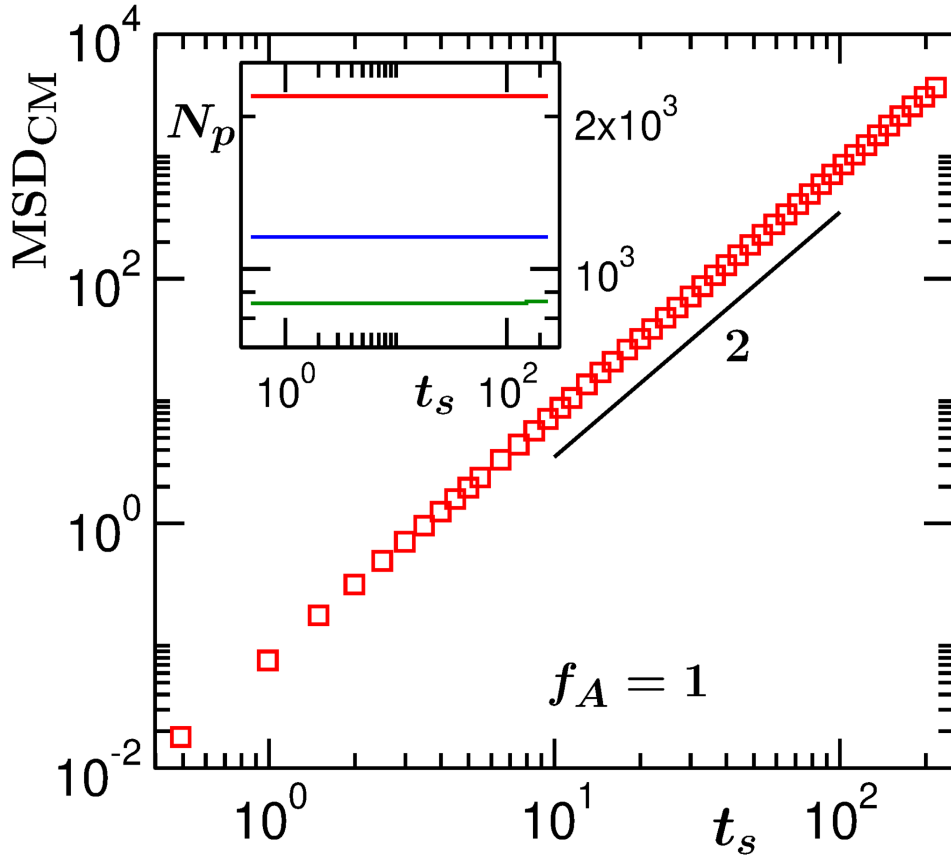
Figure 2.5: A plot of the mean-squared displacement MSD_{CM} of the centre of mass of a cluster versus translated time $t_s = t - t_0$ (t_0 being the beginning of an observation) has been shown for $f_A = 1$. In the inset the numbers of particles, N_p, inside a cluster are shown versus t_s. Here results from three different clusters are included. The presented data are for the Vicsek-like particles.

where n is the number density of cluster and C is a constant that arises from the Stokes–Einstein–Sutherland relation [1, 46, 54]. From the conservation of mass one has $n \propto 1/m$.

As seen in Fig. 2.3, the growth exponent β is rather strong in the present case. The value is much higher than any known value in the context of phase separation in passive matters. The reason may be the directional motions of clusters, originating from the Vicsek activity. Note that we expect a coalescence mechanism behind the growth. To check the motion of clusters we have calculated the mean-squared-displacement (MSD_{CM}) of the center of mass of the clusters [46].

In Fig. 2.5 we have shown a representative plot of MSD_{CM} versus translated time t_s ($= t - t_0$, t_0 referring to the beginning of an observation), on a log-log scale. The
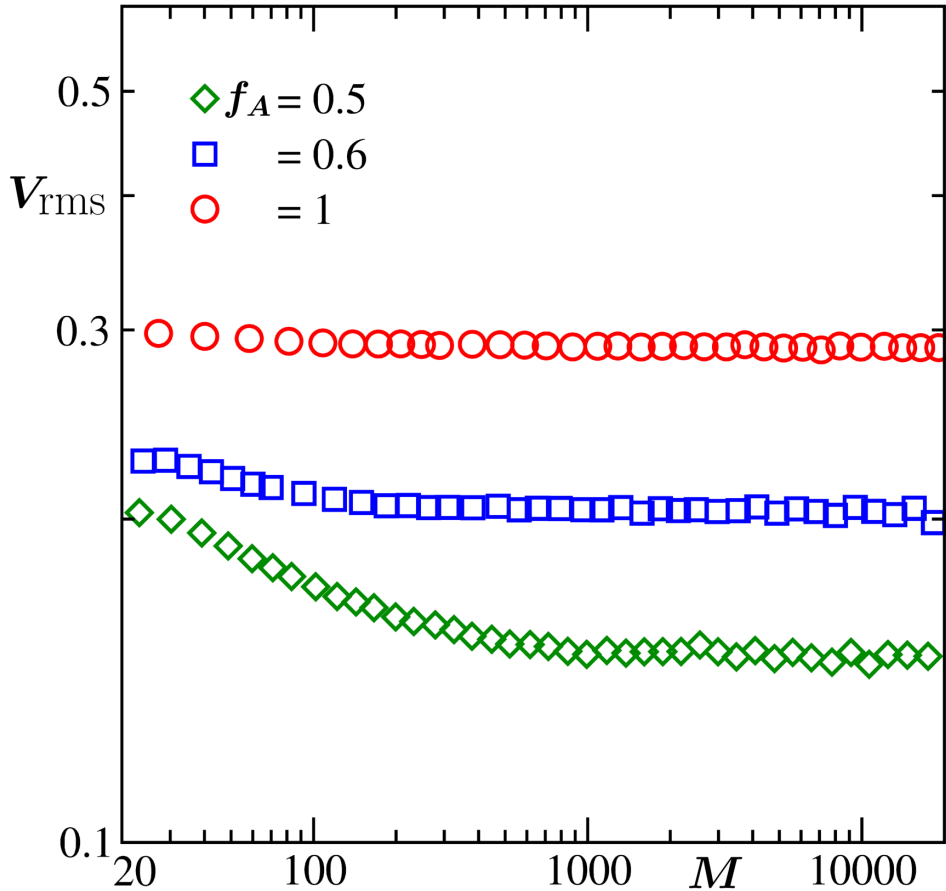
Figure 2.6: The root mean squared velocity, V_{rms}, has been plotted against M. Results from different f_A have been included. These are for Vicsek-like particles.

quadratic behavior is indicative of the ballistic movement of the clusters. In the inset of Fig. 2.5 we show the numbers of particles N_p inside a few clusters, as a function of t_s. The near-constant values of N_p discard the possibility of any significant contribution due to the Lifshitz–Slyozov particle diffusion mechanism [5, 55–57].

As the motion of the clusters is ballistic in nature, we look for a theory of ballistic aggregation mechanism (BAM) [58–62]. In BAM a standard equation for binary collisions reads [58–62]

$$\frac{dn}{dt} = -\sigma_{\mathrm{coll}} V_{\mathrm{rms}} n^2, \tag{2.14}$$

where σ_{coll} is the collision cross-section and V_{rms} is the root mean squared velocities of the clusters. In $d = 2$, σ_{coll} is the radius of gyration R_g, i.e., $\sigma_{\mathrm{coll}} \sim M^{1/d_f}$ [see Eq. (2.10)]. From the conservation of mass one obtains $M \propto 1/n$. Typically V_{rms} depends on the average mass (M) of the clusters as $V_{\mathrm{rms}} \sim M^z$. Using these information, Eq. (2.14) can

be written as

$$\frac{dM}{dt} = M^{z+\frac{1}{d_f}}.$$ (2.15)
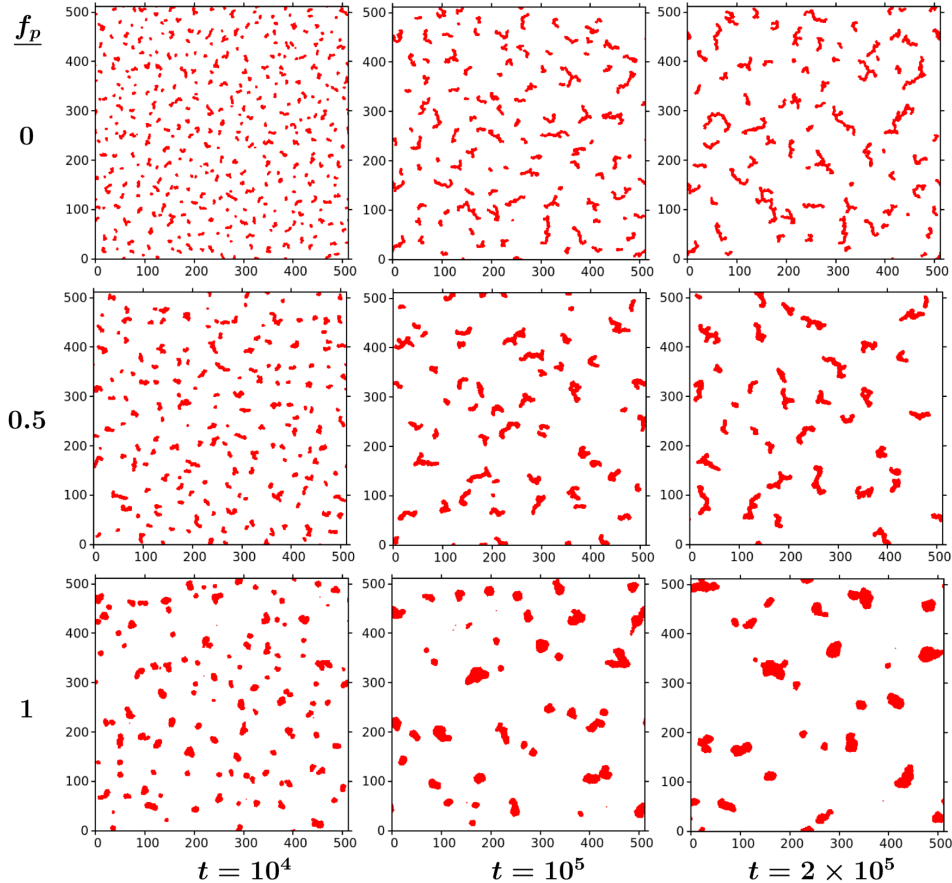
Figure 2.7: Snapshots demonstrating evolutions of ABP systems with different self-propulsion force f_p.

From the solution of Eq. (2.15) one obtains [60–62]

$$M \sim t^{\beta},$$ (2.16)

with $\beta = \frac{d_f}{d_f(1-z)-1}$.

Now if BAM is true for the present problem, then for $\beta \approx 2$ and $d_f \approx 1.7$, one obtains $z \approx -0.1$, a value much different from -0.5, which is expected in situations when the velocities of the clusters are uncorrelated, observed in many passive matter systems [14, 58–60, 62]. We have calculated $V_{\rm rms}$ of the clusters and plotted versus M, on a log-log scale, in Fig. 2.6. We obtain the value of z to be practically 0 in the large M
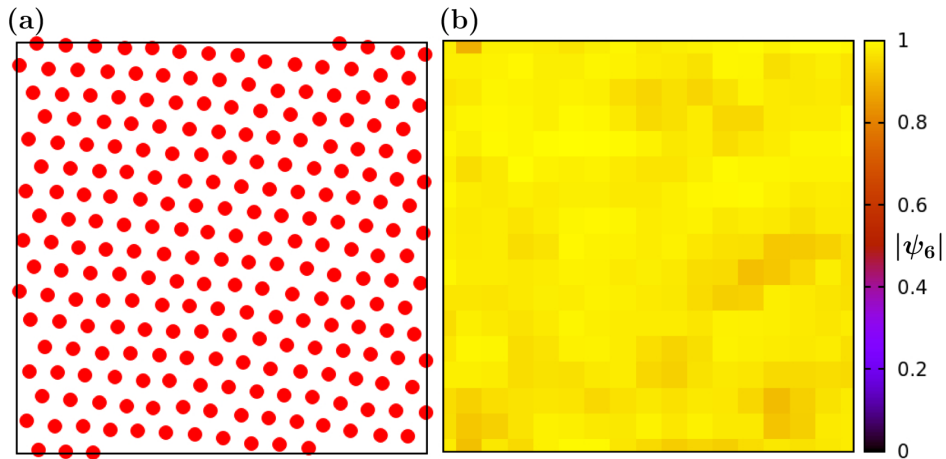
Figure 2.8: (a) A part of a cluster from the snapshot of a system with $f_p = 1$ is shown from time $t = 2 \times 10^5$ (b) Hexatic order parameter, $|\psi_6|$, for the arrangement shown in (a). The selected part here has the size 16×16. These are for an ABP system.

regime. The discrepancy between the observation and the expected value from BAM may occur due to the following reasons. It is possible that on an average $\mathrm{MSD_{CM}}$ deviates from the quadratic time-dependence to some extent. To ascertain that, of course, a more accurate study, with very good statistics, is needed. This is true for the other associated quantities as well. However, our results are already in very good agreement with the theoretical picture, even at a quantitative level.

2.3.2   Active Brownian Particles

In this section we discuss results from systems consisting of active Brownian particles. We have taken the standard model in an overdamped limit that has been used commonly to study ABP systems [22–24, 40, 41]. In addition, we have considered the same passive interaction potential that was incorporated in the Vicsek case. Here we vary the self-propulsion force (f_p) of the particles and investigate how the dynamics of the system changes. In Fig. 2.7 we show the evolution snapshots of systems having different values of f_p. Note that $f_p = 0$ corresponds to the passive Brownian particles. For $f_p = 0$ filament-like structures are visible at late times, while for $f_p = 1$ at the late time the clusters are less fractal. There is a strong dependence of the shape of the clusters with the self-propulsion speed in ABP case.

In Fig. 2.8(a) we have shown a portion of a cluster, for $f_p = 1$, from $t = 2 \times 10^5$. The hexatic arrangement of particles is seen. This has been confirmed in Fig. 2.8(b), where we have shown the local hexatic order-parameter ψ_6 for the same portion that is shown
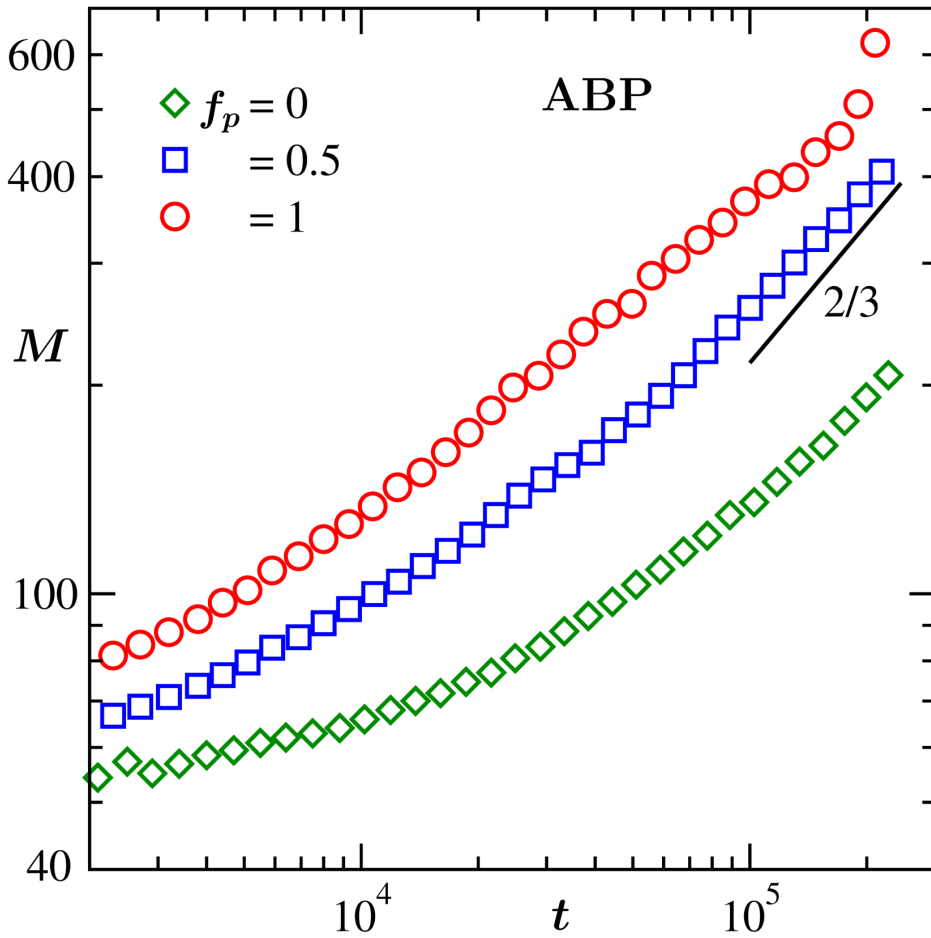
Figure 2.9: Average mass (M) is shown versus t. Results from three values of f_p are included. The solid line is indicative of a power-law growth with the mentioned exponent. These results are for ABP systems.

in (a). The higher value of ψ_6 is indicative of 'solid' clusters. Thus, here also we are dealing with vapor-'solid' transition.

In Fig. 2.9 we have shown the growth of the average mass (M) of the clusters with time. Power-law growth at a late time can be appreciated for all considered values of f_p. This growth exponent is much smaller than the Vicsek case. For this model, the exponent is approximately 2/3. In Fig. 2.10 we have presented the $\mathrm{MSD_{CM}}$ for a typical cluster. The motion here is diffusive, contrary to the Visek-like activity. This growth exponent is expected when the growth of clusters primarily happens via the diffusive deposition of particles. The latter is referred to as the Lifshitz–Slyozov (LS) mechanism [5, 55–57]. Note that the cluster displacements here are negligible. Thus, the diffusive coalescence mechanism is naturally discarded.
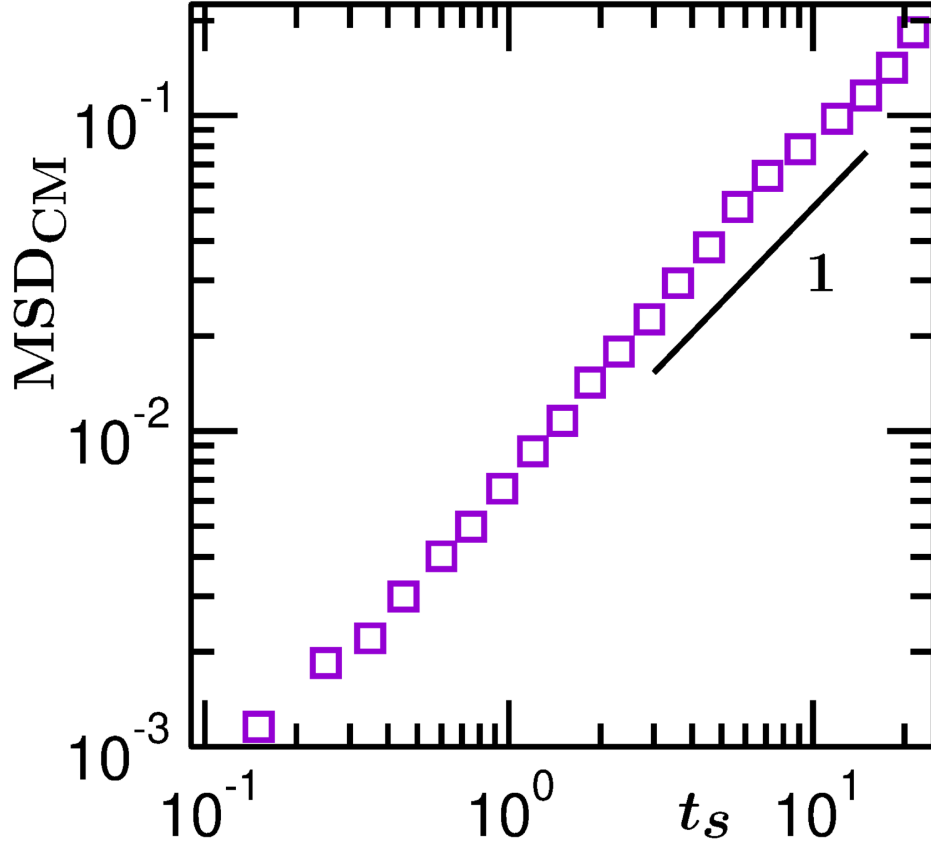
Figure 2.10: The time dependence of the mean-squared displacement (MSD_{CM}) of the center of mass of a cluster has been shown for $f_p = 1$. The presented data set is for an ABP system.

The average mass of the clusters is plotted versus the radius of gyration R_g in Fig. 2.11. The power-law dependence is valid in this case also and we have quantified the fractal dimensions of the clusters d_f for different values of f_p. With the increase of f_p the fractality decreases, i.e., d_f increases.

2.4   Conclusion

In this work we have carried out a study of the dynamics of cluster growth during vapor-'solid' phase-separation in two-dimensional systems containing Vicsek-like [34] and active Brownian particles [22–24, 40, 41]. We have worked at a very low temperature with an overall density close to the vapor branch of the coexistence curve. In such region of the parameter space, we observe disconnected fractal clusters. In the case of Vicsek
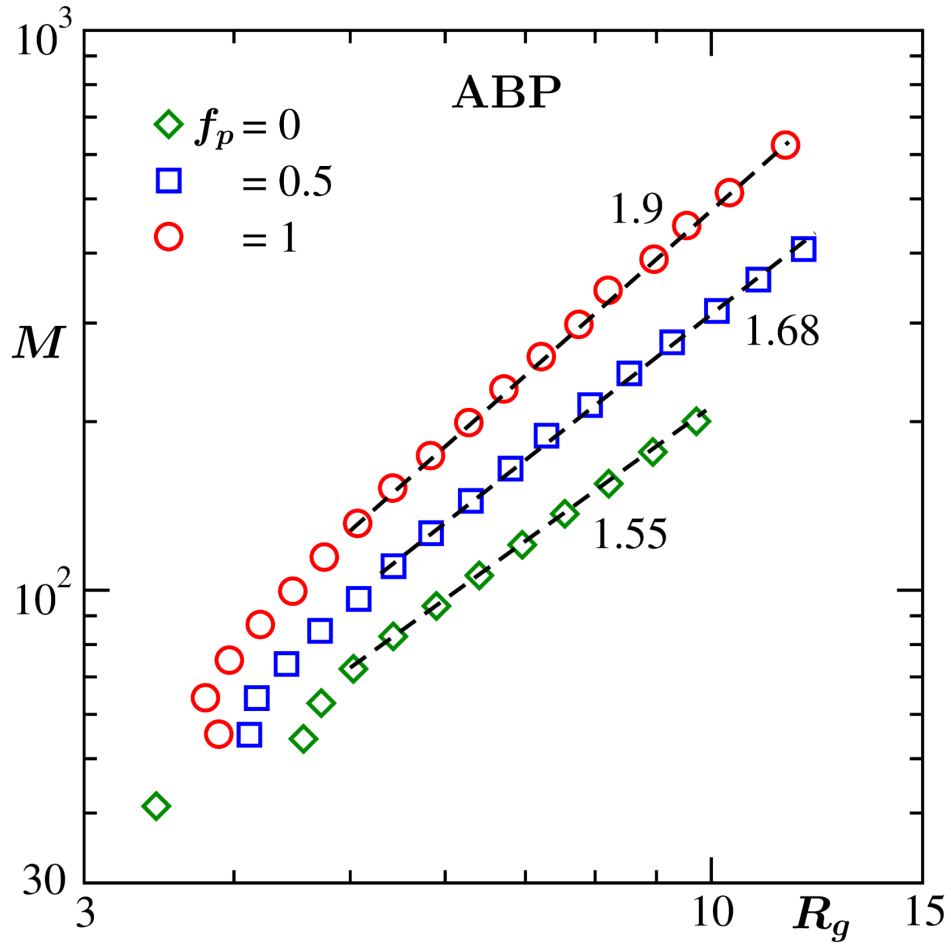
Figure 2.11: The variation of M, versus R_g, is plotted on a double-log scale, for a few f_p values. The dashed lines represent power-laws with different exponents. These results are for ABP systems.

activity, the growth of these clusters occurs via the ballistic aggregation mechanism. The growth exponent is rather high, viz., $\beta \approx 2$. This can be explained via a theory.

For active Brownian particles, the growth is much slower. In this case, the clusters appear to move diffusively. However, the exponent resembles that of Lifshitz-Slyozov [5] mechanism. With the increase in activity, the fractal dimension, in this case, shows a noticeable change towards the space dimension of the system.

Copyright and Permission

A part of the results in this chapter has been published in the article:

S. Paul, A. Bera, and S. K. Das, "How do clusters in phase-separating active matter systems grow? A study for Vicsek activity in systems undergoing vapor-solid transition", Soft Matter **17**, 645 (2021).

We reproduced these results with kind permission from the Royal Society of Chemistry. See the publication link below:

https://pubs.rsc.org/en/content/articlepdf/2021/sm/d0sm01762k

Bibliography

[1] A. Onuki, *Phase Transition Dynamics*, Cambridge University Press, Cambridge, England, 2002.

[2] K. Binder, in *Phase Transformation of Materials*, edited by R.W. Cahn, P. Haasen, and E.J. Kramer, VCH, Weinheim, 1991, p. 405, Vol. 5.

[3] A. J. Bray, Adv. Phys. **51**, 481 (2002).

[4] R. A. L. Jones, *Soft Condensed Matter*, Oxford University Press, Oxford, 2008.

[5] I. M. Lifshitz and V. V. Slyozov, J. Phys. Chem. Solids **19**, 35 (1961).

[6] K. Binder and D. Stauffer, Phys. Rev. Lett. **33**, 1006 (1974).

[7] K. Binder, Phys. Rev. B **15**, 4425 (1977).

[8] E. D. Siggia, Phys. Rev. A **20**, 595 (1979).

[9] H. Furukawa, Phys. Rev. A **31**, 1103 (1985).

[10] H. Furukawa, Phys. Rev. A **36**, 2288 (1987).

[11] S. Roy and S. K. Das, Phys. Rev. E **85**, 050602 (2012).

[12] S. Roy and S. K. Das, Soft Matter **9**, 4178 (2013).

[13] R. Shimizu and H. Tanaka, Nature Comm. **6**, 7407 (2015).

[14] J. Midya and S. K. Das, Phys. Rev. Lett. **118**, 165701 (2017).

[15] M. C. Marchetti, J. F. Joanny, S. Ramaswamy, T. B. Liverpool, J. Prost, M. Rao, and A. Simha, Rev. Mod. Phys. **85**, 1143 (2013).

[16] S. Ramaswamy, Annu. Rev. Condens. Matter Phys. **1**, 323 (2010).

[17] M. E. Cates and J. Tailleur, Annu. Rev. Condens. Matter Phys. **6**, 219 (2015).

[18] S. Mishra and S. Ramaswamy, Phys. Rev. Lett. **97**, 090602 (2006).

[19] J. M. Belmonte, G. L. Thomas, L. G. Brunnet, R. M. C. de Almeida, and H. Chaté, Phys. Rev. Lett. **100**, 248702 (2008).

[20] S. Mishra, A. Baskaran, and M. C. Marchetti, Phys. Rev. E **81**, 061916 (2010).

[21] M. E. Cates, D. Marrenduzzo, I. Pagonabarraga, and J. Tailleur, Proc. Natl. Acad. Sci. U.S.A. **107**, 11715 (2010).

[22] G. S. Redner, M. F. Hagan, and A. Baskaran, Phys. Rev. Lett. **110**, 055701(2013).

[23] G. S. Redner, A. Baskaran, and M. F. Hagan, Phys. Rev. E **88**, 012305 (2013).

[24] A. Wysocki, R. G. Winkler, and G. Gompper, Europhys. Lett. **105**, 48004 (2014).

[25] E. Méhes, E. Mones, V. Németh, and T. Vicsek, PLOS ONE **7**, e31711 (2012).

[26] F. Peruani and M. Bär, New J. Phys. **15**, 065009 (2013).

[27] S. Mishra, S. Puri, and S. Ramaswamy, Phil. Trans. R. Soc. A **372**, 20130364 (2014).

[28] P. Cremer and H. Löwen, Phys. Rev. E **89**, 022307 (2014).

[29] J. Schwarz-Linek, C. Valeriani, A. Cacciuto, M. E. Cates, D. Marenduzzu, A. N. Morozov, and W. C. K. Poon, Proc. Natl. Acad. Sci. U.S.A. **109**, 4052 (2012).

[30] J. Palacci, S. Sacanna, A. P. Steinberg, D. J. Pine, and P. M. Chaikin, Science **339**, 936 (2013).

[31] N. Kumar, H. Soni, S. Ramaswamy, and A. K. Sood, Nat. Commun. **5**, 4688 (2014).

[32] S. K. Das, S. A. Egorov, B. Trefz, P. Virnau, and K. Binder, Phys. Rev. Lett. **112**, 198301 (2014).

[33] B. Trefz, S. K. Das, S. A. Egorov, P. Virnau, and K. Binder, J. Chem. Phys. **144**, 144902 (2016).

[34] T. Vicsek, A. Czirôk, E. Ben-Jacob, I. Cohen, and O. Schochet, Phys. Rev. Lett. **75**, 1226 (1995).

[35] A. Czirôk and T. Vicsek, Phys. A **281**, 17 (2000).

[36] G. Baglietto, E. V. Albano, and J. Candia, Interface Focus **2**, 708 (2012).

[37] H. Chaté, F. Ginelli, G. Grégoire, F. Peruani, and F. Raynand, Eur. Phys. J. B **64**, 451 (2008).

[38] S. K. Das, J. Chem. Phys. **146**, 044902 (2017).

[39] S. Chakraborty and S.K. Das, J. Chem. Phys. **153**, 044905 (2020).

[40] L. Caprini, U. M. B. Marconi, and A. Puglisi, Phys. Rev. Lett. **124**, 078001 (2020).

[41] J. Stenhammer, D. Marenduzzo, R. J. Allen, and M. E. Cates, Soft Matter **10**, 1489 (2014).

[42] A. Callegari, G. Volpe, *Numerical Simulations of Active Brownian Particles*. In: F. Toschi, M. Sega (eds) *Flowing Matter. Soft and Biological Matter*, Springer, Cham. 2019.

[43] D. Loi, S. Mossa, and L.F. Cugliandolo, Soft Matter **7**, 10193 (2011).

[44] D. Frenkel and B. Smit, *Understanding Molecular Simulations: From Algorithm to Applications*, Academic Press, California, 2002.

[45] M. P. Allen and D. J. Tildesley, *Computer Simulations of Liquids*, Clarendon, Oxford, 1987.

[46] J.-P. Hansen and I. R. McDonald, *Theory of Simple Liquids*, Academic Press, London, 2008.

[47] E. Platen, Acta Numerica **8**, 197 (1999).

[48] W. Mickel, S. C. Kapfer, G. E. Schröder-Turk and K. Mecke, J. Chem. Phys. **138**, 044501 (2013).

[49] P. J. Steinhardt, D. R. Nelson and M. Ronchetti, Phys. Rev. B: Condens. Matter Mater. Phys. **28**, 784 (1983).

[50] B. Bhattacherjee and D. Chaudhuri, Soft Matter **15**, 8483 (2019).

[51] T. Vicsek, *Fractal Growth Phenomena*, World Scientific, Singapore, 1992.

[52] T. Vicsek, M. Shlesinger, and M. Matushita, editors, *Fractals in Natural Sciences*, World Scientific, Singapore, 1994.

[53] H. Goldstein, C.P. Poole, and J.F. Safko, *Classical Mechanics*, 3rd Ed., Addison-Wesley, 2001.

[54] S. K. Das, J. V. Sengers and M. E. Fisher, J. Chem. Phys. **127**, 144506 (2007).

[55] J. G. Amar, F. E. Sullivan, and R. D. Mountain, Phys. Rev. B **37**, 196 (1988).

[56] S. Majumder and S. K. Das, Phys. Rev. E **84**, 021110 (2011).

[57] D. A. Huse, Phys. Rev. B **34**, 7845 (1996).

[58] G.F. Carnevale, Y. Pomeau, and W.R. Young, Phys. Rev. Lett. **64**, 2913 (1990).

[59] E. Trizac and P.L. Krapivsky, Phys. Rev. Lett. **91**, 218302 (2003).

[60] E. Trizac and J.-P. Hansen, J. Stat. Phys. **82**, 1345 (1996).

[61] S. Paul and S. K. Das, Phys. Rev. E **96**, 012105 (2017).

[62] S. Paul and S. K. Das, Phys. Rev. E **97**, 032902 (2018).

Chapter 3

Dynamics of Velocity Ordering in Systems of Vicsek-like Active Particles

3.1   Introduction

Systems having self-propelling constituents appear rather common in nature, covering a wide range of scale [1–15]. Several active matter systems contain particles with dynamic alignment interactions [3–7]. There the movement of each particle tends to get strongly correlated with the average propulsion directions of particles within its neighborhood. Such systems can display interesting pattern formation in velocity fields. There exists different kinds of alignment interactions. One such aligning interaction was introduced in a model by Vicsek et. al. [4]. This has important implications in understanding phenomena associated with flocking of birds [16, 17] and other living entities [18, 19].

In the Vicsek model each particle tends to align its direction of motion with the average direction of its neighbors in a somewhat noisy environment. Interesting steady states, showing flocking of active particles, have been observed for low noise strength and high particle density in this model. Emergence of fascinating topological defects is rather common in these systems, like in magnetic systems [20–24], superconductors [25, 26] and liquid crystals [27, 28]. In this work we will explore these while studying the dynamics of velocity ordering in a Vicsek-like aligning active matter system.

To understand the morphology in typical phase-ordering systems one calculates the equal-time density-density correlation function [29, 30]

$$C_{\rho\rho}(r = |\vec{r}|, t) = \langle \rho(\vec{r}, t)\rho(0, t)\rangle - \langle \rho(\vec{r}, t)\rangle \langle \rho(0, t)\rangle. \qquad (3.1)$$

Here $\rho(\vec{r}, t)$ is local density at position $\vec{r}$ and time t, while $\langle ... \rangle$ represents statistical averaging. Similarly, one can calculate the correlation function, $C_{vv}(r, t)$, for the velocity fields of particles in the system. This can be defined as [29–31]

$$C_{vv}(r, t) = \langle \vec{v}(\vec{r}, t) \cdot \vec{v}(\vec{0}, t)\rangle - \langle \vec{v}(\vec{r}, t)\rangle \cdot \langle \vec{v}(\vec{0}, t)\rangle. \qquad (3.2)$$

If there exists growth in the velocity field there will be slower decay of $C_{vv}(r, t)$, as a function of interparticle distance r, with the progress of time t. The characteristic length scale, ℓ_v, associated with the growth in velocity ordering, may increase with time in power-law fashion, i.e.,

$$\ell_v = t^{\alpha_v}. \qquad (3.3)$$

For self-similar growth one can obtain the scaling of $C_{vv}(r, t)$ as

$$C_{vv}(r, t) \equiv \tilde{C}_{vv}(r/\ell_v(t)). \qquad (3.4)$$

Analytical forms of this scaling function for the correlations of vector order parameter are obtained in earlier studies [32, 33], in connection with ferromagnetic ordering. The Bray-Puri-Toyoki analytical function [32, 33], derived being aided by certain integral representation of the n-component vector field ($\vec{\phi}$), is given by

$$C_{\vec{\phi}}(r, t) = \frac{n\gamma}{2\pi}\left[\mathbf{B}\left(\frac{n+1}{2}, \frac{1}{2}\right)\right]^2 \mathbf{F}\left(\frac{1}{2}, \frac{1}{2}; \frac{n+2}{2}; \gamma^2\right), \qquad (3.5)$$

where $\mathbf{B}(x, y)$ $\left[=\Gamma(x)\Gamma(y)/\Gamma(x + y)\right]$ is the beta function [$\Gamma(a)$: gamma function], $\mathbf{F}(a, b; c; z^2)$ is a hypergeometric function and γ is related to the characteristic length scale $\ell(t)$ as $\gamma = \exp\{-r^2/2\ell(t)^2\}$. For scalar order parameter ($n = 1$), this leads to the Ohta-Jasnow-Kawasaki (OJK) functional form, i.e., $C(r, t) = \frac{2}{\pi}\sin^{-1}\gamma$. The correlation of phases in two component systems, e.g., in XY model and Kuramoto model, exhibits scaling behavior that may follow the BPT form [34]. For non-conserved Ising model during evolution from para-magnetic to ferromagnetic phase, the correlation function satisfying this OJK form [35].

In this work we have studied the dynamics of velocity ordering primarily in a high density system of aligning active particles in space dimension $d = 2$.

3.2   Model and Methods

The passive and active interactions are the same as in the previous chapter. We consider a two dimensional ($d = 2$) square box with periodic boundary condition (PBC) having side L. The number density of particles in the system is calculated as $\rho = N/L^2$. While we present results for multiple values of ρ, primarily we have studied the kinetics of velocity ordering for a dense system with $\rho = 1$. All our results will be presented for $L = 512$, unless otherwise mentioned. The initial arrangements of particle positions and velocities have been taken to be random, with velocities obeying the Maxwell-Boltzmann distribution at high temperatures. The evolution dynamics of ordering in velocity fields has been investigated after quenching such configurations to a final temperature $T = 0.25$, unless otherwise mentioned. Final quantitative results are presented after averaging over runs with 50 independent initial configurations.

3.3   Results

We will show first the evolution of the system with density $\rho = 0.3$ for both density and velocity fields. Then we will investigate a high density case with $\rho = 1$. We will also present results from a phase-ordering passive system, viz., XY model in $d = 2$, that has connection with planar ferromagnet.

In Fig. 3.1 we have shown evolution snapshots of the systems for particle density $\rho = 0.3$, for $f_A = 0$ and 10, the former corresponding to the passive case. In both cases, phase separation is clearly visible in the density field. The growth is significantly faster in the active case. The coarsening in density field and related aging dynamics in this case have been studied in earlier works [36, 37]. The aspects of dynamics of velocity ordering, however, generally remained less explored.

We calculate the phase angle (θ_i) of velocity field as $\theta_i = \tan^{-1}(v_{i,y}/v_{i,x})$, where $v_{i,x}$ and $v_{i,y}$ are the two Cartesian components of velocity $\vec{v}_i$ of the ith particle. In Fig. 3.2(a) we have shown the velocities of particles for $f_A = 10$ at $t = 10$ by representing the phase angles, lying in the range $[-\pi : \pi]$, in different colors. In Fig. 3.2(b) we show the velocity directions inside a small portion [that is shown in a square box in 3.2(a)] of the full
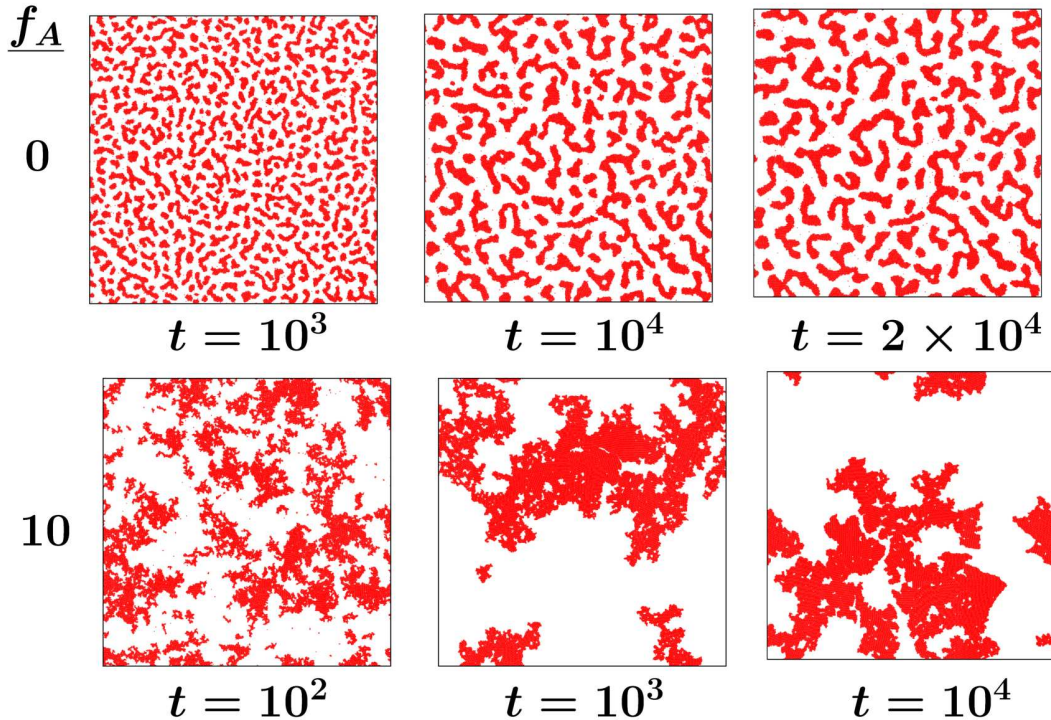
Figure 3.1: Demonstration of phase separation in the active matter system for $\rho = 0.3$ and $T = 0.25$, for two different alignment strengths f_A, viz., 0 and 10. In each of the cases evolution snapshots from a few different times have been shown for $L = 512$. The dots mark the location of particles. As stated, $f_A = 0$ corresponds to the passive case.

system, where we see a circulation of particles around a defect core. This indicates the existence of vortex-like topological defects in the system.

As there exist many void regions in the system for this considered "low" overall density, the identification of defects becomes technically difficult. That is why in the following we have considered a system with much higher density ($\rho = 1$). Recall that our interest is in quantifying the dynamics of ordering of the velocity field.

In Fig. 3.3 we show the evolution of the velocity phases of particles for different activity strength f_A. We observe that there is no ordering in the velocity field without any alignment strength. With the increase of f_A the ordering gets more prominent.

To estimate the degree of ordering in the system we calculate the magnitude of normalized average velocity,

$$V_a = \left| \frac{1}{N} \sum_{i=1}^{N} \frac{\vec{v}_i}{|\vec{v}_i|} \right|, \tag{3.6}$$

which is the typical Vicsek order parameter [4]. In Fig. 3.4 we show the variation of V_a with time for few values of f_A. We observe different saturation values of V_a for different
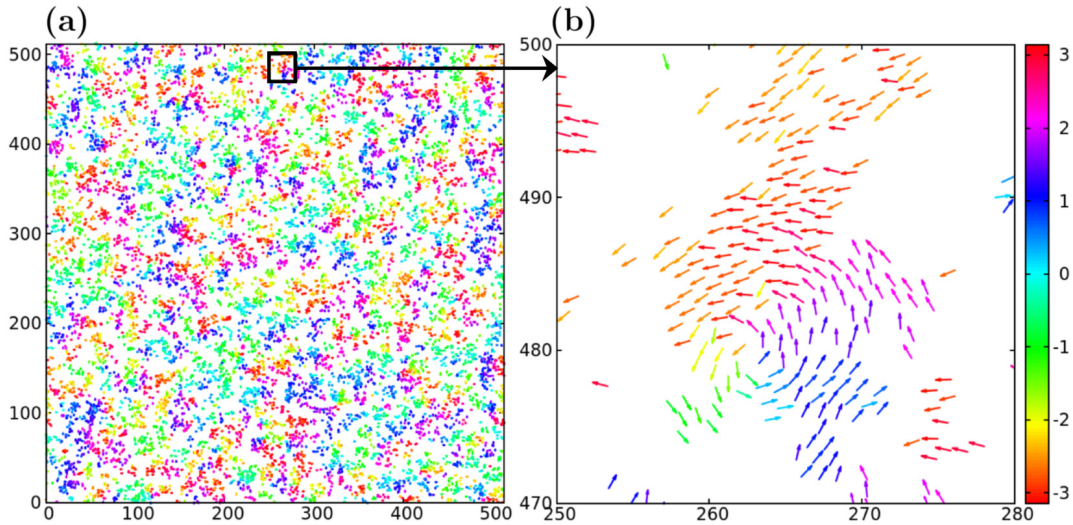
Figure 3.2: (a) The velocity directions of particles of a system with $\rho = 0.3$ and $f_A = 10$ at time $t = 10$. Here different values of θ_i are shown in different colors. The color coding is illustrated at the rightmost part of the figure. (b) An enlarged view of the box shown in (a). Here velocity directions are shown by arrowheaded lines. Color coding is same as in part (a).

f_A. This indicates that the degree of parallelization in velocity field is controlled by the activity strength.

We will investigate such ordering in velocity fields. For this we will look for the topological defects in velocity fields. The topological charge around a defect core is defined as [29, 30]

$$n = \frac{1}{2\pi} \oint \vec{\nabla}\theta \cdot \vec{d\ell}, \tag{3.7}$$

where θ is the continuous phase angle corresponding to the velocity field and the integral is carried over the closed path around the defect core. The topological charge $n = +1$ corresponds to a vortex and $n = -1$ corresponds to an anti-vortex with unit charge. The average length under a defect is defined as [29, 30]

$$\ell_v = \frac{L}{\sqrt{N_d}}, \tag{3.8}$$

where N_d is the total number of defects and L is the system size.

In Fig. 3.5(a) we present the phase angle (θ_i), similar to Fig. 3.3, but for a part of the simulation box, for $f_A = 10$, at $t = 5$. In Fig. 3.5(b) we have shown the velocity directions for the same part. The corresponding color plot of $\sin^2(2\theta_i)$ is shown in Fig. 3.5(c), that has an altered range $[0, 1]$. For all of the cases, the locations of vortices and
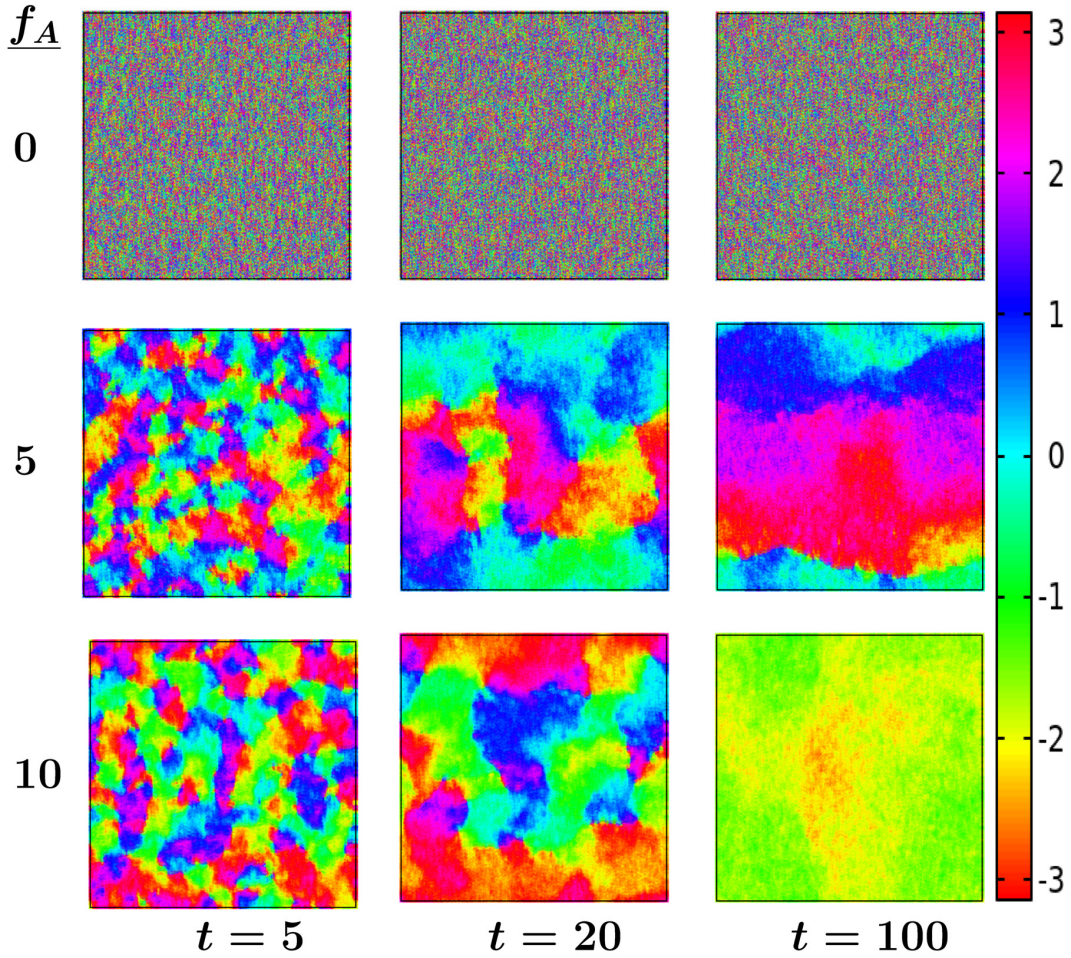
Figure 3.3: The phase angles, θ_i ($\in [-\pi : \pi]$), for the velocities of the particles are shown during evolutions of the systems with different values of the alignment strength f_A.

anti-vortices are shown by filled and void circles, respectively. Vortices and anti-vortices can be found on the meeting points of different colored regions in phase-angle plot (see Fig. 3.5(a)). On the other hand, these topological defects are positioned at the merging points of same colored branches when the system is presented in Schlieren patterns [23, 34] with color intensity corresponding to $\sin^2(2\theta_i)$, as shown in Fig. 3.5(c).

This vortex-antivortex structure formation resembles phase-ordering in typical passive systems, e.g., in XY model in $d = 2$. Here we discuss this case briefly. In this model evolution also there exist similar topological defects in the system and the synchronization in phases occurs via the annihilation of defect and anti-defect pairs below certain
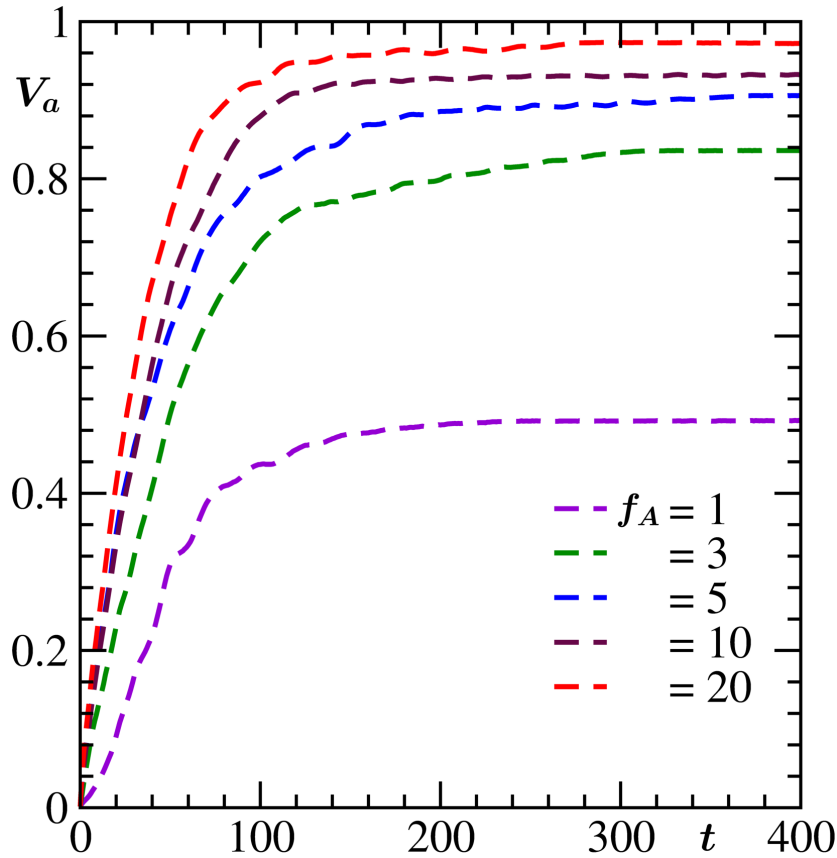
Figure 3.4: The order parameter V_a, versus time (t), for different f_A values are shown.

temperature. The Hamiltonian for XY model is written as [20, 21]

$$H = -J \sum_{<ij>} \vec{S}_i \cdot \vec{S}_j = -J \sum_{<ij>} \cos(\theta_i - \theta_j), \tag{3.9}$$

where one has $J > 0$ and the sum is carried over the nearest neighbors only. $\vec{S}_i$ (= $\cos\theta_i, \sin\theta_i$) is a spin variable, that is represented by a unit vector in $d = 2$ and can rotate by 2π in XY-plane. This model undergoes the Berezinskii–Kosterlitz–Thouless (BKT) transition from bound vortex-antivortex pairs at low temperatures to unpaired vortices and anti-vortices at the temperature $T_{BKT} \approx 0.89 J/k_B$ [22, 24]. This model does not exhibit second order phase transition in $d = 2$ and the synchronized phases of the spins are open to transverse fluctuations. Below T_{BKT} the spin-spin correlations decay in power-law manner with a temperature dependent exponent.

In Fig. 3.6 we have shown the phase evolution of the XY-model at $T = 0.4 J/k_B$ from a random initial orientations of the spins. In Fig. 3.7(a) we show an enlarged portion of the system at $t = 100$. Corresponding vector field of the spins is shown in Fig. 3.7(b).
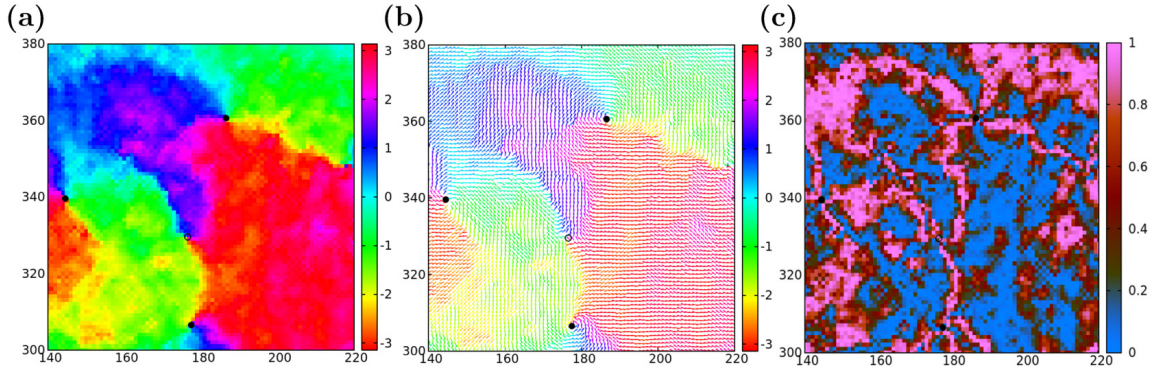
Figure 3.5: (a) Phase angles (θ_i) for a part of 512×512 system are shown. (b) The normalized velocity fields corresponding to the picture shown in (a) have been plotted. (c) Same as (a) but the color intensity here is arranged according to $\sin^2(2\theta_i)$, like in Schlieren patterns. The vortices and anti-vortices are marked in black filled and empty circles, respectively. These snapshots are for $f_A = 10$ at $t = 5$.

$$t = 10^2 \qquad t = 10^3 \qquad t = 10^4$$
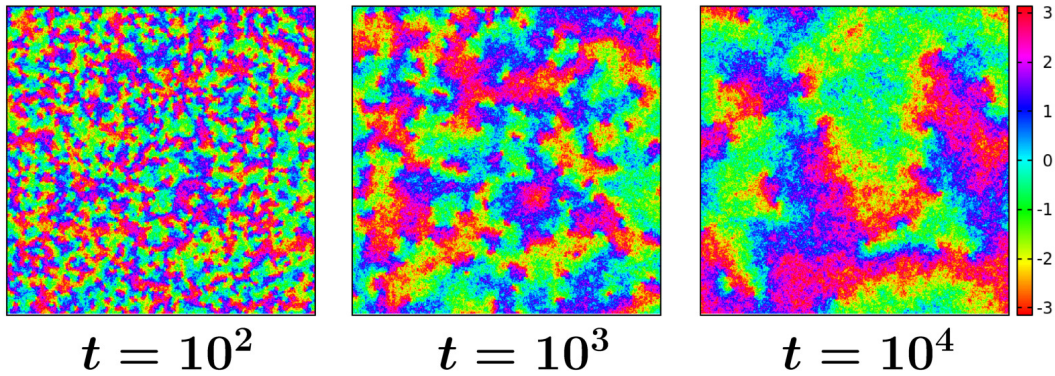
Figure 3.6: Phase evolution in XY model starting from random initial directions after quench to $T = 0.4$. The phase angles are plotted with the progress of time for $L = 512$.

The vortices and anti-vortices are marked in both of the cases. Next we return to the active matter case.

In Fig. 3.8 we show the growth of average characteristic length, ℓ_v, versus time, for different f_A. Here we observe the enhancement of growth with the increase in f_A. Also, for each value of f_A, it appears that there exists crossover from an early time slower growth to a late time faster evolution.

We have further calculated the velocity-velocity correlation function. In Fig. 3.9(a) we have shown $C_{vv}(r,t)$, versus r, from different times for $f_A = 10$. The slower decay of correlation functions with the increase of time indicates the growth of characteristic length for the velocity field with time. In Fig. 3.9(b) we have shown the scaling of $C_{vv}(r,t)$ with r/ℓ_v. Here the length ℓ_v is calculated from the drop of $C_{vv}(r,t)$ to a certain
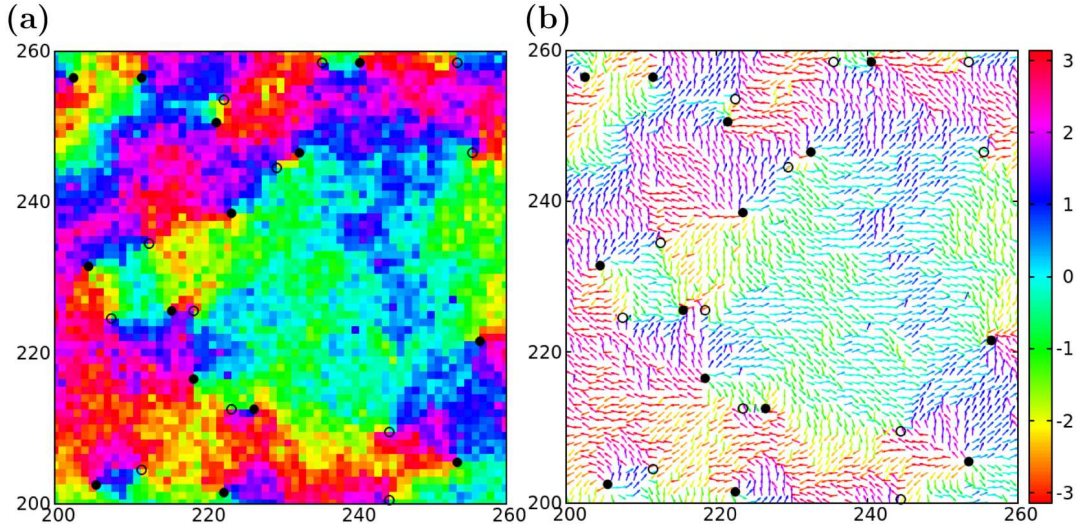
Figure 3.7: (a) Same as 3.6 but here only a portion of the XY model system is shown at $t = 100$. (b) Vector fields corresponding to the picture in (a) are shown. The locations of vortices and anti-vortices are shown in filled and empty circles, respectively.

value, viz., 0.1, i.e., $C_{vv}(r = \ell_v, t) = 0.1$. It appears that the BPT function describes the decay of $C(r, t)$ reasonably well. However, the initial jump needs to be understood. This may be the temperature effect. However, further investigation is necessary. While comparing with the BPT function, the latter has been normalized in such a way that matching is obtained only in the post-jump part. It is possible that over the period of evolution various synchronization models get arrested in phase locked state. The system is said to be phase locked if

$$\lim_{t \to \infty} |\theta_i(t) - \theta_j(t)| = K, \quad \text{for } i \neq j. \tag{3.10}$$

where K is a constant. For complete ordering/perfect synchronized phases $K = 0$. We calculate an average phase difference in velocity field of the particles during the evolution as [34]

$$C_\theta = \left\langle \sqrt{\frac{2}{N(N-1)} \sum_{<ij>} (\Delta \theta_{ij})^2} \right\rangle, \tag{3.11}$$

where the sum is carried over all the particle pairs and $\langle ... \rangle$ represents the statistical average. Here $\Delta \theta_{ij}$ $(= |\theta_i - \theta_j|)$ is the absolute value of minimum phase difference between particle i and j, i.e., $\Delta \theta_{ij} \in [0, \pi]$. In Fig. 3.10 we have shown the decay of C_θ with time for different f_A. The different saturation values at late time indicate different velocity order in the system. From this decay of C_θ, we can estimate the time to reach
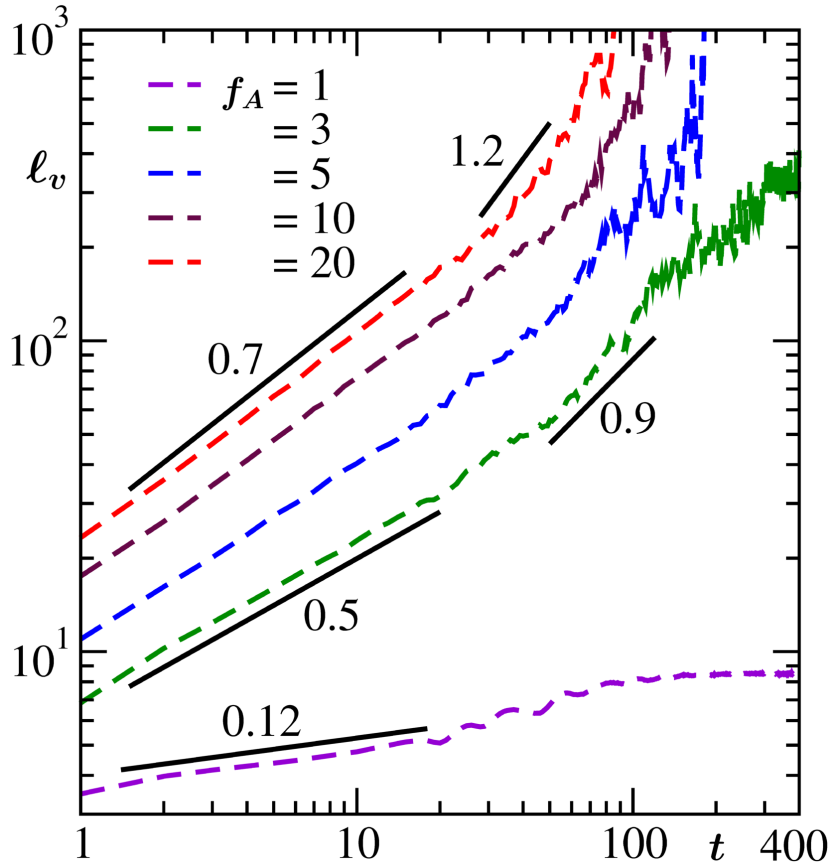
Figure 3.8: Plots of ℓ_v versus time for different f_A. The solid lines represent power-laws with different exponents.

phase locked state. The decay of C_θ is faster for higher f_A value. This phase locking is related to lack of perfect long range order due to competition between thermal noise and aligning interaction. In any case, these results are analogous to those of the growth of global order parameter V_a with time in Fig. 3.2. However, such plots can provide additional information in special situations, e.g., when there is band formation in Vicsek model.

We have also investigated these ordering dynamics for different temperatures. The evolution of V_a with time for different T and two f_A values are shown in Fig. 3.11(a). Here we observe clear thermal effect for lower f_A, but for higher f_A when alignment force dominates over thermal fluctuations there exists minor difference in global ordering. The average defect length ℓ_v is shown versus time for different T and f_A in Fig. 3.11(b). Effects are analogous to these in Fig. 3.11(a).
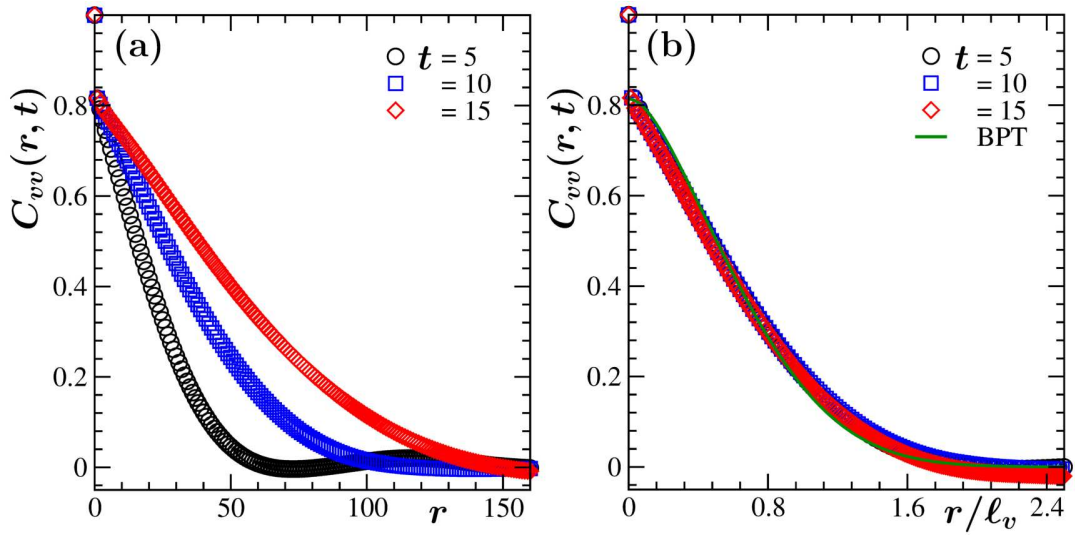
Figure 3.9: (a) $C_{vv}(r, t)$ have been plotted versus r, from different times (t), for $f_A = 10$. (b) The scaling of $C_{vv}(r, t)$, versus r/ℓ_v, is demonstrated. The solid line represents the BPT function.
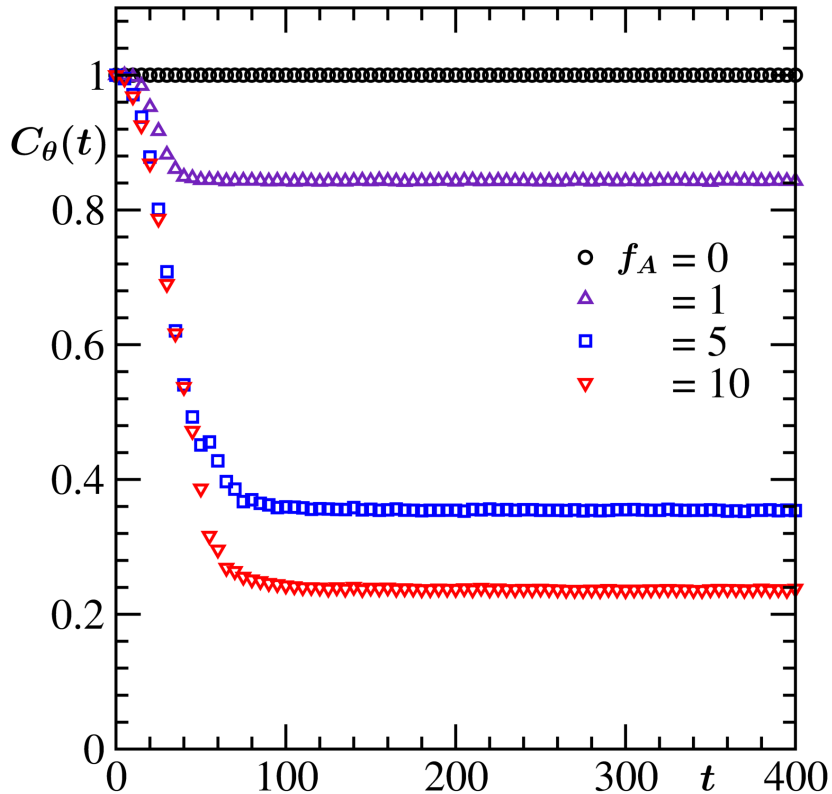
Figure 3.10: $C_\theta(t)$ have been shown versus t for different f_A. We have divided $C_\theta(t)$ by $C_\theta(t = 0)$, so that the decay starts from unity. These data are presented for $L = 256$.
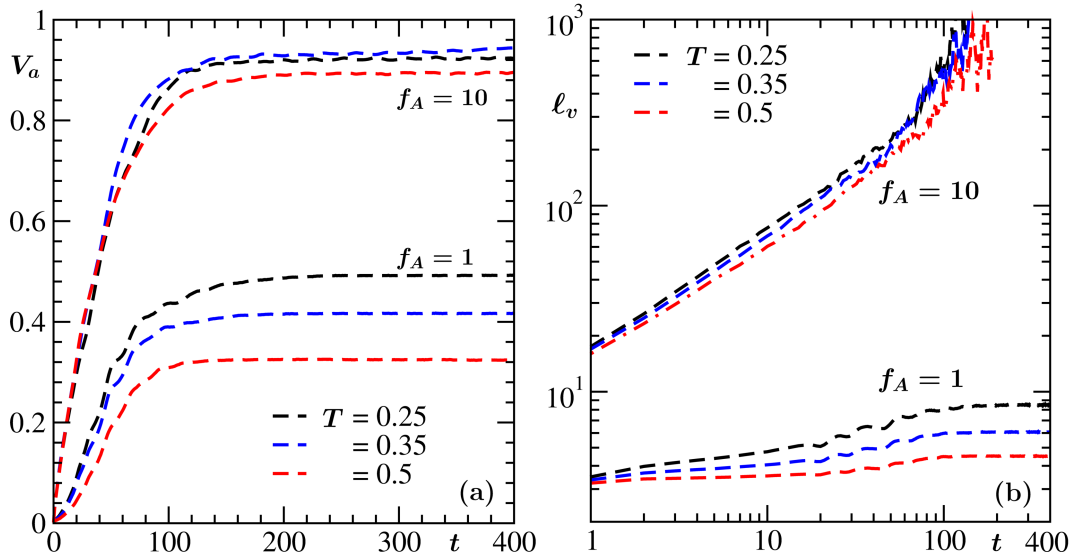
Figure 3.11: (a) V_a versus t plots are shown for different temperatures T for two values of f_A. (b) Here ℓ_v is plotted versus t for different T, for $f_A = 1$ and 10, as mentioned in the graph.

3.4   Conclusion

We have studied the dynamics of coarsening in velocity field in a system of disk-like active particles with local alignment interaction in space dimension $d = 2$. There exist Vicsek-like alignment interactions among the particles as well as passive interparticle interactions modeled by Lennard-Jones potential. We performed Molecular dynamics simulations, with Langevin thermostat, for high density of particles. We have presented results on the dynamics of velocity ordering for different alignment strengths and temperatures. These results are discussed in the background of those from the XY model.

We have directly observed there that the ordering in the velocity field occurs with the annihilation of vortex and anti-vortex pairs, i.e., the reduction in the number of defect cores in the system. With the increase of f_A at a given temperature the growth becomes faster. It follows power-law time dependence. The exponent seems to increase with the rise in alignment strength.

There exists scaling in the velocity-velocity correlation function. This scaling form is reasonably well described by the Bray-Puri-Toyoki analytical function. This issue requires more detailed investigation though. In future we would also like to arrive at more accurate conclusion on the growth dynamics.

Bibliography

[1] M. C. Marchetti, J. F. Joanny, S. Ramaswamy, T. B. Liverpool, J. Prost, M. Rao, and R. A. Simha, Rev. Mod. Phys. **85**, 1143 (2013).

[2] S. Ramaswamy, Annu. Rev. Condens. Matter Phys. **1**, 323 (2010).

[3] G. Grégoire and H. Chaté, Phys. Rev. Lett. **92**, 025702 (2004).

[4] T. Vicsek, A. Czirôk, E. Ben-Jacob, I. Cohen, and O. Schochet, Phys. Rev. Lett. **75**, 1226 (1995).

[5] T. Vicsek and A. Zafeiris, Phys. Rep. **517**, 71 (2012).

[6] S. K. Das, J. Chem. Phys. **146**, 044902 (2017).

[7] J. Toner and Y. Tu, Phys. Rev. Lett. **75**, 4326 (1995).

[8] J. Elgeti, R. G. Winkler, and G. Gompper, Rep. Prog. Phys. **78**, 056601 (2015).

[9] J. Stenhammar, D. Marenduzzo, R. J. Allen, and M. E. Cates, Soft Matter **10**, 1489 (2014).

[10] J. Bialké, T. Speck, and H. Löwen, Phys. Rev. Lett. **108**, 168301 (2012).

[11] Y. Fily and M. C. Marchetti, Phys. Rev. Lett. **108**, 235702 (2012).

[12] M. E. Cates and J. Tailleur, Annu. Rev. Condens. Matter Phys. **6**, 219 (2015).

[13] P. Digregorio, D. Levis, A. Suma, L. F. Cugliandolo, G. Gonnella, and I. Pagonabarraga, Phys. Rev. Lett. **121**, 098003 (2018).

[14] C. B. Caporusso, P. Digregorio, D. Levis, L. F. Cugliandolo, and G. Gonnella, **125**, 178004 (2020).

[15] L. Caprini, U. Marini Bettolo Marconi, and A. Puglisi, Phys. Rev. Lett. **124**, 078001 (2020).

[16] M. Ballerini, N. Cabibbo, R. Candelier, A. Cavagna, E. Cisbani, I. Giardina, V. Lecomte, A. Orlandi, G. Parisi, A. Procaccini, M. Viale, and V. Zdravkovic, Proc. Natl. Acad. Sci. U. S. A. **105**, 1232 (2008).

[17] M. Nagy, Z. Ákos, D. Biro, and T. Vicsek, Nature **464**, 890 (2010).

[18] O. Feinerman, I. Pinkoviezky, A. Gelblum, E. Fonio, and N. S. Gov, Nature Physics **14**, 683 (2018).

[19] C. Dombrowski, L. Cisneros, S. Chatkaew, R. E. Goldstein, and J. O. Kessler, Phys. Rev. Lett. **93**, 098103 (2004).

[20] J. M. Kosterlitz and D. J. Thouless, J. Phys. C: Solid State Phys. **6**, 1181 (1973).

[21] J. M. Kosterlitz, J. Phys. C: Solid State Phys. **7**, 1046 (1974).

[22] R. Gupta, J. DeLapp, G. G. Batrouni, G. C. Fox, C. F. Baillie, and J. Apostolakis, Phys. Rev. Lett. **61**, 1996 (1988).

[23] B. Yurke, A. N. Pargellis, T. Kovacs, and D. A. Huse, Phys. Rev. E **47**, 1525 (1993).

[24] M. Hasenbusch, J. Phys. A **38**, 5869 (2005).

[25] B. I. Halperin and D. R. Nelson, J. Low Temp. Phys. **36**, 599 (1979).

[26] B. Chen, W. P. Halperin, P. Guptasarma, D. G. Hinks, V. F. Mitrović, A. P. Reyes, and P. L. Kuhns, Nat. Phys. **3**, 239 (2007).

[27] S. Shankar and M. Cristina Marchetti, Phys. Rev. X **9**, 041047 (2019).

[28] N. Kumar, R. Zhang, J. J. de Pablo, and M. L. Gardel, Sci. Adv. **4**, 7779 (2018).

[29] A. J. Bray, Adv. Phys. **43**, 357 (1994).

[30] *Kinetics of Phase Transitions*, edited by S. Puri and V. Wadhawan (CRC, Boca Raton, FL, 2009).

[31] S. Paul and S. K. Das, Europhys. Lett. **108**, 66001 (2014).

[32] A.J. Bray and S. Puri, Phys. Rev. Lett. **67**, 2670 (1991).

[33] H. Toyoki, Mod. Phys. Lett. B **7**, 397 (1993).

[34] D. Levis, I. Pagonabarraga, and A. Díaz-Guilera, Phys. Rev. X **7**, 011028 (2017).

[35] N. Vadakkayil, S. Chakraborty, and S. K. Das, J. Chem. Phys. **150**, 054702 (2019).

[36] S. Chakraborty and S. K. Das, J. Chem. Phys. **153**, 044905 (2020).

[37] S. Paul, A. Bera, S. K. Das, Soft Matter **17**, 645 (2021).

Chapter 4

Dynamics of Clustering in Systems of Active Particles in Explicit Solvent

4.1 Introduction

The phenomena of clustering is observed in natural active matter systems in a wide range of scale [1–7], e.g., colony of bacteria, school of fish, flock of birds, etc. Like in passive systems where the clustering and coarsening phenomena have been well studied [8–23], there exists studies related to the statics and dynamics in such phase-separating active matters also [1–7, 24–35]. A recent interest in these domain of active matters is in developing meaningful methodologies to understand the dynamics of clustering [3, 4, 6, 7]. Associated interest in the branch of statistical mechanics is also in quantifying the universality in the context of critical and coarsening phenomena [24–34].

In passive systems it is well established that hydrodynamics plays an important role in both equilibrium [12] and nonequilibrium [9, 15, 18, 21, 23] dynamics. In the presence of hydrodynamic interaction, the progress of phase separation, following a quench of a homogeneous system inside the coexistence region, occurs much faster. Such effects may be expected in the active case also. The understanding of these requires simulation techniques that can take well care of hydrodynamic conservations in computers, while dealing with large numbers of active particles and an adequately high density of solvent. In this chapter we consider a collection of Vicsek-like [5, 36] active particles immersed in an explicit solvent. The overall dynamics is carried out via an advanced combination of multi-particle collision dynamics (MPCD) [37] and molecular dynamics (MD) [38, 39] techniques. To the best of our knowledge, phase separation models having explicit solvent are very limited even for passive systems [40–44], leaving aside the implementation of

an advanced hydrodynamic method for studying large scale phenomena exhibited by active microswimmers [45, 46, 44, 47, 48]. Our study fills this crucial gap, in addition to obtaining important simulation results and explaining these via an appropriate theoretical picture.

In passive fluids, the influence of hydrodynamics on the evolution or growth rate, during phase separation, depends on the overall density or composition of particles [9, 15, 17–23]. For low overall density, say, in a vapor-liquid transition, the evolving morphology consists of clusters (of particles) that are disconnected from each other [20–22]. The growth of such a morphology is expected to occur via coalescence of the clusters [15, 16, 18, 21, 49]. Here, we investigate the structure and dynamics in such a region of the phase diagram, for active as well as passive systems, the emphasis being on the former. We observe that the method leads to appropriate hydrodynamic mechanisms. In the passive case this provides growth via the diffusive coalescence (DC) mechanism which is in good quantitative agreement with a picture proposed by Binder and Stauffer [15]. When the activity is turned on we show that the growth occurs via the ballistic aggregation (BA) mechanism [49–55]. The emerging growth law has been quantified and explained via an appropriate theoretical consideration [50].

During phase separation, the average mass, M, of domains or clusters typically evolves [9] with time (t) as $M \sim t^\beta$. For a disconnected morphology, in the presence of hydrodynamics, one expects $\beta = 1$ for DC of clusters [15, 17, 18, 21]. The expectation is different for BA [50–55]. For the latter, the value of β should be 1.2 in space dimension $d = 3$ [50–56] that may, however, change when the velocities of the clusters are correlated [49, 50]. For $\beta = 1.2$, the root-mean-squared velocity, v_{rms}, behaves [50, 56, 57] as $v_{\mathrm{rms}} \sim M^z$, with $z = -1/2$. However, z may deviate from $z = -1/2$, leading to different values of β. E.g., the latter can be rather large, for $z = 0$. In this chapter, unlike in chapter 2, we do not consider the fractal features of the clusters. The reason will be become clear later.

4.2   Model and Methods

In our model N_a active particles, each of mass m_a and diameter σ, are immersed in a solvent consisting of N_s point-like particles, each having mass m_s. The overlap-preventing interaction between two active particles, a distance r apart, is implemented, like in the

previous chapters, via versions of the Lennard-Jones potential [39]:

$$U(r) = 4\epsilon\left[\left(\frac{\sigma}{r}\right)^{12} - \left(\frac{\sigma}{r}\right)^{6}\right], \tag{4.1}$$

with σ, ϵ being, respectively, the particle diameter and interaction strength. We have considered two different passive potentials to study the clustering dynamics.

(I) Primarily we have used a cut-off radius $r_c = 2.5\sigma$, and a force correction term so that the modified potential reads

$$u(r) = U(r) - U(r_c) - (r - r_c)\left(\frac{dU}{dr}\right)_{r=r_c}, \quad r < r_c. \tag{4.2}$$

This has an attractive tail and will be referred to as the passive attractive (PA) model.

(II) For a limited set of results, we have also considered the Weeks-Chandler-Andersen (WCA) potential [58], given by

$$u(r) = U(r) + \epsilon, \quad r < 2^{\frac{1}{6}}\sigma. \tag{4.3}$$

This will be referred to as the passive repulsive (PR) potential.

The interaction between the active and solvent particles is incorporated via the WCA potential [58]:

$$u_s(r) = 4\epsilon\left[\left(\frac{\sigma}{2r}\right)^{12} - \left(\frac{\sigma}{2r}\right)^{6} + \frac{1}{4}\right], \quad r < 2^{\frac{1}{6}}(\sigma/2). \tag{4.4}$$

Here the factor $1/2$ modifies the interaction diameter to $\sigma/2$ in this case.

The self-propulsion is achieved via the Vicsek interaction [5, 28], like in the previous chapters, i.e., an active particle i experiences a dynamic force $\mathbf{f}_i = f_A\hat{n}$, due to its neighbors, implemented in such a way that only its direction of motion is changed. Here, $\hat{n}$ ($= \sum_j \mathbf{v}_j/|\sum_j \mathbf{v}_j|$, $\mathbf{v}_j$ being the velocity of particle j that falls within the neighborhood defined by the distance r_c from particle i) is the mean direction of motion of neighbors and f_A is the strength of the active force. Please see Fig. 4.1 for a schematic demonstration of the implementation of the activity.

In our mesoscopic description, the interactions among the solvent particles are incorporated by the MPCD technique [37, 59], while the rest are through MD. In the hybrid MD-MPCD simulations, the positions and velocities of all the particles are updated via the velocity Verlet algorithm [38] with a time step Δt. The multi-particle collisions
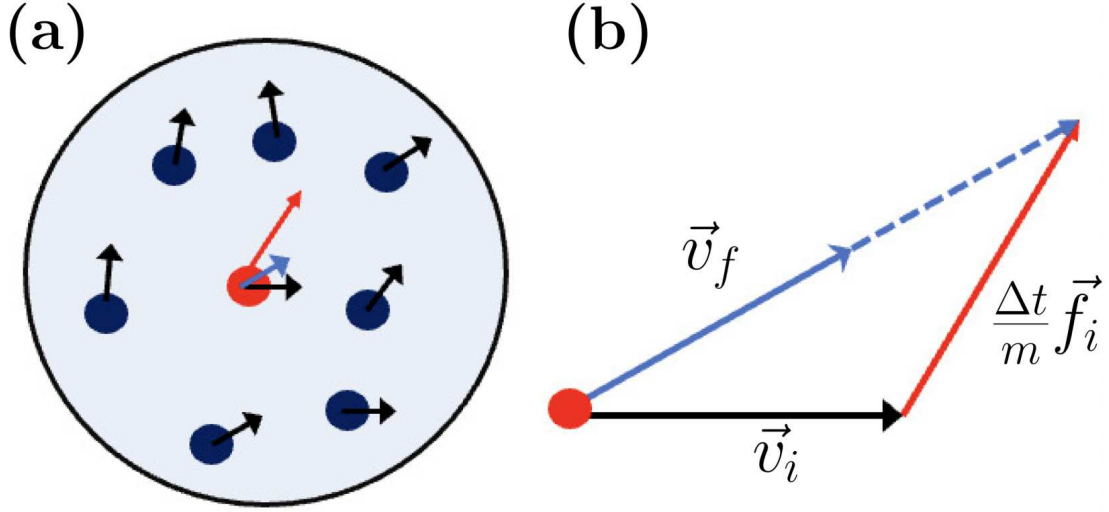
Figure 4.1: (a) Directions of particles within a neighborhood are schematically shown. (b) A diagram that shows the rotation of a velocity vector ($\vec{v}_i$) to the final velocity $\vec{v}_f$ due to the application of the alignment force $\vec{f}_i$. The continuous part in the sketch of $\vec{v}_f$ shows only the directional change due to the active force.

in the solvent are performed periodically via the exchange of momentum among particles within a cubic cell of side σ, at time intervals τ. This is achieved via rotations of the relative velocity $\delta\mathbf{v}$ of the kth solvent particle ($\mathbf{v}_{s,k}$) with respect to the velocity of the centre of mass of the corresponding cell ($\mathbf{v}_{s,cm}$), about a randomly selected axis, by an angle γ:

$$\mathbf{v}_{s,k} = \mathbf{v}_{s,cm} + \mathbf{R}(\gamma)\delta\mathbf{v} \tag{4.5}$$

Here $\mathbf{R}$ is a rotation matrix. Application of this satisfies the hydrodynamic requirements, i.e., the conservations of mass, momentum and energy. A random grid shifting is implemented in every collision step to restore the Galilean invariance in the small mean free path limit ($\lambda < \sigma$) [37, 59, 60].

We choose $m_a = 8m_s$, set by considering certain solvent density equivalence. The quenched temperature of the system is $T = 0.6\epsilon/k_B$ (k_B being the Boltzmann constant), unless otherwise mentioned. This falls well inside the miscibility gap. We set ρ_s, the solvent number density, at $10/\sigma^3$ and ρ_a, the active particle density, at $0.05/\sigma^3$. Furthermore, we have $\Delta t = 0.005t_0$ ($t_0 = \sqrt{\sigma^2 m_s/\epsilon}$), $\tau = 0.05t_0$ and $\gamma = 130°$. The above chosen [61] values of various parameters ensure the fluidic behavior of the solvent, with Reynolds number $Re < 1$ and Schmidt number $Sc \sim 10^2$. For convenience, we fix m_s, σ, ϵ and k_B to unity. All quantitative results correspond to averaging over more

than 80 independent initial realizations. The simulations for the PA active cases with hydrodynamics are performed in a periodic cubic box of side $L = 64\sigma$. Results without hydrodynamics, PR active and pure passive cases are obtained for $L = 48\sigma$.
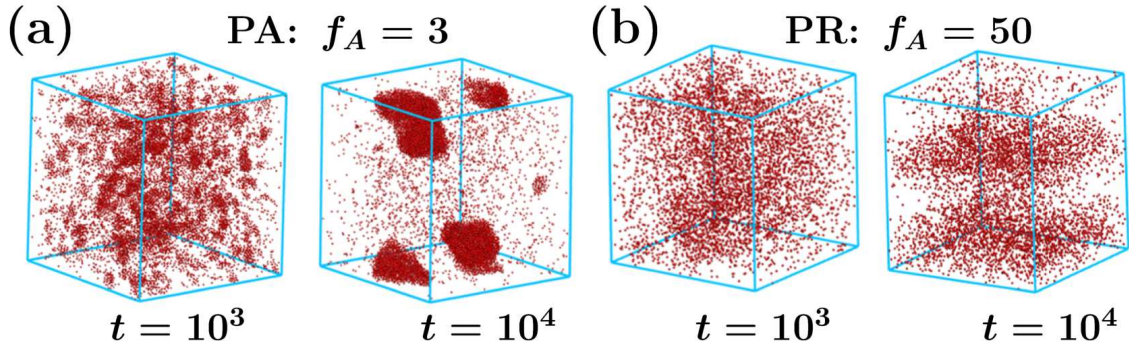
Figure 4.2: (a) Snapshots, recorded during the evolution of the model system, having PA active particles in a hydrodynamic environment, with swimmer flow, are presented from different times, with $f_A = 3$ and $T = 0.6$. Locations of only the active particles are marked. Strong fractal features of the clusters that we observed in Chapter 2, are missing here. (b) Same as (a) but here we have displayed the snapshots for PR active system with $f_A = 50$ and $T = 0.2$. For the PR case such a low temperature was chosen to ensure that the alignment interaction can win over the passive potential and produce clustering in the system.

4.3   Results

In Fig. 4.2(a) we show snapshots from the evolution following temperature quench of a system containing PA active particles in hydrodynamic environment. In Fig. 4.2(b) of this figure we show similar results for a PR active system. The formation and growth of clusters in both cases can be identified. Note that for PR case it is essential to keep the temperature at a very low value and set a high value for f_A, so that active alignment interaction can win against the joint effects of the repulsive potential and thermal fluctuations, facilitating clustering.

In Fig. 4.3 we show the growth plots for these two cases. Note that the average mass from the snapshots was calculated in a standard fashion as the first moment of the mass distribution function. The mass of an individual cluster, M_c, was obtained, in units of m_a, by appropriately identifying the cluster boundary and calculating the number of particles inside it [19–22]. For presentation, this was normalized by $r_e{}^3$, r_e being the

inter-particle distance ($2^{1/6}\sigma$ for PA and 2σ for PR) used to identify particles as parts of certain clusters.
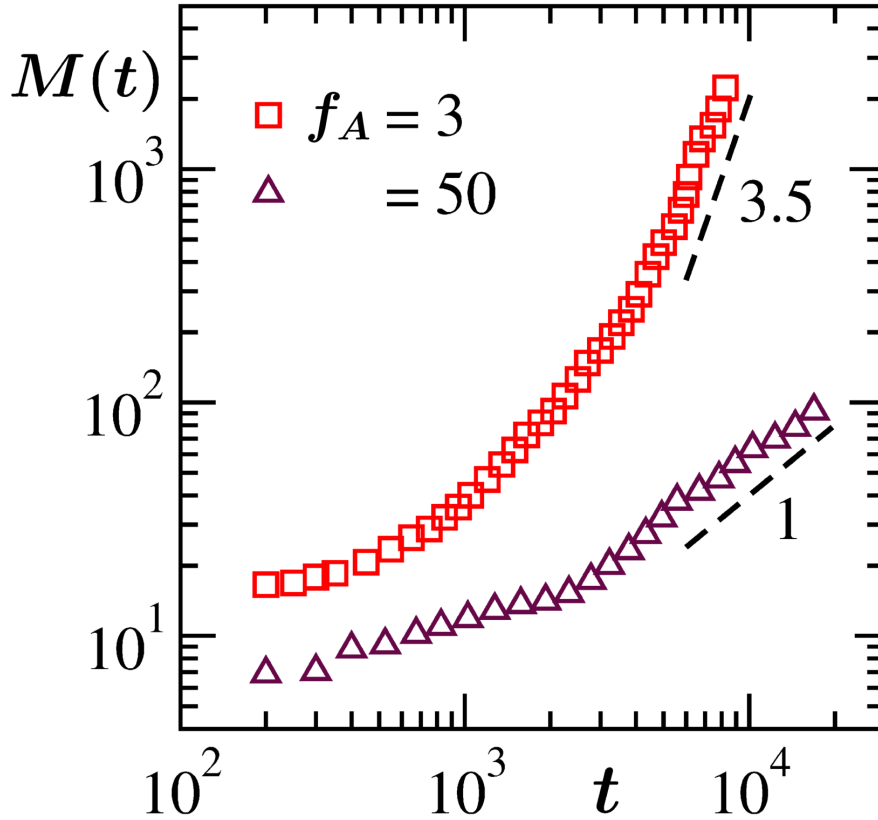
Figure 4.3: Average mass, M, as a function of time (t), for the systems in parts (a) and (b) of Fig. 4.2 are shown. The dashed lines represent power-laws with mentioned values of the exponents.

Interestingly, the Vicsek interaction can inject growth even when the passive potential is repulsive, though for very low T and high f_A. However, the growth is faster when there exists an attractive passive interaction. This is because in the repulsive case the clusters can break easily. In the rest of the paper, we focus only on the PA case and obtain a growth picture by comparing it with the corresponding outcome for its pure passive counterpart.

Consideration of PA is another interesting route to a systematic study of the dependence of aspects of phase transitions on strength of activity, given that the corresponding pure passive limit also has a phase transition. To elucidate the role of hydrodynamics, we will also present results by turning the local momentum conservation constraint off, by introducing random exchange of solvent velocities to destroy hydrodynamics [44, 62].
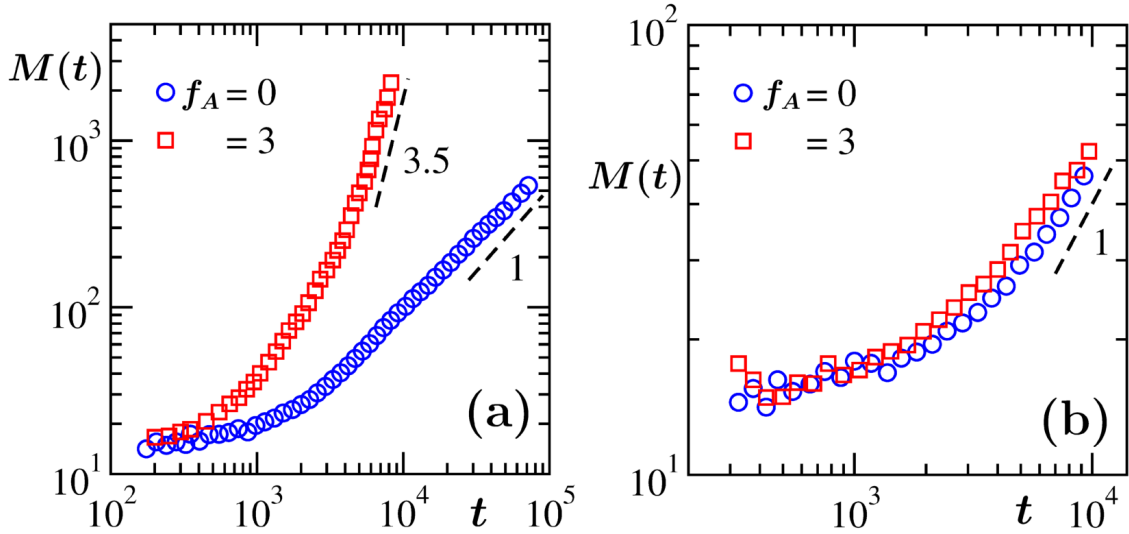
Figure 4.4: (a) Plots of M versus t are shown on a log-log scale for active ($f_A = 3$) and passive ($f_A = 0$) cases. (b) Same as (a) put these results were obtained in absence of hydrodynamics (HI-OFF). The dashed lines represent power-laws with mentioned values of the exponents.

In Fig. 4.4(a) we show the growth plots for two values of f_A, viz., 0 and 3. These, like the ones in Fig. 4.3, were obtained in the presence of hydrodynamics. Growth pictures, in absence of hydrodynamics, are presented in Fig. 4.4(b). From Figs. 4.4(a) and (b) it is clear that the growths for the active case occur faster. In the presence of hydrodynamics, the effects of activity, however, are striking. We believe that when hydrodynamics is turned off, the growth, for both $f_A = 0$ and 3, should occur via the Lifshitz-Slyozov [13] "simple" particle diffusion mechanism, for which $\beta = 1$. The simulation data agree with this. For this overall comparative picture to be true, between the hydrodynamic and non-hydrodynamic cases, there should be a difference between the ordering in the velocities of the active particles in the two situations. This difference we captured in the two-point equal time correlation function for the velocity field, viz.,

$$C_{vv}(r, t) = \langle \vec{v}_i(t) \cdot \vec{v}_j(t) \rangle, \tag{4.6}$$

where r is the scalar separation between the ith and j^{th} particles inside a cluster. The corresponding results are shown in Fig. 4.5. Expectedly, the ordering in the velocity directions is reflected in the hydrodynamic case. This confirms the role of hydrodynamics.

The hydrodynamic mechanism in the passive case leads to $\beta \simeq 1$, in agreement with the discussion above on DC. This value results from the solution of the dynamical
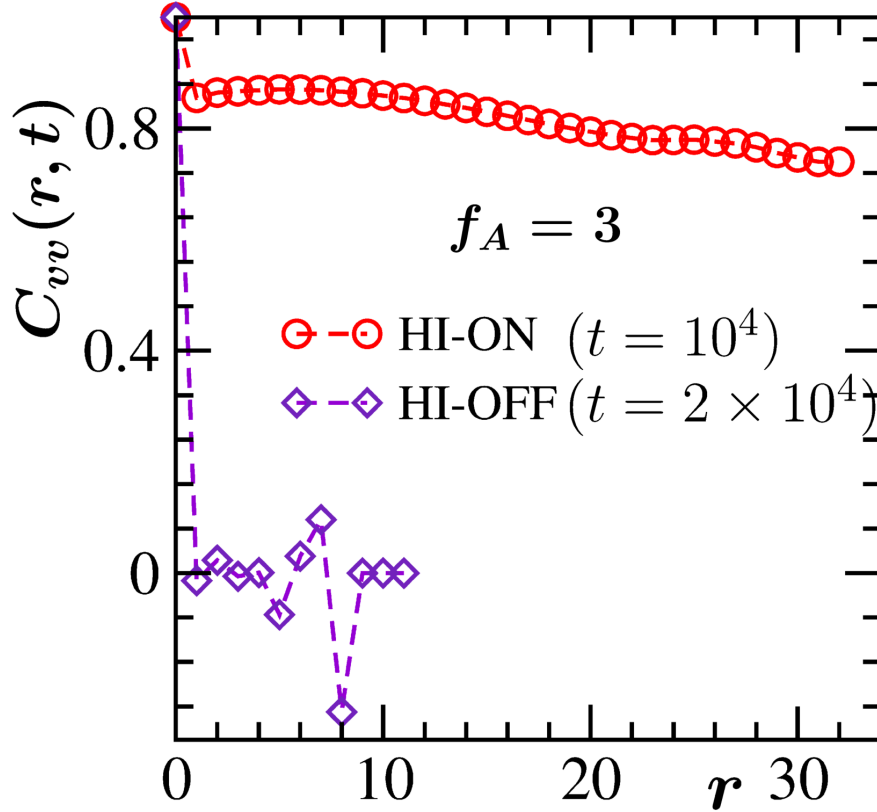
Figure 4.5: The velocity correlation C_{vv} is shown as a function of r, for $f_A = 3$. Results for both HI-ON and HI-OFF cases are included.

equation [15–22], as was also written previously,

$$\frac{\mathrm{d}n}{\mathrm{d}t} = -Cn^2, \tag{4.7}$$

for the droplet density n. Here C is a constant, arising from the generalized Stokes-Einstein-Sutherland relation [63]. This solution satisfies the mass conservation constraint, implying that nM equals the total number of particles in the droplet phase at all times. For the active case, as suggested by the plot in Fig. 4.3, we have $\beta \simeq 3.5$, which cannot be straight-forwardly guessed. In Fig. 4.6(a) we show plots for masses in typical clusters [20–22], two from each of $f_A = 0$ and 3, versus t', the translated time with respect to the beginnings of the observations at t_0, i.e., $t' = t - t_0$. Periods are chosen in such a way that within these intervals the considered clusters did not undergo collisions. Near-constant values in both the cases, over long periods, true for other droplets as well, imply that the growths are not happening via the simple particle diffusion mechanism. Hence, it is
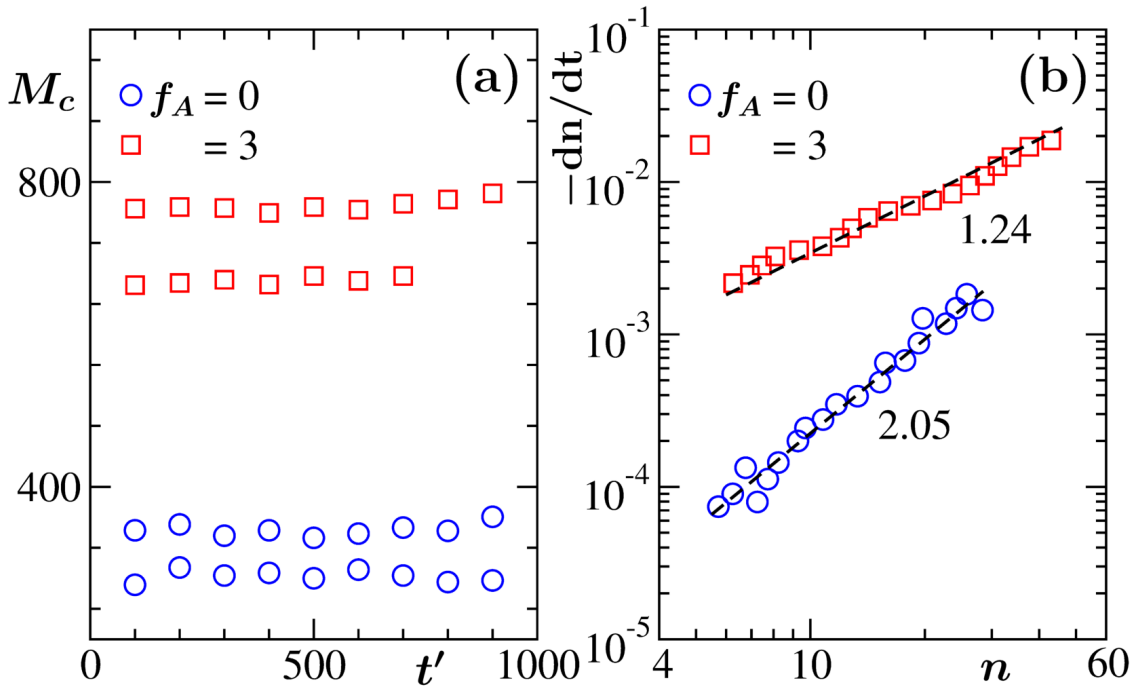
Figure 4.6: (a) Plots of masses in several clusters, from $f_A = 0$ and $f_A = 3$, are shown as a function of translated time $t' = t - t_0$, t_0 being the beginning of an observation. (b) Log-log plots of $-\mathrm{d}n/\mathrm{d}t$ versus n, for $f_A = 0$ and 3. The dashed lines represent power-laws, exponents for which are mentioned.

the coalescence of droplets [15, 49–53, 64, 65], via one or the other mechanism, that is responsible for growth in each of the cases.

In Fig. 4.6(b) we show plots of $-\mathrm{d}n/\mathrm{d}t$ versus n, on a double-log scale, for both the values of f_A, by restricting ourselves to being within the post-nucleation regimes. For the passive case, the quadratic trend of $-\mathrm{d}n/\mathrm{d}t$ in the simulation data hints towards the presence of the DC mechanism. The data set for the active case exhibits a behavior that is significantly weaker than quadratic.

In Fig. 4.7(a) we show the mean-squared displacement (MSD) of typical clusters [57], versus t', for both active and passive cases. For the passive case the time dependence is linear, confirming the DC mechanism for the growth [15–22, 57]. The quadratic enhancement in the active case suggests the BA mechanism [49–55]. For BA, as discussed in Chapter 2, the dynamical equation for collisions is:

$$\frac{\mathrm{d}n}{\mathrm{d}t} = -\sigma_{\mathrm{coll}} v_{\mathrm{rms}} n^2, \tag{4.8}$$
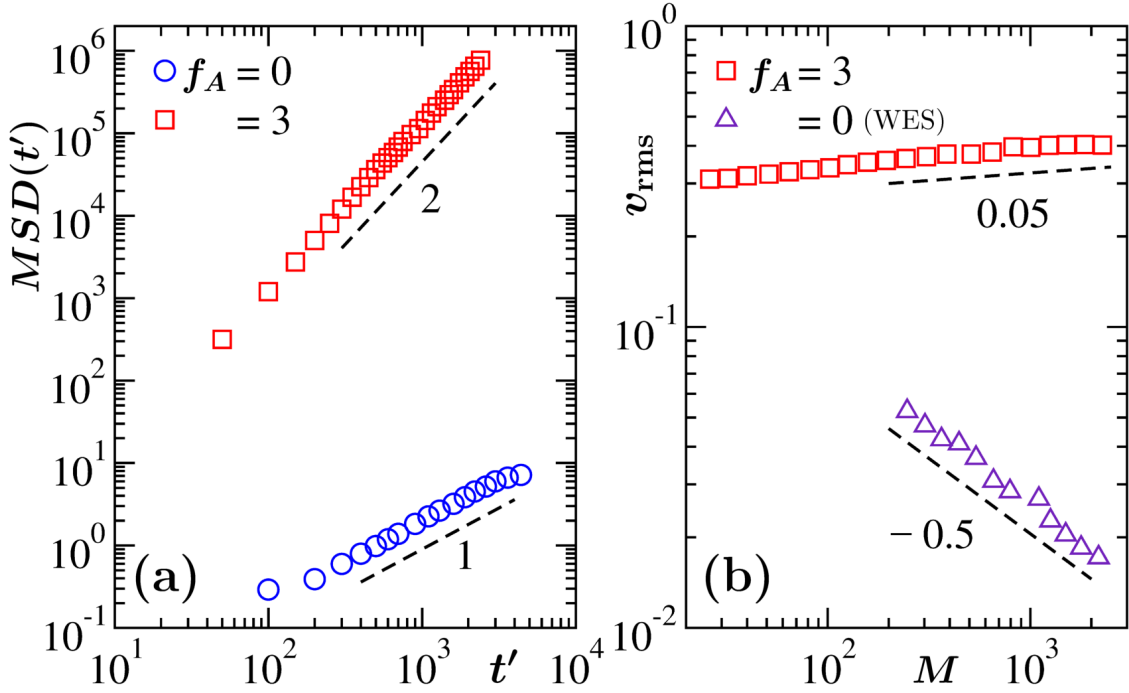
Figure 4.7: (a) Plots of mean-squared-displacement (of clusters) versus t', on a log-log scale. Typical results for passive and active cases have been included. (b) Root-mean-squared velocity of clusters is plotted versus M, on a double-log scale, for active case. For comparison, data from a passive system [49] with same LJ interaction, without explicit solvent (WES), showing $z = -1/2$, expected for uncorrelated motion of particles, are also included. These results correspond to HI-ON. The dashed lines represent power-laws, with mentioned values of the exponents.

where σ_{coll} is the collision cross-section. By taking $\sigma_{\text{coll}} \sim M^{(d-1)/d}$, one has $\beta = d/(1-dz)$. For $\beta \simeq 3.5$, one expects $z \simeq 0.05$. This is much different from $-1/2$ that is observed for uncorrelated motion of clusters [49]. In Fig. 4.7(b) we have shown v_{rms} versus M plots. There we have included data for $f_A = 3$ for the present hydrodynamic model, as well as from the same passive LJ system [49] without explicit solvent (WES), exhibiting ballistic aggregation. For the latter, $z \simeq -1/2$, for $T = 0.3$ and $\rho = 0.05$. On the other hand, in our active case, the value of z is consistent with 0.05, as predicted above. Thus, the overall picture in Fig. 4.7 supports the observation in Fig. 4.6(b), thereby validating the ballistic aggregation mechanism. Interestingly the theory works reasonably well even for z deviating from $-1/2$.

4.4 Conclusion

We use a combination of molecular and multi-particle collision dynamics methods for studying clustering in systems of Vicsek-like active particles in a hydrodynamic environment. For the chosen parameter values, the non-equilibrium morphology consists of disconnected clusters [21]. This has the advantage of checking the effects of hydrodynamics in an efficient manner. If the clusters are immersed in a high density solvent it is expected that between collisions these will exhibit diffusive motion, at least in the passive case.

In addition to presenting results for the passive case, we asked a further interesting question: How does the motion of clusters get changed when the constituents are active? It appears that for a Vicsek-type rule in activity the clusters eventually move ballistically. We have quantified the growth for this and explained it via the mass dependence of the velocities of the clusters [49, 50]. By tuning the system parameters [62] we have checked that our model provides hydrodynamic environment for both the passive and active cases. Such hydrodynamic methods were not used before to explore coalescence mechanisms, neither for passive nor for active matter systems. Though there exist reports on the role of hydrodynamics in the passive case [20–22], the explicit solvent for coalescence mechanism is new. Our conclusions are drawn after accurately analyzing the simulation data over long periods of time for large enough system sizes.

It is of interest to look at the dependence of kinetics on f_A. While in general, we expect faster growth compared to the passive case, the dependence of β on f_A can be nontrivial. For a meaningful conclusion, one requires a systematic study which we leave for the future. Nontriviality should exist for a transition from DC to BA also, depending upon the competition between f_A and T.

and Research (IISER) Bhopal. Thus, the chapter has resemblance with Chapter 5 of the Ph.D. Thesis by S. Sahoo entitled "Dynamics and aggregation of active colloids in different fluidic environments", IISER Bhopal (2021). However, whatever similarity may appear with those in the above mentioned thesis, differ either in system size or statistics or in other parameter values. Documents concerning the permission from the journal are attached towards the end of the thesis.

Bibliography

[1] M. E. Cates and J. Tailleur, Annu. Rev. Condens. Matter Phys. **6**, 219 (2015).

[2] J. Schwarz-Link, C. Valeriani, A. Cacciuto, M. E. Cates, D. Marenduzzo, A. N. Morozov, and W. C. K. Poon, Proc. Natl. Acad. Sci. U.S.A. **109**, 4052 (2012).

[3] J. Palacci, S. Sacanna, A. P. Steinberg, D. J. Pine, and P. M. Chaikin, Science **339**, 936 (2013).

[4] N. Kumar, H. Soni, S. Ramaswamy, and A. K. Sood, Nature Communications **5**, 4688 (2014).

[5] T. Vicsek, A. Czirôk, E. Ben-Jacob, I. Cohen, and O. Shochet, Phys. Rev. Lett. **75**, 1226 (1995).

[6] M. C. Marchetti, J. F. Joanny, S. Ramaswamy, T. B. Liverpool, J. Prost, M. Rao, and A. Simha, Rev. Mod. Phys. **85**, 1143 (2013).

[7] S. Ramaswamy, Annu. Rev. Condens. Matter Phys. **1**, 323 (2010).

[8] K. Binder, *in Phase Transitions of Materials*, edited by R.W. Cahn, P. Hansen, and E. J. Kramer (VCH, Weinheim, 1991), Vol. 5, p.405.

[9] A. J. Bray, Adv. Phys. **51**, 481 (2002).

[10] A. Onuki, *Phase Transition Dynamics* (Cambridge University Press, Cambridge, 2002).

[11] S. Puri and V. Wadhawan (eds.), *Kinetics of Phase Transitions* (CRC Press, Boca Raton, 2009).

[12] P. C. Hohenberg and B. I. Halperin, Rev. Mod. Phys. **49**, 435 (1977).

[13] I. M. Lifshitz and V. V. Slyozov, J. Phys. Chem. Solids **19**, 35 (1961).

[14] M. E. Fisher, Rep. Prog. Phys. **30**, 615 (1967).

[15] K. Binder and D. Stauffer, Phys. Rev. Lett. **33**, 1006 (1974).

[16] K. Binder, Phys. Rev. B **15**, 4425 (1977).

[17] H. Tanaka, J. Chem. Phys. **105**, 10099 (1996).

[18] E. D. Siggia, Phys. Rev. A **20**, 595 (1979).

[19] S. Roy, A. Bera, S. Majumder, and S.K. Das, Soft Matter **15**, 4743 (2019).

[20] S. Roy and S. K. Das, Soft Matter **9**, 4178 (2013).

[21] S. Roy and S. K. Das, Phys. Rev. E **85**, 050602 (2012).

[22] S. Roy and S. K. Das, J. Chem. Phys. **139**, 044911 (2013).

[23] S. K. Das, S. Roy, S. Majumder, and S. Ahmed, Europhys. Lett. **97**, 66006 (2012).

[24] A. Wysocki, R. G. Winkler, and G. Gompper, Europhys. Lett. **105**, 48004 (2014).

[25] J. M. Belmonte, G. L. Thomas, L. G. Brunnet, R. M. C. de Almeida, and H. Chaté, Phys. Rev. Lett. **100**, 248702 (2008).

[26] L. Caprini, U. M. B. Marconi, and A. Puglisi, Phys. Rev. Lett. **124**, 078001 (2020).

[27] C. Bechinger, R. D. Leonardo, H. Löwen, C. Reichhardt, G. Volpe, and G. Volpe, Rev. Mod. Phys. **88**, 045006 (2016).

[28] S.K. Das, J. Chem. Phys. **146**, 044902 (2017).

[29] S. K. Das, S. A. Egorov, B. Trefz, P. Virnau, and K. Binder, Phys. Rev. Lett. **112**, 198301 (2014).

[30] B. Trefz, S. K. Das, S. A. Egorov, P. Viranau, and K. Binder, J. Chem. Phys. **144**, 144902 (2016).

[31] J. T. Siebert, F. Dittrich, F. Schmid, K. Binder, T. Speck, and P. Virnau, Phys. Rev. E **98**, 030601(R) (2018).

[32] S. Thakur and R. Kapral, Phys. Rev. E **85**, 026121 (2012).

[33] T. Yu, P. Chuphal, S. Thakur, S. Y. Reigh, D. P. Singh, and P. Fisher, Chem. Comm. **54**, 11933 (2018).

[34] S. Thakur and R. Kapral, J. Chem. Phys. **135**, 024509 (2011).

[35] O. Pohl and H. Stark, Phys. Rev. Lett. **112**, 238303 (2014).

[36] F. Ginelli, Eur. Phys. J. Special Topics **225**, 2099 (2016).

[37] R. Kapral, Adv. Chem. Phys. **140**, 89 (2008).

[38] D. Frenkel and B. Smit, *Understanding Molecular Simulations: From Algorithms to Applications* (Academic Press, San Diego, California, 2002).

[39] M. P. Allen and D. J. Tildesley, *Computer Simulations of Liquids* (Clarendon, Oxford, 1987).

[40] A. Furukawa and H. Tanaka, Phys. Rev. Lett. **104**, 245702 (2010).

[41] H. Tanaka and T. Araki, Phys. Rev. Lett. **85**, 1338 (2000).

[42] S. Das, J. Riest, R. G. Winkler, G. Gompper, J. K. G. Dhont, and G. Nägele, Soft Matter **14**, 92 (2018).

[43] A. Winkler, P. Virnau, K. Binder, R. G. Winkler, and G. Gompper, J. Chem. Phys. **138**, 054901 (2013).

[44] S. Li, H. Jiang, and Z. Hou, Soft Matter **11**, 5712 (2015).

[45] R. M. Navarro and S. M. Fielding, Soft Matter **11**, 7525 (2015).

[46] R. M. Navarro, R. Golestanian, T. B. Liverpool, and S. M. Fielding, Phys. Rev. E **90**, 032304 (2014).

[47] A. Zöttl and H. Stark, Phys. Rev. Lett. **112**, 118101 (2014).

[48] J. Blaschke, M. Maurer, K. Menon, A. Zöttl, and H. Stark, Soft Matter **12**, 9821 (2016).

[49] J. Midya and S. K. Das, Phys. Rev. Lett. **118**, 165701 (2016).

[50] G. F. Carnevale, Y. Pomeau, and W. R. Young, Phys. Rev. Lett. **64**, 2913 (1990).

[51] E. Trizac and P. L. Krapivsky, Phys. Rev. Lett. **91**, 218302 (2003).

[52] E. Trizac and J.-P. Hansen, J. Stat. Phys. **82**, 1345 (1996).

[53] N. Brilliantov, P. L. Krapivsky, A. Bodrova, F. Spahn, H. Hayakawa, V. Stadnichuk, and J. Schmidt, Proc. Natl. Acad. Sci. U.S.A. **112**, 9536 (2015).

[54] S. Paul and S. K. Das, Phys. Rev. E **96**, 012105 (2017).

[55] S. Paul and S. K. Das, Phys. Rev. E **97**, 032902 (2018).

[56] S. N. Pathak, D. Das and R. Rajesh, Europhys. Lett. **107**, 44001 (2014).

[57] J.-P. Hansen and I. R. McDonald, *Theory of Simple Liquids* (Academic Press, London, 2008).

[58] J.D. Weeks, D. Chandler and H.C. Andersen, J. Chem. Phys. **54**, 5237 (1971).

[59] G. Gompper, T. Ihle, D. Kroll, and R. Winkler, Avd. Polym. Sci. **221**, 1 (2008).

[60] T. Ihle and D. M. Kroll, Phys. Rev. E **63**, 020201(R) (2001).

[61] J. T. Padding and A. A. Louis, Phys. Rev. E **74**, 031402 (2006).

[62] I. Ali, D. Marenduzzo, and J.M. Yeomans, J. Chem. Phys. **121**, 8635 (2004).

[63] S. K. Das, J.V. Sengers and M.E. Fisher, J. Chem. Phys. **127**, 144506 (2007).

[64] N. V. Brilliantov and F. Spahn, Math. Comput. Simul. **72**, 93 (2006).

[65] S. Roy, Europhys. Lett. **121**, 34001 (2018).

Chapter 5

Macroscopic Rotation of Active Colloids in a Colloid-Polymer Mixture inside a Spherical Cavity

5.1 Introduction

Understanding how phase transitions and collective behavior of particles in active matter systems differ from their equilibrium counterparts in passive systems has become a grand challenge problem [1–6]. A key observation, dating back to the Vicsek [7] model for the formation of bird swarms, is the "motility induced phase separation" (MIPS) [2, 4, 8] between high-density (liquid-like) and low density (vapor-like) phases. Experimentally, MIPS was found in suspensions of motile bacteria [9] or of self-propelled colloids [10], for instance.

As a "fruitfly model" of MIPS, the model of active Brownian particles (ABP) was proposed [11–14]. These particles interact via pairwise repulsive forces in the absence of hydrodynamics, each particle having an intrinsic speed of fixed absolute value v_0, with the direction decorrelating by rotational diffusion. Unlike Ref. [7], there is no explicit alignment interaction in this model.

Recent studies [15, 16] revealed that the phase behavior of this ABP model is apparently very complicated in space dimension $d = 3$: liquid-vapor-like phase coexistence typically is metastable against separation between vapor-like and crystalline phases. Thus, we focus here on an alternative model [17–20], viz., an Asakura-Oosawa (AO) type model for colloid-polymer mixtures [21–24] amended by a Vicsek-like interaction, the colloids

being self-propelling. Choosing a size ratio $q_s = 0.8$ between the radius of the polymer coils (that are modeled as soft spheres) and the colloids, the phase behavior in the passive case has been precisely characterized: a vapor-liquid-like separation occurs, with Ising critical behavior [24–27] remaining unaffected, the crystal phase of the colloids does not interfere with this vapor-liquid critical behavior.

A strange feature of the simulation studies of the above mentioned active AO model [17–19] is the anomalous behavior at the interfaces between the coexisting phases. This is enforced by the periodic boundary conditions (PBC) of the cubic box, standard for obtaining the bulk behavior of quasi-macroscopic systems [28]: the slab-like liquid domain is separated from the vapor by a planar interface at which the "local temperature" is enhanced by a factor of 2 to 4 compared to the rest of the system [18]. Here the temperature is defined kinetically in terms of the mean-squared fluctuation of the particle velocities. No such effects occur in equilibrium. There the temperature is homogeneous, and PBC do not cause such unphysical artifacts. In this active AO model, an almost uniform flow of colloid particles parallel to the interfaces occurs in the colloid-rich domain, while the polymer rich domain stays at rest. Thus, small finite systems with PBC are well suited to elucidate the bulk behavior of real systems in equilibrium, while the use of PBC can cause problems for simulations of active matter.

A physically more reasonable behavior is expected for a system in a closed container confined by walls. The equilibrium behavior of the AO model in spherical confinement has revealed interesting core-shell or Janus-particle type structures, depending on the particle-wall interactions [29]. Thus, to investigate the interesting case of active matters enclosed in vesicles or living cells, we study here an active version of the AO model [17–20] under spherical confinement, where, as stated before, the colloids are made self-propelling. We observe that the region of phase coexistence between colloid-rich and polymer-rich phases in the confined system becomes wider with increasing "activity strength" f_A: this can be understood by the fact that an additional "effective" pairwise attraction arises between colloids due to the activity. Even more interesting feature is a macroscopic rotation of the colloid-rich phase, characterized by an angular momentum $\vec{L}$. No such motion is possible in equilibrium. Here $\vec{L}$ is not strictly a constant of motion. Slow random reorientation of the direction of $\vec{L}$ occurs, however, the magnitude of $\vec{L}$ stays almost unchanged.

Coherent motions in dense active matters have been reported for active nematics, mostly in (quasi-) two-dimensional (2D) systems. Simulations of active nematics in a quasi-1D microchannel, by Shendruk et. al. [30], observed transitions from laminar to

oscillatory flow and finally to "dancing disclinations", as the strength of the activity is increased. Experiments on confined cellular nematics, such as Retinal cells and mouse myoblasts that form nematic phases, show spontaneous shear flow in monolayers formed on micropatterned glass substrates with adhesive widths in the 100 micrometer range [31]. Spiral vortical flow was observed in quasi-2D suspensions of Bacillus subtilis in flattened drops with about 50 micrometer diameter [32]. Simulations of these [33, 34] and related flows in annuli and channels are reviewed in Ref. [35]. Studies of 3D active fluids in toroidal channels and cylinders (with flows parallel to the cylinder surface) [36] revealed a transition between turbulent motion and coherent flow. The system contained microtubule filaments and depleting polymers (inducing tubuli bundling, i.e., an attraction similar to the AO model) in which activity was generated by the presence of kinesin motor clusters, causing interfilament sliding. Interesting long range effects due to planar boundaries on active matters were also discussed in various contexts [37–39]. Recent experiments [40] on motile Escherichia coli inside spherical confinement showed that depending on conditions, the bacteria are either uniformly distributed in the spherical water drops (in an oil emulsion) or enriched near the surface. Here the bacteria are elongated, the interaction is via hydrodynamic forces, and the persistence length of the ballistic trajectories is very large. For two dimensional active particles confined inside a square box, it is reported that the active particles accumulate preferentially near the walls [41]. The study related to confinement between parallel plates in Ref. [42] showed an interesting crossover in the concentration profile with changing volume fraction. Again, the coupling between swimmers here is hydrodynamic and Vortex-like flows are found. The existence of a striped phase where collective motion occurs in the direction perpendicular to the high density stripes is reported in Vicsek model [43]. As is well known [44], colloid-polymer mixtures are a key model for the description of depletion interactions and of many phenomena resulting from them, including biological processes in living cells. While previous works [45–49] have studied flows of active nematics confined to the surface of a sphere, we are not aware of any work on the spontaneous coherent flow of active spherical particles confined inside a sphere. While most of these works deal with strongly elongated objects, we find interesting coherent motion in a system of spherical active particles.

5.2   Model and Methods

We study the phase behavior and dynamical properties of binary mixtures consisting of active colloids and passive polymers under spherical confinement. While in the original AO model the colloids are hard spheres, for Molecular Dynamics (MD) [28] a smooth repulsion is convenient. Here we use the repulsive part of the Lennard-Jones potential, with strength $\varepsilon = 1$ and range $\sigma = 1$, the latter taken as the unit of length. The same potential is used for the colloid (c)-polymer (p) interaction as well, but with different interparticle interaction diameter. The polymers repel each other with a much weaker potential that allows strong polymer-polymer (pp) overlap [27], closely resembling the "no" pp interaction in the original version.

In our model, the passive interactions among the particles are taken from a variant of the well-known Asakura-Oosawa (AO) model [21–24] of colloid (c) and polymer (p) mixtures. For $\alpha = c$ and $\beta = c, p$, particles i and j interact with each other via the Weeks-Chandler-Andersen (WCA) potential [50]

$$U_{\alpha\beta} = \begin{cases} 4\varepsilon_{\alpha\beta}\left[\left(\frac{\sigma_{\alpha\beta}}{r}\right)^{12} - \left(\frac{\sigma_{\alpha\beta}}{r}\right)^{6} + \frac{1}{4}\right], & \text{for } r < 2^{\frac{1}{6}}\sigma_{\alpha\beta} \\ 0, & \text{otherwise;} \end{cases} \tag{5.1}$$

and we have for pp pairs

$$U_{pp}(r) = \begin{cases} 8\varepsilon_{pp}\left[1 - 10\left(\frac{r}{r_{c,pp}}\right)^{3} + 15\left(\frac{r}{r_{c,pp}}\right)^{4} - 6\left(\frac{r}{r_{c,pp}}\right)^{5}\right], & \text{for } r < r_{c,pp} = 2^{\frac{1}{6}}\sigma_{pp} \\ 0, & \text{otherwise.} \end{cases} \tag{5.2}$$

Here $\varepsilon_{\alpha\beta}$ and $\sigma_{\alpha\beta}$ are the interaction strengths and interaction diameters for various combinations of species. We set [17, 18] $\varepsilon_{cc} = \varepsilon_{cp} = \varepsilon = 1$, $\varepsilon_{pp} = 0.0625$, $\sigma_{cc} = \sigma = 1$, $\sigma_{cp} = 0.9$ and $\sigma_{pp} = 0.8$.

All particles are confined in a sphere of radius $R = 10$, the wall potential being the same as in equilibrium studies [29, 51]. The wall-particle interactions are modeled by smooth repulsion described by the WCA potential [50]

$$U_{wb}(r_w) = \begin{cases} 4\varepsilon_{wb}\left[\left(\frac{\sigma_{wb}}{r_w}\right)^{12} - \left(\frac{\sigma_{wb}}{r_w}\right)^{6} + \frac{1}{4}\right], & \text{for } r_w < 2^{\frac{1}{6}}\sigma_{wb} \\ 0, & \text{else.} \end{cases} \tag{5.3}$$

Here $b = (c, p)$ and r_w is the shortest distance between the particle and the spherical wall. The interaction strength between the wall and the particles (c or p) are taken to be

unity, i.e., $\varepsilon_{wc} = \varepsilon_{wp} = 1$. The relative influence of the wall on the particles is controlled by the ratio of the repulsive ranges [29], viz., $q_w = \sigma_{wp}/\sigma_{wc}$, where σ_{wc} and σ_{wp} are the diameters for wall-colloid and wall-polymer interactions, respectively.

Molecular dynamics (MD) simulations have been performed via the numerical solutions of the Langevin equation ($\vec{r}_n$ is the position of nth particle)

$$m\ddot{\vec{r}}_n = -\vec{\nabla}U_n - \gamma m\dot{\vec{r}}_n + \vec{F}_n^r(t) + \vec{f}_n. \tag{5.4}$$

Here the mass m is same for all colloid and polymer particles. In Eq. (5.4), the friction coefficient γ is related to the random force $\vec{F}_n^r(t)$ via the standard fluctuation-dissipation relation at thermal energy $k_B T = 1$. The Cartesian components of the random force satisfy $\langle F_n^{r,\mu}(t) \rangle = 0$ and $\langle F_n^{r,\mu}(t) F_{n'}^{r,\nu}(t') \rangle = 2m\gamma k_B T \delta_{\mu\nu}\delta_{nn'}\delta(t - t')$, $[\mu, \nu \equiv x, y, z]$.

We have $\vec{f}_n = 0$ for all polymers and the self-propelling activity among the colloids is introduced via the Vicsek model in which the velocity of the nth colloid ($\vec{v}_{c,n}$) gets influenced by the average direction $\hat{p}_n$ ($= \sum_k \vec{v}_{c,k}/|\sum_k \vec{v}_{c,k}|$) of colloids within its neighbourhood (including n^{th} colloid) that is defined by a distance r_{int} from $\vec{r}_n$. The active force, $\vec{f}_n$, on the nth colloid is proportional to $f_A\hat{p}_n$, where f_A is the strength of activity. The activity has been incorporated in such a way that only the direction of velocity changes, not the magnitude. The choice of the Vicesek model is motivated by the fact that an aligning interaction between the motions of bacteria, which are propagated by their moving flagellas, results from the hydrodynamic interactions between these bacterias in the aqueous solution inside the cells. Similar interactions may also arise between colloids in suspensions, when one hemisphere is coated such that a chemical reaction in the suspension takes place providing the energy for the ballistic motion of the colloids. Explicit demonstrations that hydrodynamic interactions cause collective motions of confined spherical colloids has been given by Zöttl and Stark [52] for a quasi-twodimensional model of squirmers. We are not aiming at a faithful description of a particular system, however, and rather study a generic model. This way of implementation of activity will allow the system to be in the assigned temperature [53–55]. The mass, length and time in our simulations were measured in units of m, σ and $t_s = \sqrt{\sigma^2 m/\varepsilon}$, respectively. The time step in the MD simulations is taken to be $\Delta t = 0.002t_s$. We have fixed m, σ, ε, k_B, T and γ to unity and used $r_{\text{int}} = 2^{2/3}$. All the results are presented for $R = 10$, the radius of the spherical cavity. In this work we use $\sigma_{wc} = 0.6$ and $\sigma_{wp} = 0.4$, unless otherwise mentioned. For this choice of q_w ($=\sigma_{wp}/\sigma_{wc} = 0.667$), there is no preferential affinity of wall towards any components, in the full passive case ($f_A = 0$). In equilibrium,
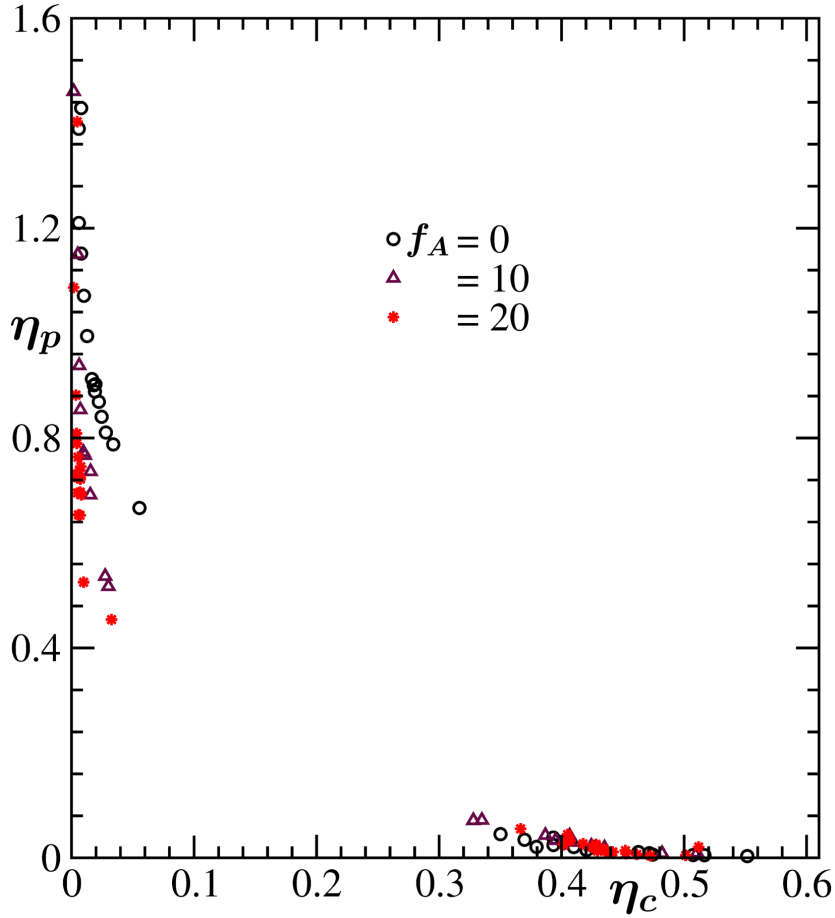
Figure 5.1: Phase diagrams of the active AO model in spherical confinement of radius $R = 10$ are shown in the η_c–η_p plane, for different strengths of f_A. These results are obtained via MD simulations.

in this case, both components wet the wall forming Janus particle-like structure under conditions where the system exhibits phase separation in the bulk. The introduction of activity to the colloids leads to a drastic change in configurations in steady states with respect to passive configurations in equilibrium. We have chosen these particular values for the parameters σ_{wb} for certain reasons. Note that the wetting properties of this model in the passive limit have been studied by Statt et. al. [51]. Complete wetting of the sphere surface by the colloids was observed for up to $\sigma_{wc} = 0.59$ and partial wetting picture emerged for σ_{wc} lying approximately between 0.59 and 0.7, for $\sigma_{wp} = 0.4$. The case of "neutral" walls, i.e., a contact angle of 90^0, was found for $\sigma_{wc} = 0.65$. All data are for packing fractions $\eta_c = 0.3$ and $\eta_p = 0.3$ of both polymers and colloids unless otherwise mentioned.

5.3 Results

The "phase diagrams" in the plane of packing fractions η_c and η_p, obtained from the simulations, are shown in the main frame of Fig. 5.1, for several choices of f_A, including the passive case $f_A = 0$. States above the symbols are in the immiscible region, the left branches quantifying the polymer-rich and the right ones the colloid-rich phases. The region near the critical point, where the branches are expected to merge, is not displayed here. When f_A increases the phase boundaries move towards the coordinate axes, since activity enhances phase separation. Here η_c and η_p are related to the colloid and polymer densities ρ_c and ρ_p as [27] $\eta_c = 0.5484\rho_c$ and $\eta_p = 0.2808\rho_p$ [$\rho_b = N_b/V$, $b = (c, p)$; where N_b is the number of particles of type b and V ($= 4\pi R^3/3$) is the volume of the cavity].
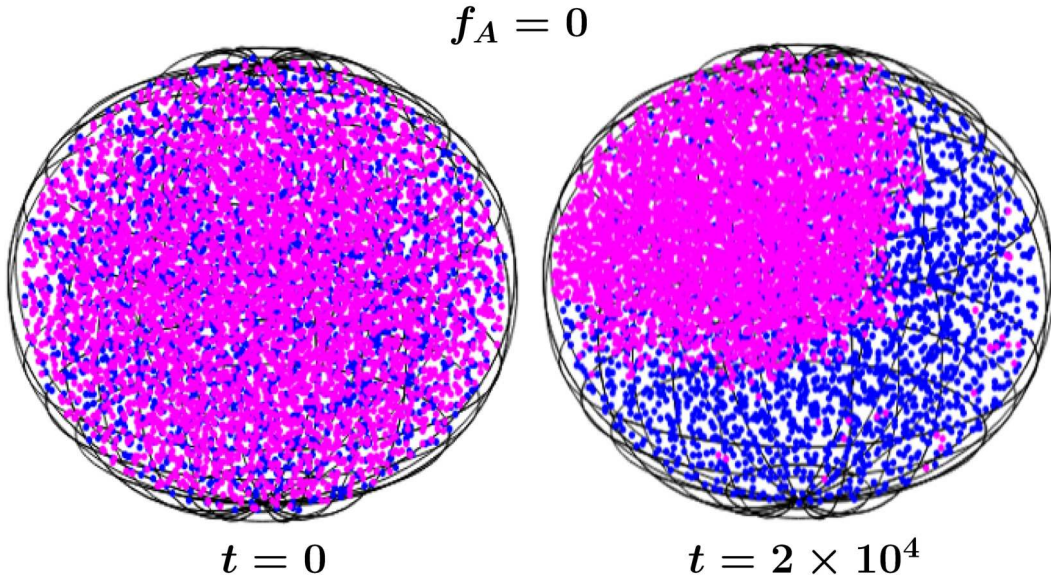
Figure 5.2: Typical evolution snapshots at different times for a passive case $f_A = 0$. Colloids (polymers) are represented by blue (magenta) dots. These are for $\eta_c = \eta_p = 0.3$.

To obtain the simulation data in Fig. 5.1, runs for different sets of state points (η_c, η_p) are performed. For active cases ($f_A > 0$) typically steady state exhibits phase separation with the inner cluster containing mostly polymers, while the colloids accumulate mostly outside this cluster, i.e., near the sphere surface. The phase diagram here is obtained via the calculation of the density profile along the axis of a cylinder of unit radius that passes through the cavity center and having the axis in such directions where both high density phases of colloids and polymers coexist. From the plateau of density profiles of colloids and polymers, we have obtained the coexistence points presented in Fig. 5.1.
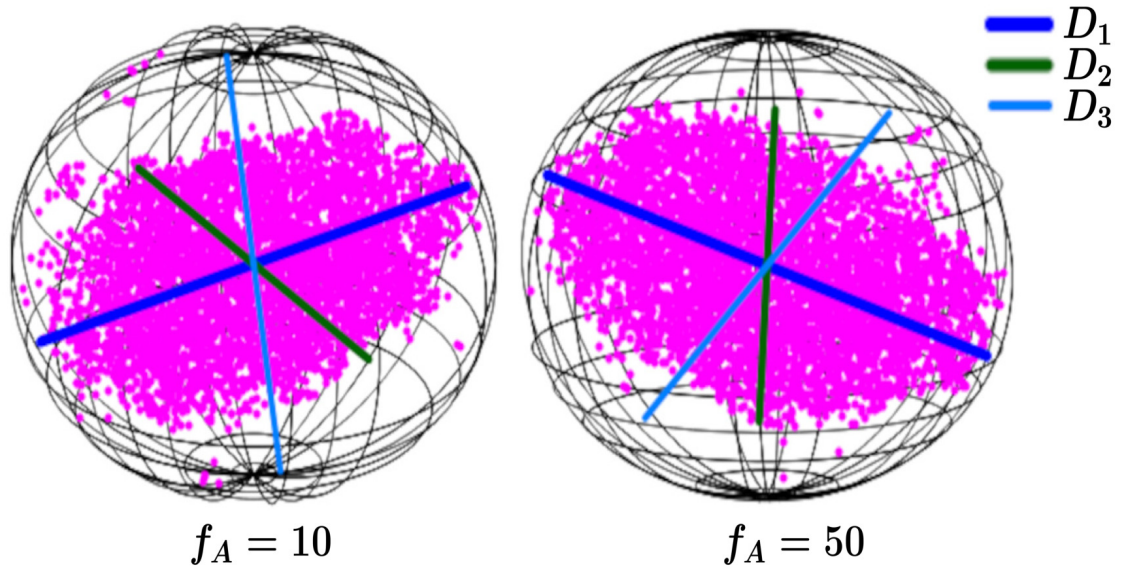
Figure 5.3: Two typical configurations, at time $t = 2 \times 10^4 \sqrt{m\sigma^2/\varepsilon}$, showing only the polymers inside the sphere, for phase separated states that resulted by fixing the packing fractions at $\eta_c = \eta_p = 0.3$, for $f_A = 10$ (left) and $f_A = 50$ (right). The principal axes D_1, D_2 and D_3, corresponding to the eigenvalues $\lambda_1^2, > \lambda_2^2, > \lambda_3^2$ of the gyration tensors of the clusters, are indicated by lines.

From here onwards we will focus on the structural and dynamical aspects of the system for a state point $(\eta_c, \eta_p) \equiv (0.3, 0.3)$ that resides well inside the coexistence region. All the results onwards are for $(\eta_c, \eta_p) \equiv (0.3, 0.3)$. In the left frame of Fig. 5.2 we have shown an initial homogeneous configuration of colloid and polymer mixture. When this configuration evolves without any alignment interactions $f_A = 0$, a nearly Janus-particle structure is observed in steady state and that is shown in the right frame of Fig. 5.2. As mentioned earlier this represents a nearly neutral wall for the particles of different types.

With the introduction of activity to colloids, this shape changes drastically. Fig. 5.3 shows two typical configurations of polymer clusters when colloids are active. While in the equilibrium case the need to minimize the total interfacial excess free energy should lead to an approximately spherical shape of such a cluster, which actually is observed [29] under wetting conditions by the colloids, we here find a rather elongated, ellipsoidal cluster shape. Defining the center of mass coordinates $X^i = \sum_{n=1}^{N_p} x_n^i / N_p$ ($i = 1, 2, 3$ in space dimension $d = 3$ and the sum runs over the position coordinates x_n^i of all N_p
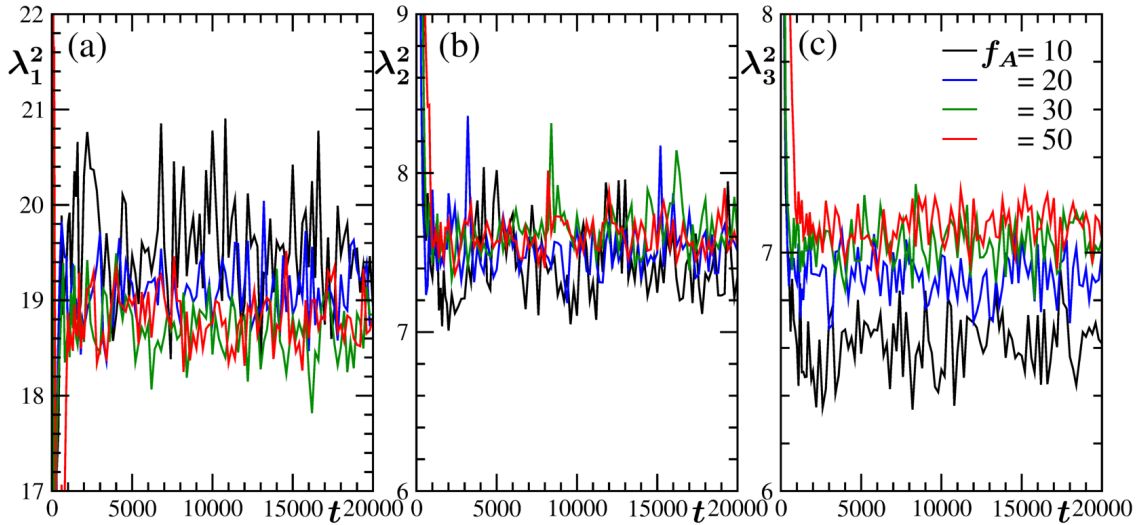
Figure 5.4: (a)-(c) The eigenvalues λ_i^2 $(i = 1, 2, 3)$ have been plotted, for different values of the activity strength f_A, as a function of time.

polymers inside the cluster), the gyration tensor Q_{ij} can be calculated as [56, 57]

$$Q_{ij} = \frac{1}{N_p} \sum_{n=1}^{N_p} (x_n^i - X^i)(x_n^j - X^j), \quad i, j = 1, 2, 3. \tag{5.5}$$

Transforming this tensor to principal axes, we find the the eigenvalues λ_i^2 $(i = 1, 2, 3)$ that have been presented in 5.4. For the system with active colloids, however, the polymer-rich ellipsoid almost extends to the poles at the sphere surface (see Fig. 5.3). We have found that the related average eigenvalues $\lambda_1^2 \gg \lambda_2^2 \simeq \lambda_3^2$ correspond to a prolate ellipsoidal shape: e.g., $\lambda_1^2 \simeq 19$ and $\lambda_2^2 \simeq \lambda_3^2 \simeq 7.5$ in the example of $f_A = 50$ in Fig. 5.3. In the steady state the λ_i^2s show fluctuations of the magnitude of only about 0.5, without any systematic change with time (see Fig. 5.4).

Furthermore, the motion of the colloidal particles relative to this structure is interesting. In Fig. 5.5 the snapshot of colloid velocities indicates a coherent collective rotational flow of the particles inside the sphere. This is despite the fact that we have no hydrodynamics in our model.

To capture these phenomena and various other symmetries along the rotation axis D_1 of the colloids, we have divided the sphere into many circular disks, each of width dz, along the principal axis diameter D_1, corresponding to λ_1^2, of the ellipsoid that is formed by the polymers in the interior of the sphere (see a schematic diagram in Fig. 5.6). Let us consider a disk C_z, situated at a distance z along D_1 from the centre of the cavity,
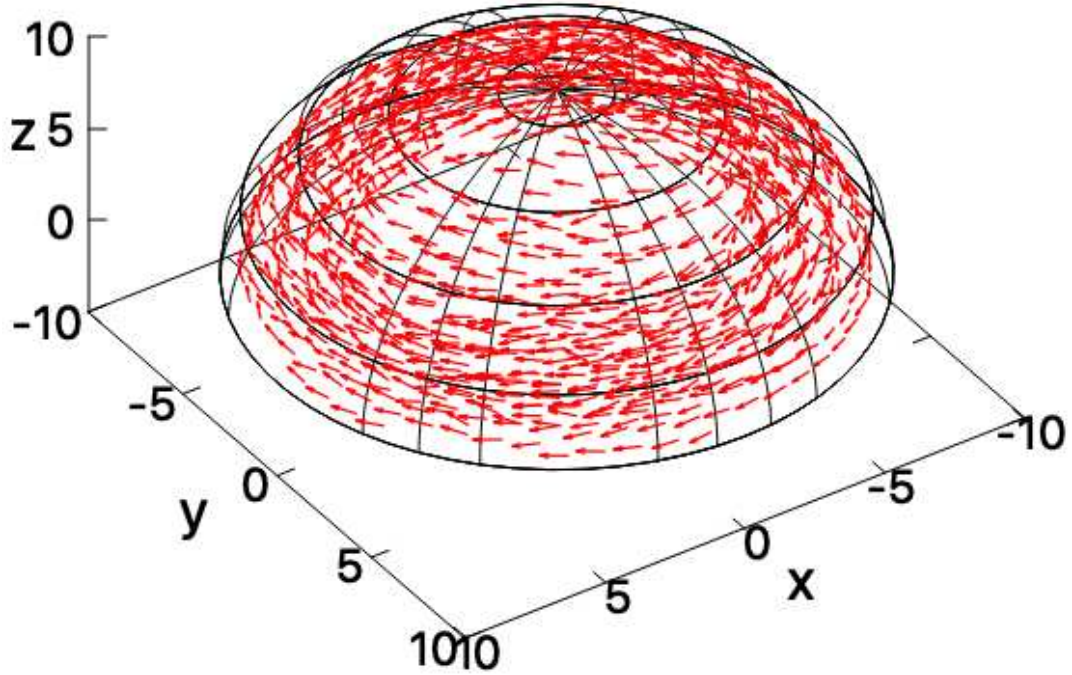
Figure 5.5: Velocity vectors of the colloidal particles inside the sphere. We have bisected the sphere by choosing an equatorial plane that is perpendicular to the eigenvector along D_1. Only one hemisphere is shown relative to this plane, by normalizing the velocity magnitudes to unity. The snapshot refers to the same system as in Fig. 5.3, with $f_A = 50$ at $t = 2 \times 10^4$.

having $N_{c,z}$ colloids and $N_{p,z}$ polymers. To quantify this whirling motion of colloids as shown in Fig. 5.5, we calculate the average angular momentum $\vec{L}(z)$, with respect to the diameter D_1, of the colloids inside C_z, defined as

$$\vec{L}(z) = \frac{1}{N_{c,z}} \sum_{k \in C_z} \vec{r}_{\perp c,k} \times \vec{v}_{c,k}. \tag{5.6}$$

The sum is carried over the colloidal particles (c) within the disk C_z. Here $\vec{r}_{\perp c,k}$ is the perpendicular distance of the kth colloid particle from D_1: $\vec{r}_{\perp c,k} = \vec{r}_{c,k} - \hat{e}_1(\hat{e}_1 \cdot \vec{r}_{c,k})$, $\hat{e}_1$ being the unit vector along D_1. Note that $\vec{r}_{c,k}$ is the position vector of the kth colloid. Fig. 5.7 shows then (a) the average of the magnitude of this angular momentum as well as (b) of an alignment parameter $q = \langle \hat{e}_1 \cdot \vec{L}/|\vec{L}| \rangle$. Note that q is a measure of how well the axis of this rotation is correlated with the distribution of the polymers in the system. It is seen that in the center of the sphere the magnitude of $\vec{L}$ is maximal and the alignment indeed is nearly perfect.
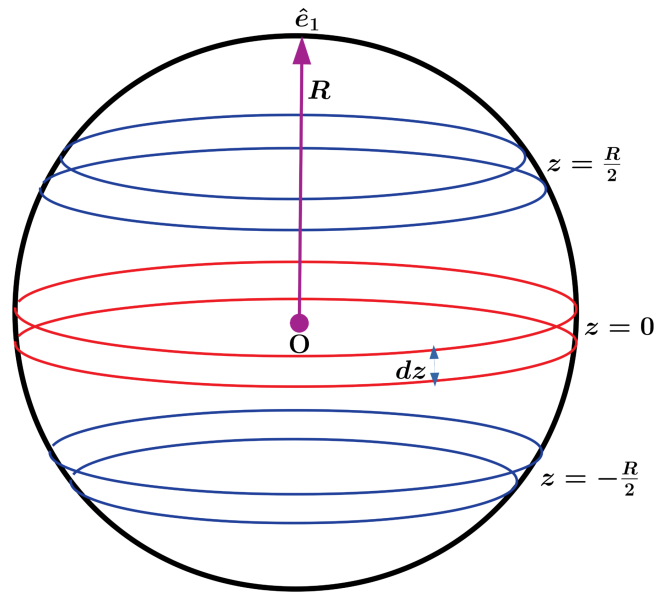
Figure 5.6: A schematic diagram that shows the division of the spherical cavity into quasi circular disks along the rotation axis ($\hat{e}_1$). A circular disk of width dz at equatorial region ($z = 0$) and two similar disks at $z = R/2$ and $-R/2$ (R being the radius of the cavity) have been shown. The direction of the rotation axis ($\hat{e}_1$) is marked by arrow-headed line.
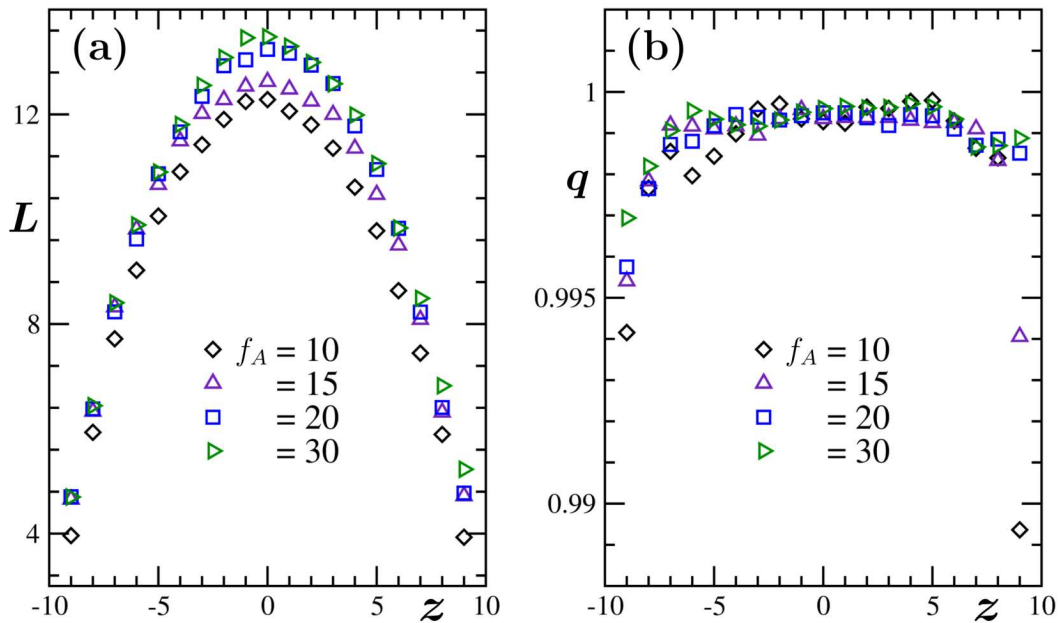
Figure 5.7: For the colloidal particles, the average absolute value of the angular momentum L (a) and of the alignment parameter q (b) are plotted versus the distance z from the center of the sphere along the diameter D_1. Results from different choices of f_A are included, as indicated.
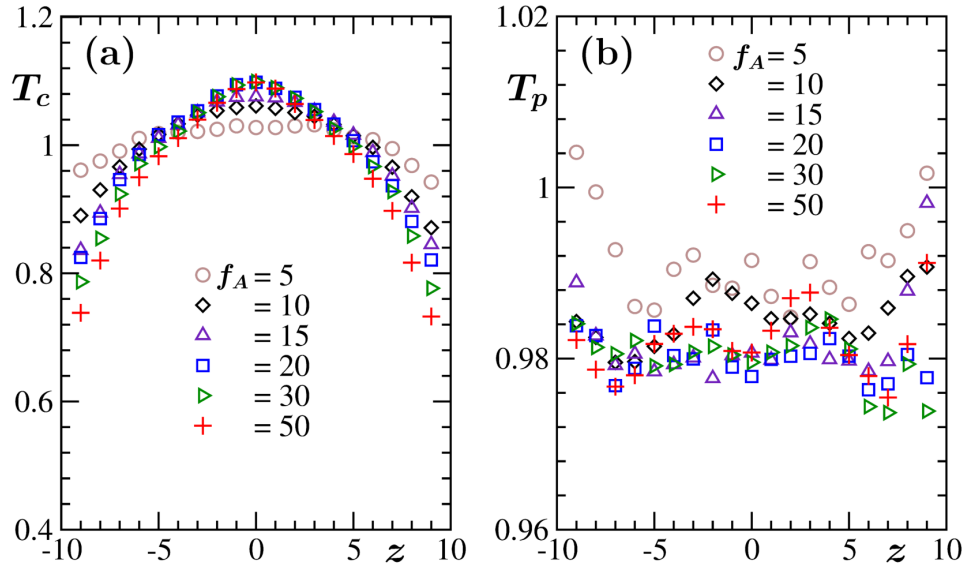
Figure 5.8: The average temperature of colloids, T_c, in (a), and of polymers, T_p, in (b), are plotted versus the distance z along the diameter D_1. Data for several f_A have been shown.
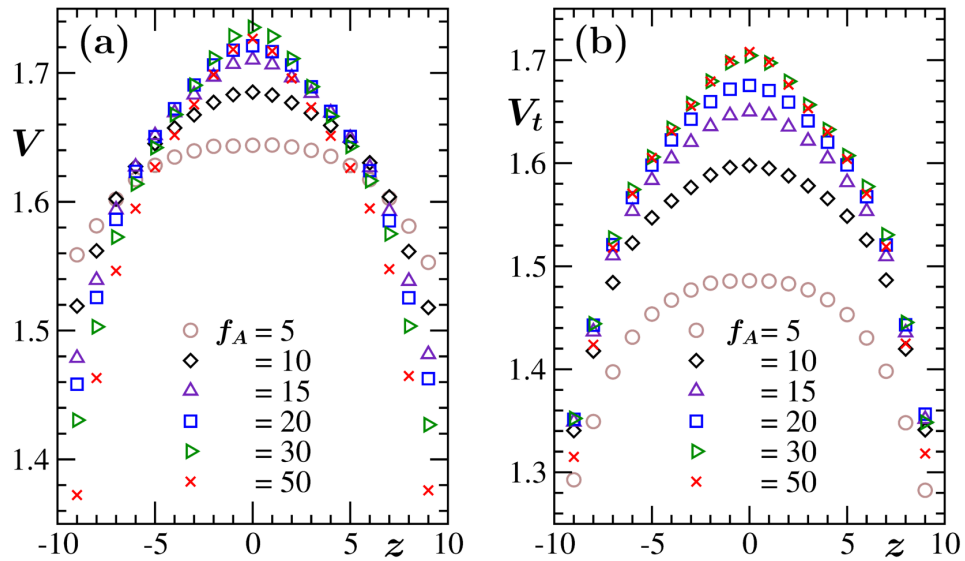
Figure 5.9: The average of the magnitudes of the velocities of the colloids, as a function of z, are shown in (a) and the average of the tangential components of the colloid velocities, with respect to D_1, are plotted versus z in (b), for different f_A.

With the same spirit we calculate the average effective temperatures of colloids (T_c) and polymers (T_p) from their kinetic energies as in Ref. [18], belonging to the disk C_z,

given by

$$T_c(z) = \frac{1}{3k_B N_{c,z}} \sum_{k \in C_z} \vec{v}_{c,k}^2,$$
$$T_p(z) = \frac{1}{3k_B N_{p,z}} \sum_{k \in C_z} \vec{v}_{p,k}^2. \tag{5.7}$$

The sum is carried over the particles (c or p) within the disk C_z. Here $\vec{v}_{c,k}$ and $\vec{v}_{p,k}$ are the velocities of the kth colloid and polymer, respectively. We have shown the variation of T_c and T_p with z, for different f_A, in Fig. 5.8(a) and (b), respectively. We find that T_p is almost uniform but somewhat smaller than the value implied via the noise in Eq. (5.4), while T_c is slightly enhanced near the sphere center and depressed near the sphere surface.

To obtain a better understanding of the time scale of these rotations of colloids around the spheroid that is formed by the polymer, we calculate the average magnitude of the velocities of colloids (V) inside the disk C_z, given by

$$V(z) = \frac{1}{N_{c,z}} \sum_{k \in C_z} |\vec{v}_{c,k}|, \tag{5.8}$$

and the corresponding tangential component of the velocities of colloids, that is

$$V_t(z) = \frac{1}{N_{c,z}} \sum_{k \in C_z} |\vec{v}_{c,k} - \hat{r}_{\perp c,k}(\vec{v}_{c,k} \cdot \hat{r}_{\perp c,k})|, \tag{5.9}$$

where $\hat{r}_{\perp c,k} = \frac{\vec{r}_{\perp c,k}}{|\vec{r}_{\perp c,k}|}$. In Fig. 5.9(a)-(b) we show the variation of V and V_t with z, for different f_A. This indicates that the average velocity of colloids as well as its tangential component is maximum in equator plane ($z = 0$) and decreases gradually towards the poles ($z \to R$).

The estimation of time that is required for a colloid to complete one rotation around the spheroid is given by $t_r = 2\pi r_p / V_t$, where r_p is the average perpendicular distance of colloids inside C_z from D_1, i.e.,

$$r_p(z) = \frac{1}{N_{c,z}} \sum_{k \in C_z} |\vec{r}_{\perp c,k}|. \tag{5.10}$$

In Fig. 5.10(a) we have shown the variation of r_p versus z, for different f_A. The lower value of r_p at higher $|z|$ is mainly due to the geometrical feature, viz., maximum r_p that remains inside the sphere at z is limited to $\sqrt{R^2 - z^2}$. The value of r_p here also gives an

estimation of the extent of the minor axes plane of the spheroid of polymers. The average time (t_r) for one rotation around the spheroid is shown in Fig. 5.10(b) for different f_A. As expected the colloids with higher f_A take less time to perform a rotation and this is very prominent in the equatorial plane [see Fig. 5.10(b)].

Finally, we consider the time dependence of the orientation of the eigenvector corresponding to λ_1, by defining an angle of deviation $\Delta\theta(t_0)$ as

$$\Delta\theta(t_0) = \cos^{-1}(|\hat{e}_1(t_0 + t) \cdot \hat{e}_1(t)|). \tag{5.11}$$
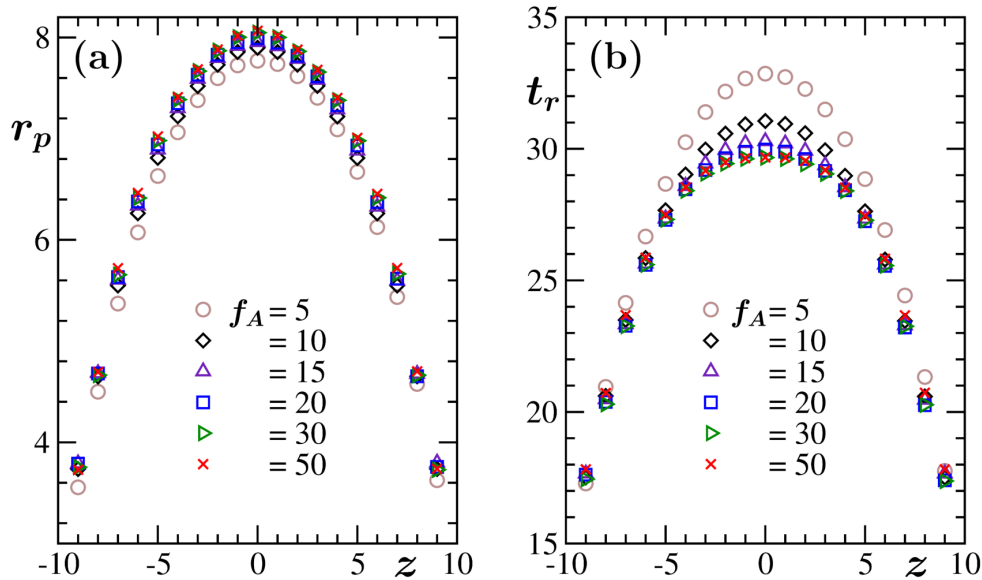
Figure 5.10: (a) The average perpendicular distance of the colloids from D_1 is shown as a function of z. Data for several choices of f_A are shown. (b) The average time t_r ($= 2\pi r_p/V_t$) for one complete rotation around D_1 by colloids are shown for different f_A, versus z.

This angular deviation of the rotation axis is between two steady states at times t and $t + t_0$. We have estimated the distributions of $\Delta\theta$ for different f_A. The probability density functions $P(\Delta\theta)$ have been obtained by fixing t_0 at 100 and are shown in Fig. 5.11(a). Fig. 5.11(b) again shows the distribution $P(\Delta\theta)$, for $t_0 = 100$, demonstrating that it is independent of f_A when $\Delta\theta$ is rescaled with its average. Since the unscaled distribution has its peak around $\Delta\theta = 0.1$, the period over which a particle near the equator takes a full "roundtrip" on the sphere is clearly less than t_0 [for $f_A = 50$ the colloids take an average of $30t_s$ ($t_s = \sqrt{\sigma^2 m/\varepsilon}$) time to perform a rotation that can be
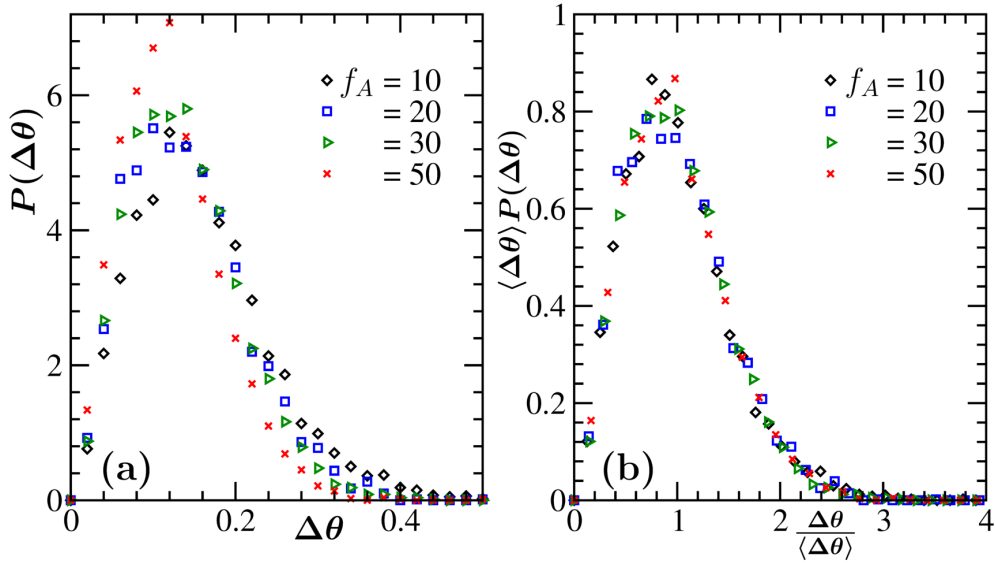
Figure 5.11: (a) The distributions of the angular displacement $\Delta\theta$ are shown for different values of f_A. $P(\Delta\theta)$ in each of the cases has been obtained by fixing t_0 at 100. The observation times (t) belong to the range $[10^4, 3 \times 10^4]$. The distribution, for each f_A, is obtained from a total of 4000 $\Delta\theta$ values (collected from different runs) lying in the above mentioned time range. (b) Plots showing the scaling collapse of the distribution function $P(\Delta\theta)$ of the angular displacement $\Delta\theta$, over time $t_0 = 100$, for different values of f_A.

extracted from Fig. 5.10(b)]. Thus, within this time there is only a small change of the orientation of the axis for the rotational flow.

Tracking one end point of the symmetry diameter D_1 during evolutions in steady states we obtained the trajectories that lie on the surface of the sphere. In Fig. 5.12(a) we have shown a typical trajectory of an end point of the symmetry axis D_1 for $f_A = 20$. From these trajectories, we calculated the mean-squared displacement (MSD) as

$$\text{MSD}(t) = \langle (\vec{r_i}(t) - (\vec{r_i}(0))^2 \rangle, \tag{5.12}$$

where $\vec{r_i}(t) = R\hat{e}_1(t)$, with the average being obtained by considering many such trajectories, for each of the f_A values. In Fig. 5.12(b) we have presented the MSD versus translated time in log-log scale. Here we show that the motion of the endpoint of the rotation axis $\vec{r}_R(t)$ [$= R\hat{e}_1(t)$] is simply diffusive. The diffusion constant has a weak dependence on f_A; it decreases only slightly when f_A increases.
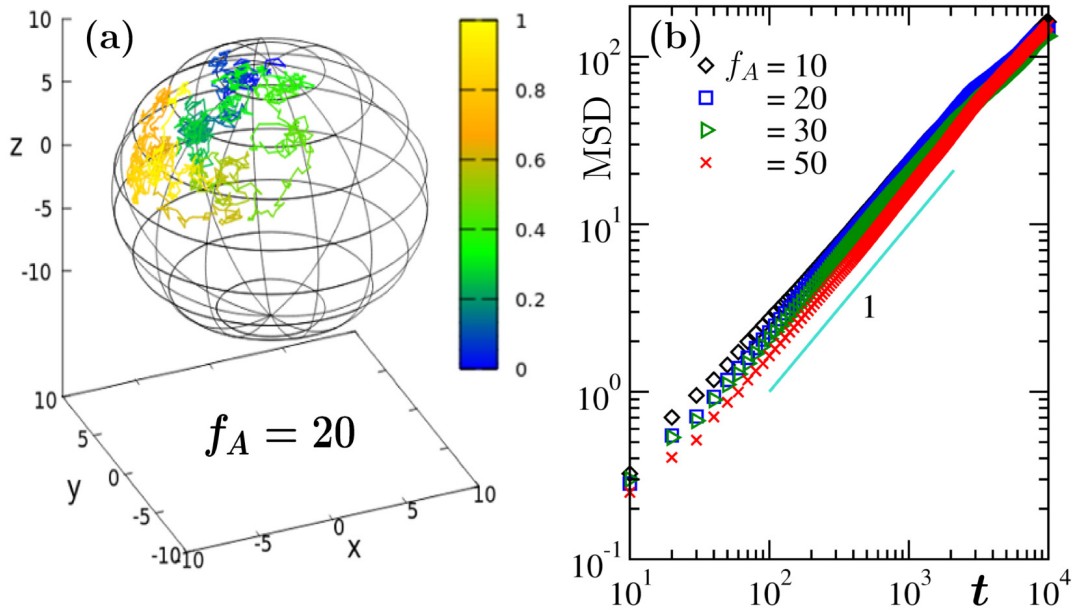
Figure 5.12: (a) A trajectory of a chosen pole of the symmetry axis D_1 for $f_A = 20$. The color code represents the time evolution of a trajectory in steady state of a system in a manner described below. The coordinate systems are transformed in such a way that the starting point is the north pole. The trajectory is shown from a starting time $t_{\min}$ $(= 10^4)$ to a maximum time $t_{\max}$ $(= 2.5 \times 10^4)$. We set the intensity of the color bar $q_{cb} = (t - t_{\min})/(t_{\max} - t_{\min})$, so that $q_{cb} \in [0, 1]$. (b) The mean-squared displacement (MSD) of a pole of the symmetry axis D_1 on the sphere is plotted versus time, for different f_A. The solid line represents a power-law with the mentioned value of the exponent.

5.4   Conclusion

The phase separation caused in colloid-polymer mixtures by depletion forces [58] is enhanced when the colloids are active particles, both in bulk and in spherical confinement. While for equal packing fractions of colloids and polymers, the confining surface remains close to neutral to colloids and polymers in the fully passive system, and, thus, a Janus-like structure is formed, one observes a different picture in the active case. In this situation, the colloids wet the sphere surface completely, with the polymers forming an ellipsoid in the interior. Coherent rotational flow of the colloids occurs around this structure. The principal axis of the ellipsoid exhibits a rotational diffusion, which is slow on the time scale characterizing the rotational flow. Increasing activity slows down the diffusion slightly. In the mixed-phase region of the system, surface enrichment of the colloids occurs, which also is enhanced by the colloid activity. All these findings are qualitatively the same, irrespective of the details of the wall-particle repulsive interactions. It could

be speculated that such collective motions in confined active systems are advantageous in the context of biological processes and functions.

Copyright and Permission

The manuscript for this chapter is submitted to arXiv: A. Bera, K. Binder, S. A. Egorov, and S. K. Das, *Macroscopic rotation of active colloids in a colloid-polymer mixture confined inside a spherical cavity.* arXiv preprint arXiv:2112.00500 (2021).
The link is https://arxiv.org/pdf/2112.00500.pdf.

Bibliography

[1] G. Gompper, R. G. Winkler, T. Speck, A. Solon, C. Nardini, F. Peruani, H. Löwen, R. Golestanian, U. B. Kaupp, and L. Alvarez, J. Phys.: Condens. Matter **32**, 193001 (2020).

[2] M. C. Marchetti, Y. Fily, S. Henkes, A. Patch, and D. Yllanes, Curr. Opin. Colloid Interface Sci. **21**, 34 (2016).

[3] C. Bechinger, R. D. Leonardo, H. Löwen, C. Reichhardt, G. Volpe, and G. Volpe, Rev. Mod. Phys. **88**, 045006 (2016).

[4] M. E. Cates and J. Tailleur, Annu. Rev. Condens. Matter Phys. **6**, 219 (2015).

[5] M. C. Marchetti, J. F. Joanny, S. Ramaswamy, T. B. Liverpool, J. Prost, M. Rao, and A. Simha, Rev. Mod. Phys. **85**, 1143 (2013).

[6] M. J. Bowick, N. Fakhri, M. C. Marchetti, and S. Ramaswamy, Phys. Rev. X **12**, 010501 (2022).

[7] T. Vicsek, A. Czirôk, E. Ben-Jacob, I. Cohen, and O. Shochet, Phys. Rev. Lett. **75**, 1226 (1995).

[8] A. P. Solon, J. Stenhammar, M. E. Cates, Y. Kafri, and J. Tailleur, Phys. Rev. E. **97**, 020602(R) (2018).

[9] G. Liu, A. Patch, F. Bahar, D. Yllanes, R. D. Welch, M. C. Marchetti, S. Thutupalli, and J. W. Shaevitz, Phys. Rev. Lett. **122**, 248102 (2019).

[10] I. Buttinoni, J. Bialké, F. Kümmel, H. Löwen, C. Bechinger, and T. Speck, Phys. Rev. Lett. **110**, 238301 (2013).

[11] Y. Fily and M. C. Marchetti, Phys. Rev. Lett. **108**, 235702 (2012).

[12] T. Speck, J. Bialké, A. M. Menzel, and H. Löwen, Phys. Rev. Lett. **112**, 218304 (2014).

[13] S. A. Mallory, C. Valeriani, and A. Cacciuto, Annu. Rev. Phys. Chem. **69**, 59 (2018).

[14] T. Speck, Phys. Rev. E **103**, 012607 (2021).

[15] F. Turci and N. B. Wilding, Phys. Rev. Lett. **126**, 038002 (2021).

[16] A. K. Omar, K. Klymko, T. GrandPre, and P. L. Geissler, Phys. Rev. Lett. **126**, 188002 (2021).

[17] S. K. Das, S. A. Egorov, B. Trefz, P. Virnau, and K. Binder, Phys. Rev. Lett. **112**, 198301 (2014).

[18] B. Trefz, S. K. Das, S. A. Egorov, P. Virnau, and K. Binder, J. Chem. Phys. **144**, 144902 (2016).

[19] B. Trefz, J. T. Siebert, T. Speck, K. Binder, and P. Virnau, J. Chem. Phys. **146**, 074901 (2017).

[20] K. Binder and P. Virnau, Soft Materials **19**, 267 (2021).

[21] S. Asakura and F. Oosawa, J. Chem. Phys. **22**, 1255 (1954).

[22] S. Asakura and F. Oosawa, J. Polym. Sci. **33**, 183 (1958).

[23] A. Vrij, Pure. Appl. Chem. **48**, 471 (1976).

[24] K. Binder, P. Virnau, and A. Statt, J. Chem. Phys. **141**, 140901 (2014).

[25] R. L. C. Vink and J. Horbach, J. Chem. Phys. **121**, 3253 (2004).

[26] R. L. C. Vink, J. Horbach, and K. Binder, Phys. Rev. E **71**, 011401 (2005).

[27] J. Zausch, P. Virnau, K. Binder, J. Horbach, and R. L. C. Vink, J. Chem. Phys. **130**, 064906 (2009).

[28] M. P. Allen and D. J. Tildesley, *Computer Simulations of Liquids* (2nd ed. Oxford Univ. Press, 2017).

[29] A. Winkler, A. Statt, P. Virnau, and K. Binder, Phys. Rev. E. **87**, 032307 (2013).

[30] T. N. Shendruk, A. Doostmohammadi, K. Thijssen, and J. M. Yeomans, Soft Matter **13**, 3853 (2017).

[31] G. Duclos, C. Blanch-Mercader, V. Yashursky, G. Salbreux, J.-F. Joanny, J. Prost, and P. Silberzan, Nat. Phys. **14**, 728 (2018).

[32] H. Wioland, F. G. Woodhuse, J. Dunkel, J. O. Kessler, and R. E. Goldstein, Phys. Rev. Lett. **110**, 268102 (2013).

[33] F. G. Woodhouse and R. E. Goldstein, Phys. Rev. Lett. **109**, 168105 (2012).

[34] T. Gao, M. D. Betterton, A. S. Jhang, and M. J. Shelley, Phys. Rev. Fluids **2**, 093302 (2017).

[35] A. Doostmohammadi and J. M. Yeomans, Eur. Phys. J. Special Topics **227**, 2401 (2019).

[36] K.-T. Wu, J. B. Hishamunda, D. T. N. Chen, S. J. DeCamp, Y.-W. Chang, A. Fernández-Nieves, S. Fraden, and Z. Dogic, Science **355**, 6331 (2017).

[37] J. Elgeti and G. Gompper, Europhys. Lett. **101** 48003 (2013).

[38] Y. Baek, A. P. Solon, X. Xu, N. Nikola, and Y. Kafri, Phys. Rev. Lett. **120**, 058002 (2018).

[39] Y. B. Dor, S. Ro, and Y. Kafri, M. Kardar, and J. Tailleur, arXiv: 2108.13409v3 (2021).

[40] I. D. Vladescu, E. J. Marsden, J. Schwarz-Linek, V. A. Martinez, J. Arlt, A. N. Morozov, D. Marenduzzo, M. E. Cates, and W. C. K. Poon, Phys. Rev. Lett. **113**, 268101 (2014).

[41] X. Yang, M. L. Manning, and M. C. Marchetti, Soft Matter **10**, 6477 (2014).

[42] J. P. Hernandez-Ortiz, C. G. Stoltz, and M. D. Graham, Phys. Rev. Lett. **95**, 204501 (2005).

[43] A. P. Solon, H. Chaté, and J. Tailleur, Phys. Rev. Lett. **114**, 068101 (2015).

[44] K. Miyazaki, K. S. Schweizer, D. Thirumalai, R. Tuinier, and E. Zaccarelli, J. Chem. Phys. **156**, 080401 (2022).

[45] F. C. Keber, E. Loiseau, T. Sanchez, S. J. DeCamp, L. Giomi, M. J. Bowick, M. C. Marchetti, Z. Dogic, and A. R. Bausch, Science **345**, 1135 (2014).

[46] R. Sknepnek and S. Henkes, Phys. Rev. E **91**, 022306 (2015).

[47] S. Shankar, M. J. Bowick, and M. C. Marchetti, Phys. Rev. X **7**, 031039 (2017).

[48] P. W. Ellis, D. J. G. Pearce, Y.-W. Chang, G. Goldsztein, L. Giomi, and A. Fernandez-Nieves, Nat. Phys. **14**, 85 (2018).

[49] S. Henkes, M. C. Marchetti, and R. Sknepnek, Phys. Rev. E **97**, 042605 (2018).

[50] J. D. Weeks, D. Chandler, and H. C. Andersen, J. Chem. Phys. **54**, 5237 (1971).

[51] A. Statt, A. Winkler, P. Virnau, and K. Binder, J. Phys: Condens. Matter **24**, 464122 (2012).

[52] A. Zöttl and H. Stark, J. Phys.: Condens. Matter **28**, 253001 (2016).

[53] S. K. Das, J. Chem. Phys. **146**, 044902 (2017).

[54] S. Chakraborty and S. K. Das, J. Chem. Phys. **153**, 044905 (2020).

[55] S. Paul, A. Bera, and S. K. Das, Soft Matter **17**, 645 (2021).

[56] K. Šolc and W. H. Stockmayer, J. Chem. Phys. **54**, 2756 (1971).

[57] H. Arkin and W. Janke, J. Chem. Phys. **138**, 054904 (2013).

[58] A. Milchev and A. Bhattacharya, J. Chem. Phys. **117**, 5415 (2002).

Chapter 6

Structure and Dynamics in a Mixture of Active and Passive Particles on Curved and Flat Surfaces

6.1 Introduction

Active particles consume energy continuously and the supplies from the environment can keep the systems in steady state which is the counterpart of equilibrium for systems consisting only of passive particles. Active particles and systems appear in nature covering a wide span of length scales, from nanoscopic molecular motors [1] to microscopic bacterial colony [2] to flock of birds [3] at the macro scale. There has been immense interest in understanding the structure and dynamics in such systems in various disciplines of sciences. These systems can exhibit phase transitions. Often they exhibit collective dynamics where particles show coherent motion and form high density clusters. A popular model to capture these features is the Vicsek model [4], in which particles align their directions along the average velocity directions of neighbors. The flocking of active clusters in Vicsek model is observed at low noise and high density of particles.

There often exist mixtures of particles having different mass, self-propulsion, diffusion constant, size, etc. The phase separation in such systems can occur due to a mismatch in any of the above aspects. Here we consider phase separation in a binary mixture of active and passive particles. The two species differ from each other only in self-propulsion,

with all the other properties remaining the same. Demixing transition in mixtures of active and passive particles have been studied in various contexts [5–9]. These studies, in two-dimensional geometry, are mainly on planar surfaces. But in nature curved surfaces are common.

The outcomes may be different in presence of curvature. While on a flat surface packing of disk-like particles are possible without any defect, say, with a hexagonal arrangement of particles. This is not true in presence of curvature, over a long spatial range. Thus, defects arise more easily in presence of curvature. This has a connection to the problem of, e.g., tiling on the surface of a soccer ball with hexagons and pentagons. The formation and growth of spherical crystals belong to this category of problems in passive systems [10, 11]. There also exists interest concerning structure formation and dynamics of growth in systems of active particles in presence of curvature [12–17]. In our study, we compare results on various aspects of demixing transitions in mixtures of active and passive particles on spherical and flat surfaces. We have considered only aligning self-propelled particles, similar to the Vicsek model [4].

6.2   Model and Methods

For both types of surfaces we have taken N_A active particles and N_B passive particles in $50 : 50$ ratio, i.e., $N_A = N_B$. We take the particles to be of equal mass and equal diameter. The total number of particles is N. The overall packing fraction on a spherical surface is given by $\phi = \frac{N\pi(\sigma/2)^2}{4\pi R^2} = \frac{N\sigma^2}{16R^2}$, where σ is the diameter of a particle and R is the radius of the sphere. In the case of a plane, $\phi = \frac{N\pi(\sigma/2)^2}{L^2} = \frac{N\pi\sigma^2}{4L^2}$, where L is length of the square box. We have considered the total packing fraction $\phi = 0.4$ for both the cases and focused on the pattern and dynamics. Below we discuss the details of the models.

6.2.1   Spherical Surface

Here all particles move on the surface of a sphere of radius R that has the center at $(0, 0, 0)$. The position vector $\vec{r}_i$ and the direction of the self-propulsion $\hat{n}_i$ of the ith particle exhibit two constraints of motion. These are $|\vec{r}_i| = R$ and $\vec{r}_i \cdot \hat{n}_i = 0$, $\forall\, i$. Note that the motion is restricted to the directions tangential to the surface. In our systems there exists no self-propulsion of passive particles. The dynamics of the system is taken care of via the over-damped Langevin equations [19–22]:

From triangle APO$'$
$$r_c^2 = h^2 + a^2$$
From triangle POO$'$
$$R^2 = (R-h)^2 + a^2$$
$$\Rightarrow 2Rh = h^2 + a^2 = r_c^2$$
Area of the cap
$$S_v = 2\pi Rh = \pi r_c^2$$
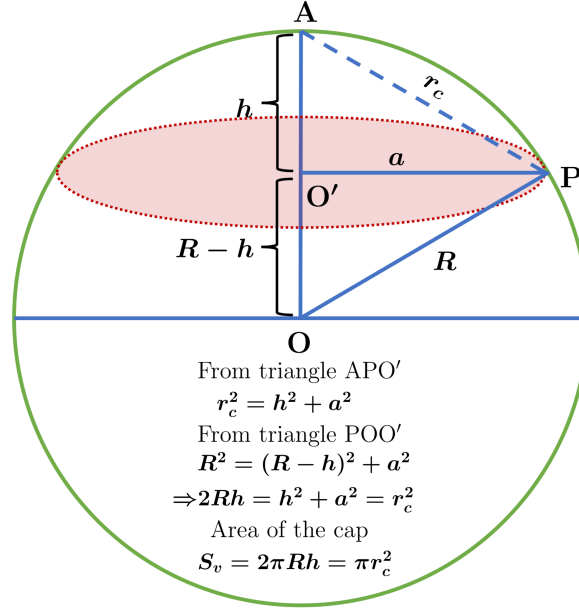
Figure 6.1: A schematic diagram is shown for alignment interaction region of a particle situated at the point A. The spherical surface above the circular plane centered at O$'$ (colored region) is the alignment interaction region $\mathbb{S}$, within which the maximum distance (Euclidean) from the point A is r_c. The area of the spherical cap $\mathbb{S}$ is given by $S_v = \pi r_c^2$.

$$\dot{\vec{r}}_i = v_0 \hat{n}_i + \mu[\vec{F}_i - (\vec{F}_i \cdot \hat{r}_i)\hat{r}_i], \tag{6.1}$$

$$\dot{\hat{n}}_i = \frac{K}{S_v} \sum_{j \in \mathbb{S}} [\hat{T}_{j,i} - (\hat{T}_{j,i} \cdot \hat{n}_i)\hat{n}_i] + \xi_i(\hat{r}_i \times \hat{n}_i). \tag{6.2}$$

In Eq. (6.1) v_0 is the self-propulsion speed that is taken to be the same for all the active particles. We have $v_0 = 0$ for all the passive particles. Here μ is the mobility and $\vec{F}_i$ is the force due to inter-particle (passive) interactions. To constrain the motion of the particles on the spherical surface we need to nullify all the normal components (with respect to the spherical surface) of force (and velocity) of each particle. The term $(\vec{F}_i \cdot \hat{r}_i)\hat{r}_i$, in Eq. (6.1), is the component of the force $\vec{F}_i$ acting along the normal direction of the spherical surface and is subtracted due to the above mentioned reason. For preventing overlap, we have taken a repulsive potential among all the particles. This has the standard Weeks-Chandler-Andersen (WCA) form [25]

$$u(r) = \begin{cases} 4\varepsilon \left[\left(\frac{\sigma}{r}\right)^{12} - \left(\frac{\sigma}{r}\right)^6 + \frac{1}{4} \right], & \text{for } r < 2^{\frac{1}{6}}\sigma \\ 0, & \text{otherwise;} \end{cases} \tag{6.3}$$
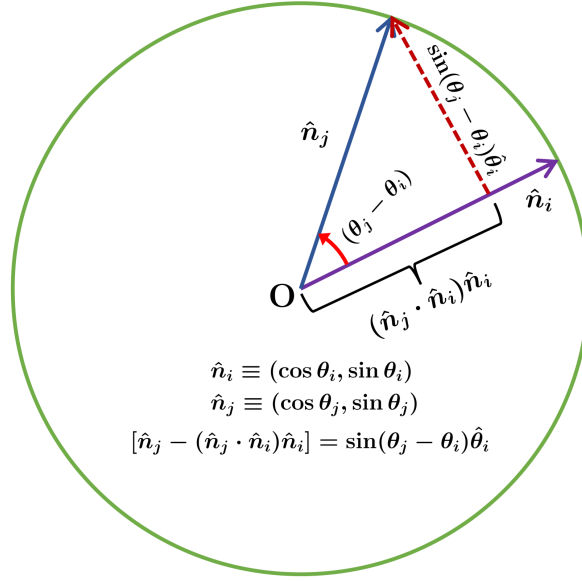
Figure 6.2: Schematic representation of the direction of alignment force due to the interactions of a particle i having propulsion direction $\hat{n}_i$ with particle j. Here $\hat{\theta}_i$ is the unit vector along the direction of increasing θ_i.

where ε is the interaction strength, σ is the diameter of each particle and r is the inter-particle Euclidean distance. The particles here move due to the forces arising from self-propulsion and the interparticle passive interactions. Note that we have neglected translational diffusion.

The dynamical equation for self-propulsion direction $\hat{n}_i$, that is written only for active particles, as noted in Eq. (6.2), contains two terms. The first term on the right hand side is the alignment interaction arising due to the coupling of self-propulsion of a particle with the self-propelling directions of its neighbors. For the range of the alignment interaction, we have considered a spherical cap $\mathbb{S}$ for a particle i that stays at the center of the cap on the spherical surface. This has been demonstrated in the schematic diagram in Fig. 6.1, that shows the position of the particle i (point A) and the corresponding sphere cap. A particle j is considered to be a neighbor of particle i, if $|\vec{r}_i - \vec{r}_j| \leq r_c$. The curved surface area of the cap is $S_v = 2\pi Rh = \pi(a^2 + h^2)$, where h is the height of the cap and a is the radius of the base of the cap. From Fig. 6.1 we have $r_c = \sqrt{a^2 + h^2}$, that gives $S_v = \pi r_c^2$. Due to different tangent planes on the spherical surface, we have transformed the propulsion direction $\hat{n}_j$ in such a way that only its component in the tangent plane at $\hat{r}_i$ is relevant. The transformed direction of $\hat{n}_j$ is $\hat{T}_{j,i}$, which is given by [23]. The interaction in Eq. (6.2) resembles the interactions in Kuramoto model [24] for synchronization of phases of oscillators in space dimension d. While the standard

Kuramoto model deals with long range interactions among oscillators, here we consider a short-range interaction. Each particle here has the tendency to align with its neighbors with a coupling strength K [24].

$$\hat{T}_{j,i} = \frac{\hat{n}_j - (\hat{n}_j \cdot \hat{r}_i)\hat{r}_i}{|\hat{n}_j - (\hat{n}_j \cdot \hat{r}_i)\hat{r}_i|}. \tag{6.4}$$
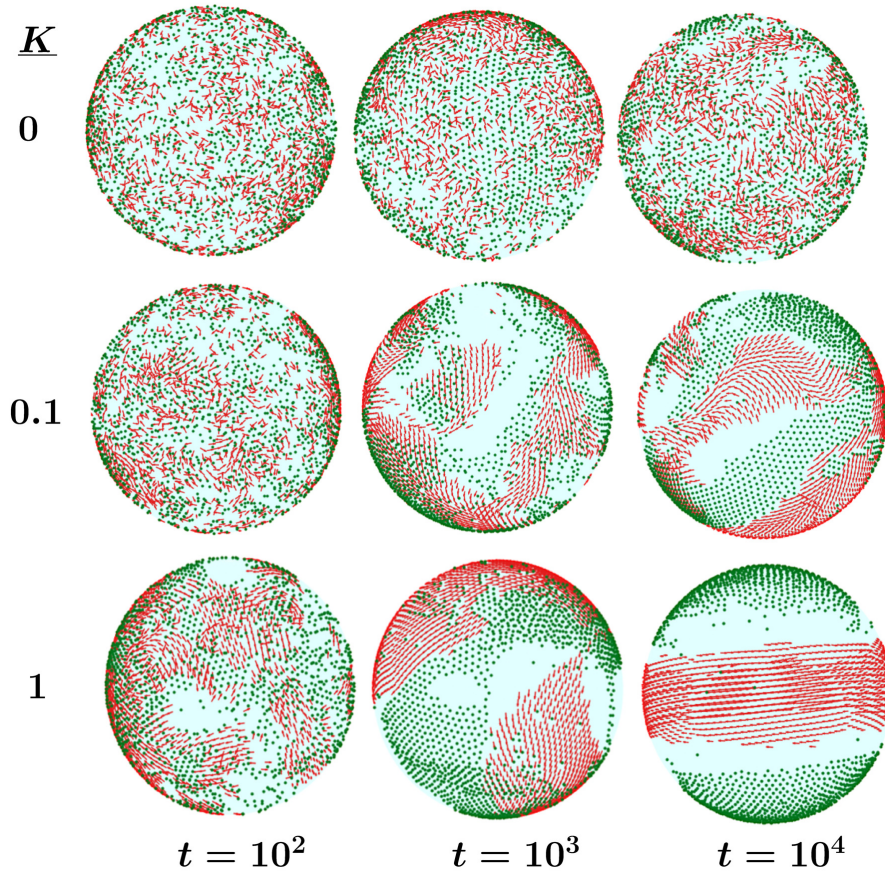
Figure 6.3: Snapshots during evolutions are presented for different K values for particles on sphere problem. The propulsion directions of the active particles are shown by arrow headed red lines. The locations of passive particles are shown in green. These results are obtained for $R = 20$, $v_0 = 0.5$, $\nu_r = 10^{-4}$ and $\phi = 0.4$.

The second term in Eq. (6.2) is related to the random rotational diffusion of particles. Here ξ_i is a Gaussian noise that is responsible for the angular rotation of $\hat{n}_i$ at the tangent plane at $\hat{r}_i$. It is delta-correlated with zero mean as

$$\langle \xi_i(t) \rangle = 0, \tag{6.5}$$
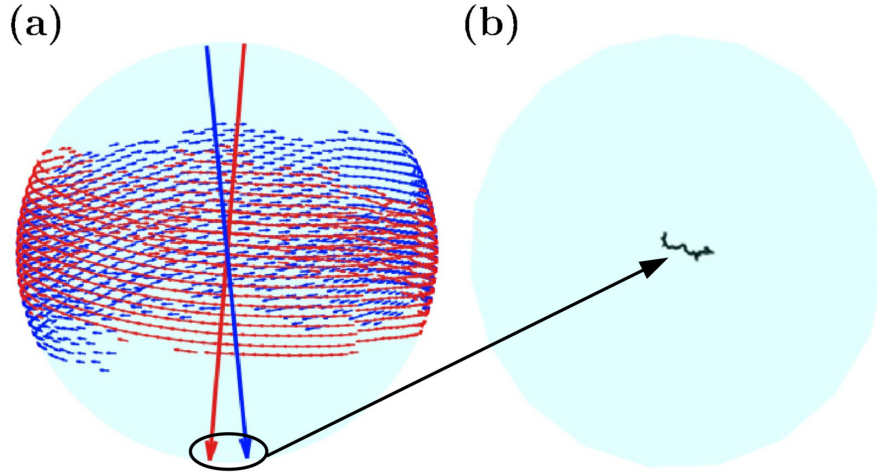
Figure 6.4: (a) The propulsion directions of the active particles are shown for $K = 10$, at time $t = 4 \times 10^3$ (blue) and 10^4 (red), with corresponding directions of rotation axis $\hat{w}$ that are shown in same color as the propulsion fields. (b) The trajectory of $\hat{w}$ on the sphere surface in a time span $t \in (2 \times 10^3, 10^4)$, for $K = 10$. In this case, for visualization purpose, the sphere is differently oriented than in (a).
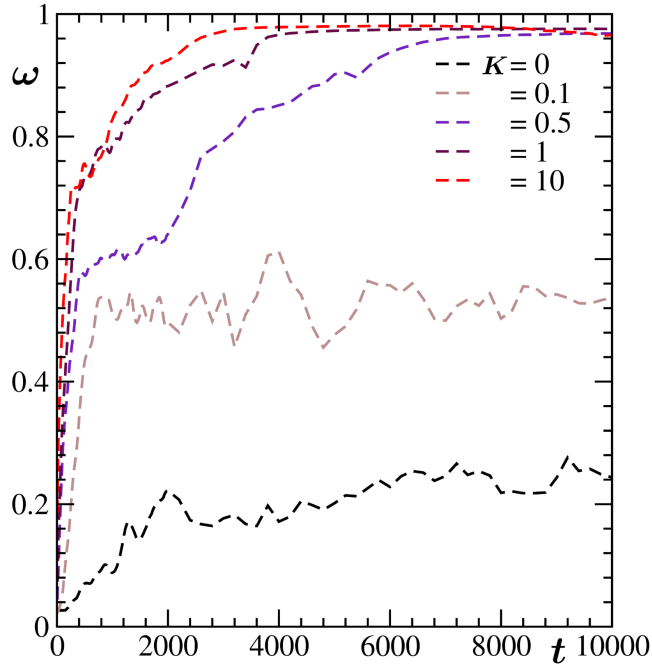
Figure 6.5: Order parameter, ω, is shown versus time. Results are included for different values of K. These are obtained for $v_0 = 0.5$.

$$\langle \xi_i(t) \xi_j(t') \rangle = \nu_r \delta_{ij} \delta(t - t'). \tag{6.6}$$
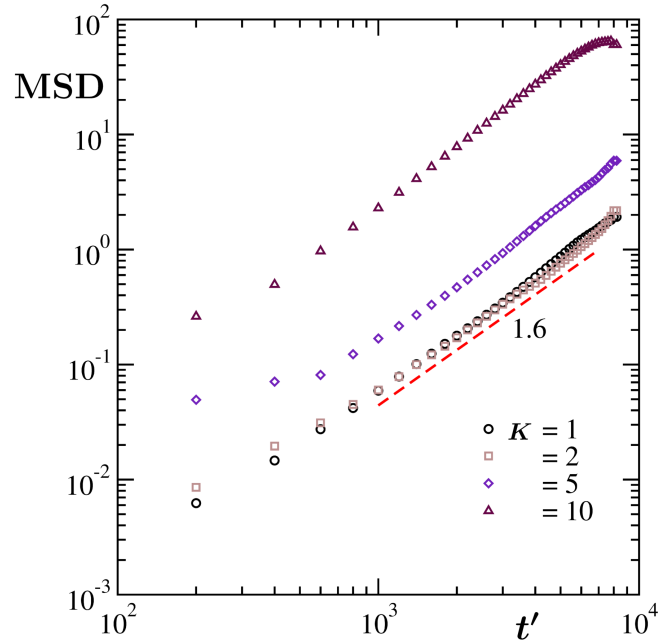
Figure 6.6: Mean-squared displacement (MSD) of the directions of the rotation axis $\hat{\omega}$ has been presented for different K. These results are for $v_0 = 0.5$.

Here ν_r is related to the rotational diffusion constant of the active particles. The competition between K and ν_r gives rise to interesting dynamics. While $K = 0$ and $\nu_r > 0$ represent active Brownian particles, $K >> \nu_r$ is the situation when alignment interaction dominates over the rotational diffusion of particles. We use $v_0 = 0$, $K = 0$ and $\nu_r = 0$, for all passive particles.

6.2.2   Flat Surface

We also study the structure and dynamics of systems of particles that are restricted to a two dimensional Euclidean plane, say, inside a square box in XY plane. In this case, directions of force and velocity remain always on the plane. Thus, the governing Eq. (6.1) simplifies to

$$\dot{\vec{r}}_i = v_0 \hat{n}_i + \mu \vec{F}_i. \tag{6.7}$$

On a flat surface, the self-propulsion direction can be represented by a scalar variable θ_i, which is the angle between the propulsion direction and X-axis, viz., $\hat{n}_i = (\cos\theta_i, \sin\theta_i)$. In a schematic diagram in Fig. 6.2 we have shown that $[\hat{n}_j - (\hat{n}_j \cdot \hat{n}_i)\hat{n}_i] = \sin(\theta_j - \theta_i)\hat{\theta}_i$, where $\hat{\theta}_i = (-\sin\theta_i, \cos\theta_i)$ is the unit direction along the increasing θ_i. Note that here transformation of $\hat{n}_j$ to $T_{j,i}$ is not needed. Furthermore, since there is no curvature
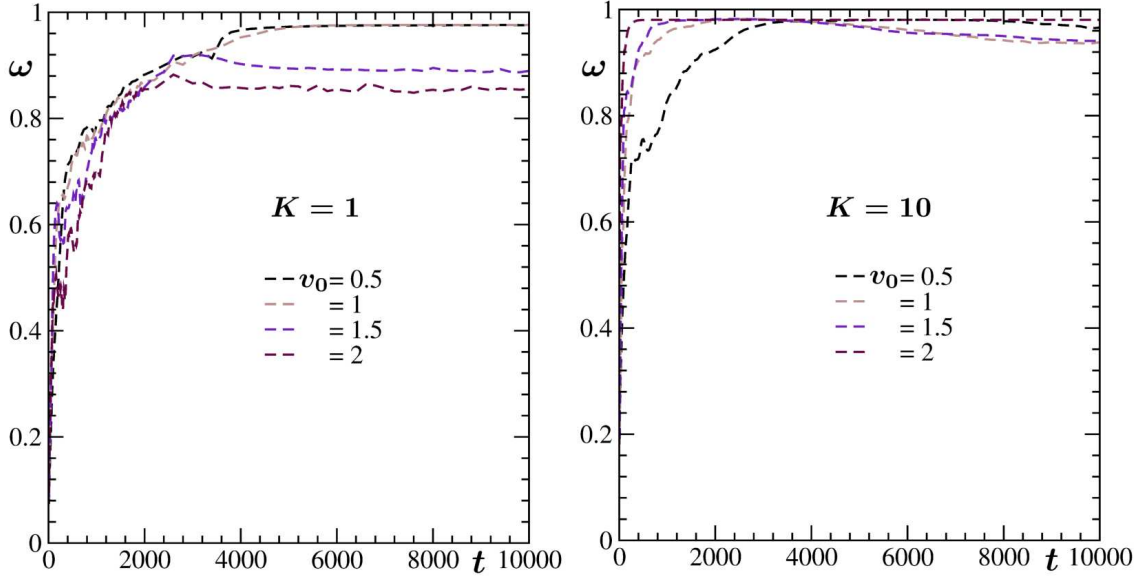
Figure 6.7: (a) Evolutions of the order parameter ω for different self-propulsion speed v_0, by fixing $K = 1$. (b) Same as (a) but for $K = 10$.

involved, $\hat{r}_i \times \hat{n}_i$ is irrelevant here. Thus, the update Eq. (6.2) for the propulsion direction can be written as

$$\dot{\theta}_i = \frac{K}{S_v} \sum_{j \in \mathbb{S}} \sin(\theta_j - \theta_i) + \xi_i. \tag{6.8}$$

Here the interaction area $\mathbb{S}$ is a circle of radius r_c, i.e., $S_v = \pi r_c^2$. For this case we have put the particles inside a square box of side L with periodic boundary conditions (PBC) in all directions.

Eq. (6.2) is a more general equation and it is expected to provide a good description for any curvature with an appropriate choice of the curvature correction term $\hat{T}_{j,i}$.

The length, energy and time scales are measured in units of σ, ε and t_s $(= \sqrt{m\sigma^2/\varepsilon})$, respectively. For both the cases we have taken $r_c = 2.5\sigma$. In all cases, the equations of motion are integrated with time step $\delta t = 10^{-4} t_s$, using a standard Euler-Maruyama method [26, 27]. Such a small step becomes necessary due to the presence of curvature.

6.3 Results

The simulations for curved surfaces are performed on a sphere of radius $R = 20$. For flat surfaces, we have considered a square box with side $L = 100$ and PBC in all directions. All results are presented by fixing $\nu_r = 10^{-4}$.
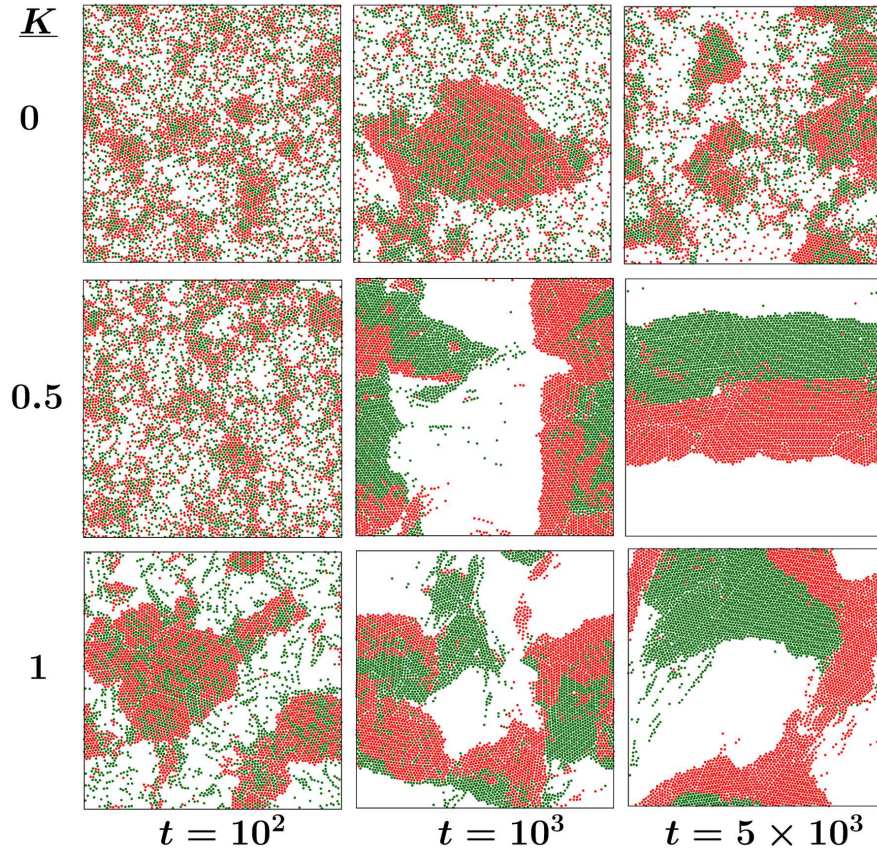
Figure 6.8: Evolution snapshots are presented for different K values, for $v_0 = 0.5$. The passive and active particles are shown in green and red filled circles, respectively. These results are obtained for $L = 100$, $v_0 = 0.5$, $\nu_r = 10^{-4}$ and $\phi = 0.4$. Here and in the rest of the chapter all results correspond to flat surface.

6.3.1 Spherical Surface

Snapshots during the evolution of the systems for different coupling strengths K are presented in Fig. 6.3, by fixing the self-propulsion speed at $v_0 = 0.5$. For $K = 0$ no clear phase separation is seen. The introduction of alignment coupling among particles has a drastic effect. While for intermediate K there exist many active clusters that are moving in different directions, higher K leads to the formation of a rotating ring of active particles. The ring occupies the equatorial part of the surface and passive particles stay near the poles. The formation of a similar kind of ring on a spherical surface has been reported also in earlier studies [21, 22]. In our study there exists a vapor phase between the ring and the passive clusters. That is due to the dancing of the ring while maintaining the overall shape. Below we focus on the steady state dynamics of the ring.
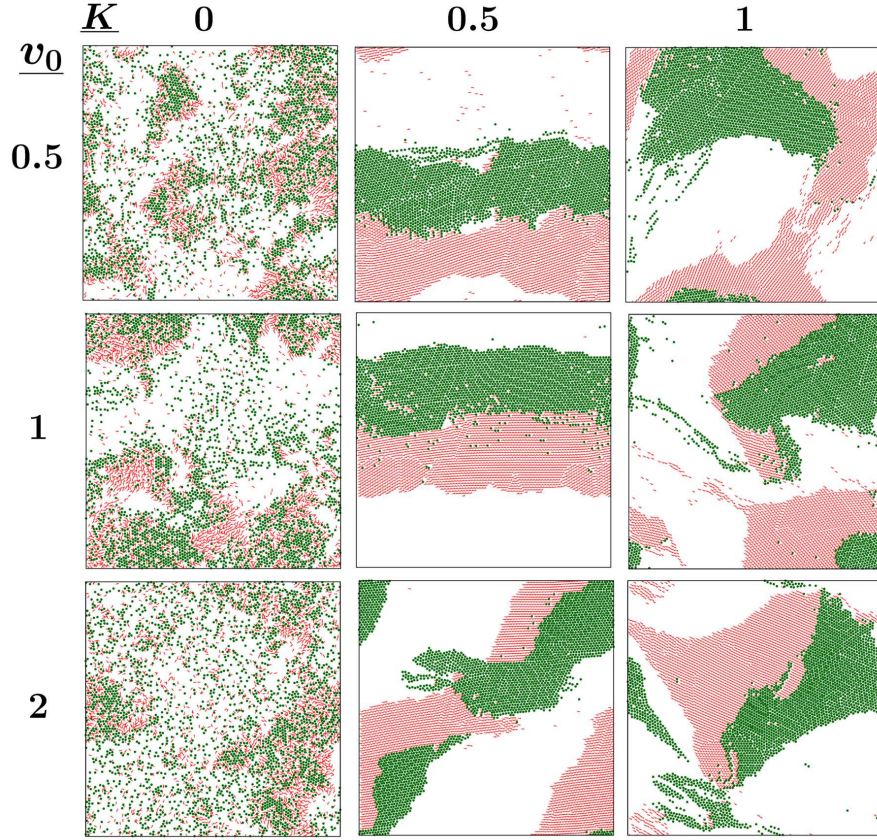
Figure 6.9: Propulsion fields of active particles and the location of passive particles are shown for different values of K and v_0. The propulsion directions of the active particles are shown in arrow headed red lines, while the locations of passive particles are marked in green circles. The snapshots are presented from $t = 5 \times 10^3$. These results are for $L = 100$, $\nu_r = 10^{-4}$.

The swarming of active particles on the spherical surface can be quantified via the average angular momentum $(\vec{\omega})$ of active particles. This is defined as [23]

$$\vec{\omega} = \frac{1}{N_A} \sum_{i=1}^{N_A} \hat{r}_i \times \hat{n}_i. \tag{6.9}$$

Here $\hat{r}_i \; (=\vec{r}_i/|\vec{r}_i|)$ and $\hat{n}_i$ are the unit vectors normal to the spherical surface and self-propulsion direction corresponding to active particle i, respectively. We consider $\omega \; (= |\vec{\omega}|)$ as the order parameter of the system. For random motion of particles on the surface ω will be small. For the aligned motion of particles, $\omega \to 1$. Note that $\hat{\omega} \; (= \vec{\omega}/\omega)$ provides the direction of the rotation axis.

(a)   **(b)**
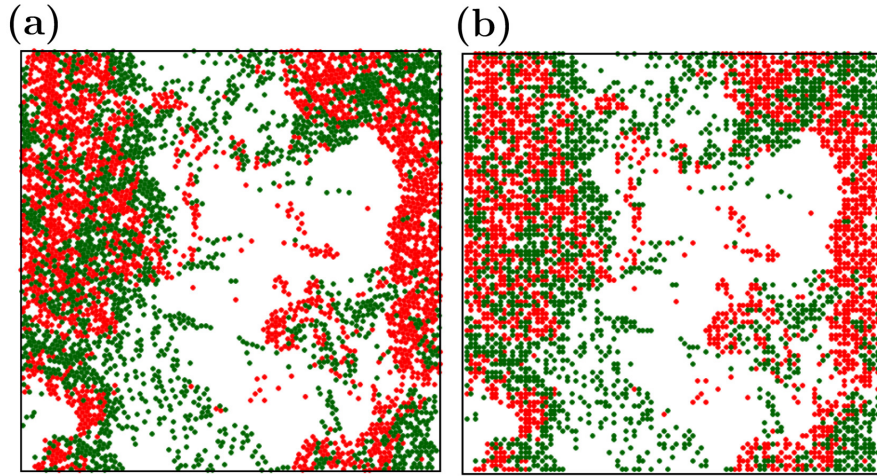
Figure 6.10: (a) A configuration with $K = 0.1$, $v_0 = 0.5$ and $t = 800$ is shown. (b) Snapshot after mapping the configuration in (a) to a square lattice is presented. Here A (B) type of particle is marked in red (green).

In Fig. 6.4(a), we have shown the directions of the rotation $\hat{\omega}$ of the ring at two different times for mentioned parameter values. The change in $\hat{\omega}$ with time is visible, though weak. We presented a trajectory of the tip of $\hat{\omega}$ on the sphere surface for the period between $t = 2 \times 10^3$ and 10^4. See Fig. 6.4(b). The trajectory covers a very small portion of the surface and that indicates fluctuations of the rotating ring of active particles. From such trajectories we have calculated the Mean-squared displacement (MSD) as

$$\text{MSD}(t') = R^2 \langle (\hat{\omega}(t_0 + t') - \hat{\omega}(t_0))^2 \rangle, \qquad (6.10)$$

where t' is the time measured from the beginning of observation at t_0.

In Fig. 6.5 we present the evolution of the order parameter ω for different K, by setting the propulsion speed $v_0 = 0.5$. As mentioned earlier, higher value of ω indicates the formation of the ring. This formation clearly becomes faster for higher value of K.

In Fig. 6.6 we present plots of MSD versus translated time (t'), for different K, by keeping $v_0 = 0.5$. These results indicate that the fluctuations of the ring are stronger for higher values of K.

To check for the effect of self-propulsion speed on the formation of ring, we have calculated ω versus t for different v_0 and presented the results in Fig. 6.7(a) for $K = 1$ and in Fig. 6.7(b) for $K = 10$. For a lower value of K, the formation of the ring gets delayed and distorted in the case of higher propulsion speed. See the lower saturation value of ω for higher v_0 in Fig. 6.7(a). For a higher value of K, the ring formation
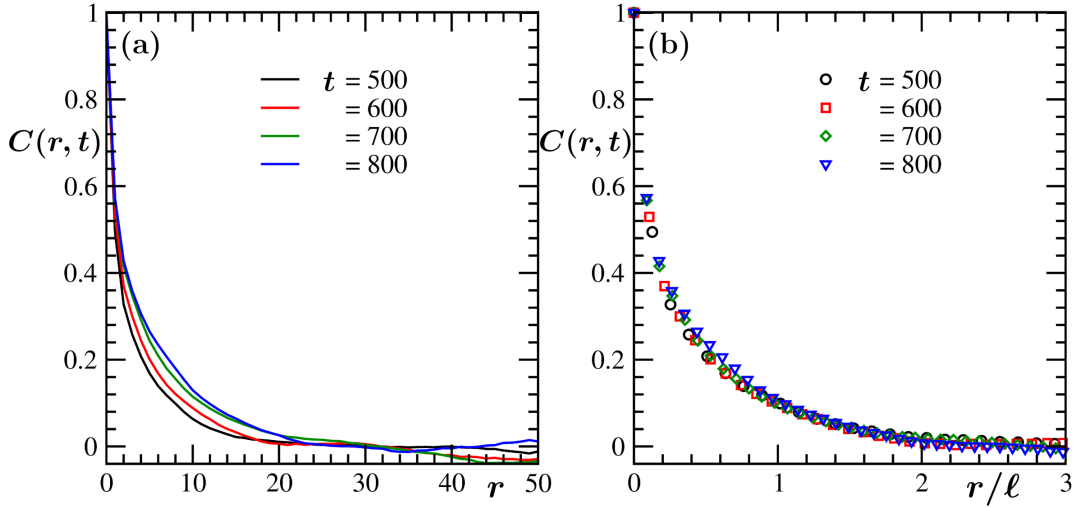
Figure 6.11: (a) $C(r,t)$ versus r from different times are shown. (b) Scaling of $C(r,t)$ is demonstrated. These results are obtained for $K = 0.1$ and $v_0 = 0.5$.

is faster for higher v_0, although there exists asymmetry in the form of dancing of the rotating ring at late times.

6.3.2   Flat Surface

In Fig. 6.8 we have shown the evolution snapshots for different values of K, for $v_0 = 0.5$. There is clustering of active particles without any alignment interactions ($K = 0$). The clustering of passive particles is not observed in this case, although the passive particles get trapped inside clusters of active particles. With the introduction of alignment strength, the process of separation between active and passive particles gets enhanced. The directional mobility of clusters of active particles leads to the clustering of passive particles. For a non-zero value of K, the clusters of active and passive particles stay in contact as shown in Fig. 6.8, unlike in the case of the spherical surface.

In Fig. 6.9 we have shown the propulsion directions of active particles as well as the locations of passive particles, at time $t = 5 \times 10^3$, for different K and v_0. For all of the cases, the directions of self-propulsion have positive non-zero components towards the passive clusters. That indicates that the clusters of active particles are pushing the clusters of passive particles along with them.

To characterize the morphology we calculate the two-point correlations. As there is similarity of this case with the morphology of q-state Potts model [28–30] with $q = 3$,
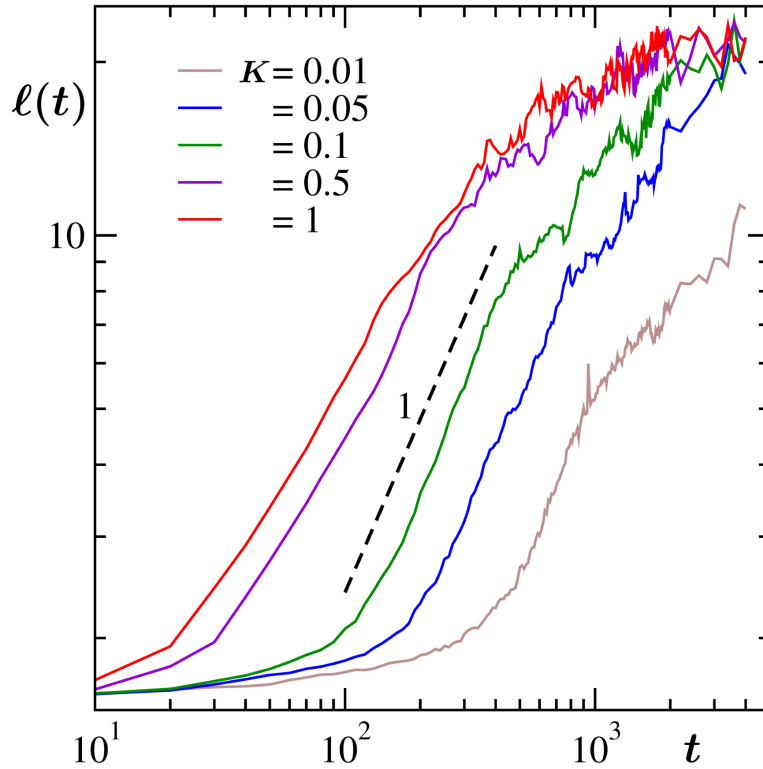
Figure 6.12: Average domain length, $\ell(t)$, is shown with time for different K values, with $v_0 = 0.5$. The dashed line represents a power-law growth with mentioned exponent.

the correlation function in this case can be defined as [30]

$$C(r,t) = \frac{q}{q-1} \left(\langle \delta_{S_i,S_j} \rangle_{|i-j|=r} - \frac{1}{q} \right). \tag{6.11}$$

Here S_i is a spin variable and the averaging is performed over all pairs of species at a distance r apart. To calculate $C(r,t)$ in the off-lattice system here, we have mapped our systems onto a square lattice, as shown in 6.10.

We have calculated $C(r,t)$ considering all the three phases ($q = 3$), e.g., A-rich, B-rich and particle-poor vapor phases that are present in the system. In Fig. 6.11(a) we have presented $C(r,t)$ versus r, at different times. The average domain length (ℓ) is obtained from the decay of $C(r,t)$ to a certain value, viz., 0.1, i.e., $C(r = \ell(t),t) = 0.1$. The scaling of $C(r,t)$ has been obtained from different times by dividing the inter-particle distance r by $\ell(t)$. This is shown in Fig. 6.11(b) for $K = 0.1$ and $v_0 = 0.5$. In Fig. 6.12 we showed the average domain length, $\ell(t)$, versus t, for different K. The growth is enhanced with the increase of K. Approximately linear growth can be appreciated. However, in the scaling region of $C(r,t)$ the growth is weaker. As there exist two different kinds of
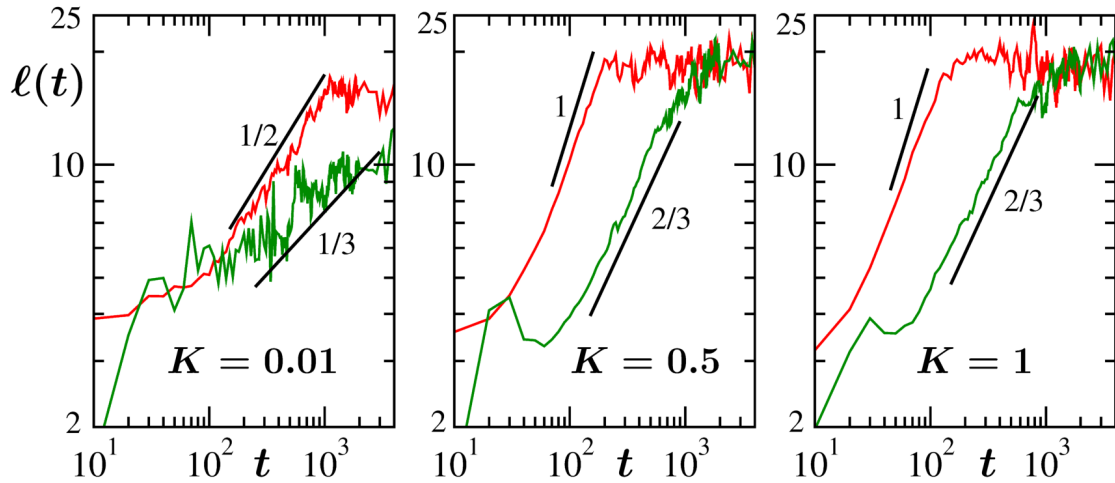
Figure 6.13: Average domain length, $\ell(t)$, of active and passive particles are shown by the red and green solid lines, respectively, for different values of coupling strength K. The black solid lines represent power-law growth with mentioned exponents. The value of v_0 is fixed at 0.5.

particles, the growth dynamics can be different for each of the species. In Fig. 6.13 we have shown the average lengths of domains for active and passive particles for different values of K. The growth is faster for the active species. Also, for the considered values of K, the onset is earlier for the active particles. The delayed growth in passive particles is indicative of the fact that clusters of active particles (forward) drag the clusters of passive particles.

6.4   Conclusion

We have studied the dynamics of phase separation in a mixture of active and passive particles spread over spherical and flat surfaces. In our model there exist local alignment interactions among active particles that self-propel. In the case of a spherical surface, for a higher value of the alignment parameter K the phase separation between active and passive particles leads to the formation of a ring of active particles near the equatorial region, while the passive particles form caps on two poles of the sphere. There exist small fluctuations of the ring that we capture via the calculation of mean-squared displacement of the trajectory of the tip of the rotation axis on the sphere surface. The fluctuation is higher for higher values of K. The same model gives rise to phase separation on the flat surface where the clusters of active and passive particles stay in contact. The propulsion directions of active particles here are towards the clusters of passive particles.

The clusters of passive particles in the flat plane move along with the clusters of active particles. While there exists a vapor phase between the ring of active particles and the cap of passive particles on the spherical surface, the clusters of active and passive particles stay in contact with each other in planer geometry. The system in planer geometry exhibits dynamical scaling of correlation functions and the average length of domains grows as power-law with time. This is an ongoing project and further analyses regarding the dynamics are in progress.

Bibliography

[1] A. Ravichandran, G. A. Vliegenthart, G. Saggiorato, T. Auth, and G. Gompper, Biophys J. **113**, 5 (2017).

[2] A. Sokolov, I. S. Aranson, J. O. Kessler, and R. E. Goldstein, Phys. Rev. Lett. **98**, 158102 (2007).

[3] I. L. Bajec and F. H. Heppner, Anim. Behav. **78**, 777 (2009).

[4] T. Vicsek, A. Czirôk, E. Ben-Jacob, I. Cohen, and O. Shochet, Phys. Rev. Lett. **75**, 1226 (1995).

[5] J. Stenhammar, R. Wittkowski, D. Marenduzzo and M. E. Cates, Phys. Rev. Lett. **114**, 018301 (2015).

[6] J. Smrek and K. Kremer, Phys. Rev. Lett. **118**, 098002 (2017).

[7] P. Dolai, A. Simha and S. Mishrac, Soft Matter **14**, 6137 (2018).

[8] S. Kumari, A. S. Nunes, N. A. M. Araujo and M. M. T. Gama, J. Chem. Phys. **147**, 174702 (2017).

[9] B. Ai, Z. Shao and W. Zhong, Soft Matter **14**, 4388 (2018).

[10] G. Meng, J. Paulose, D. R. Nelson and V. N. Manoharan, Science **343**, 634 (2014).

[11] N. Stoop and J. Dunkel, Soft Matter **14**, 2329 (2018).

[12] S. Praetorius, A. Voigt, R. Wittkowski and H. Löwen, Phys. Rev. E **97**, 052615 (2018).

[13] F. C. Keber, E. Loiseau, T. Sanchez, S. J. DeCamp, L. Giomi, M. J. Bowick, M. C. Marchetti, Z. Dogic and A. R. Bausch, Science **345**, 1135 (2014).

[14] S. Henkes, M. C. Marchetti and R. Sknepnek, Phys. Rev. E **97**, 042605 (2018).

[15] S. Ehrig, J. Ferracci, R. Weinkamer and J. W. C. Dunlop, Phys. Rev. E **95**, 062609 (2017).

[16] L. M. C. Janssen, A. Kaiser and H. Lowën, Sci. Rep. **7**, 5667 (2017).

[17] I. R. Bruss and S. C. Glotzer, Soft Matter **13**, 5117 (2017).

[18] S. Shankar, M. J. Bowick and M. C. Marchetti, Phys. Rev. X **7**, 031039 (2017).

[19] F. D. C. Farrell, M. C. Marchetti, D. Marenduzzo, and J. Tailleur, Phys. Rev. Lett. **108** 248101 (2012).

[20] A. Martin-Gomez, D. Levis, A. Diaz-Guilera, and I. Pagonabarraga, Soft Matter **14**, 2610 (2018).

[21] R. Sknepnek and S. Henkes, Phys. Rev. E **91**, 022306 (2015).

[22] B. Ai, B. Zhou, and X. Zhang, Soft Matter **16**, 4710 (2020).

[23] W. Li, Sci. Rep. **5**, 13603 (2015).

[24] S. Chandra, M. Girvan, and E. Ott, Phys. Rev. X **9**, 011002 (2019).

[25] J. D. Weeks, D. Chandler, and H. C. Andersen, J. Chem. Phys. **54**, 5237 (1971).

[26] E. Platen, Acta Numerica **8**, 197 (1999).

[27] A. Callegari, G. Volpe, *Numerical Simulations of Active Brownian Particles.* In: F. Toschi, M. Sega (eds) *Flowing Matter. Soft and Biological Matter*, Springer, Cham. 2019.

[28] K. Kaski, J. Nieminen, and J. D. Gunton, Phys. Rev. B **31**, 2998 (1985).

[29] S. Kumar, J. D. Gunton, and K. K. Kaski, Phys. Rev. B **35**, 8517 (1987).

[30] M. P. O. Loureiro and J. J. Arenzon, Phys. Rev. E **81**, 021129 (2010).

Chapter 7

Summary of the Thesis

Below we summarize the thesis. We proceed in a chapter-wise fashion.

The introductory Chapter provides a brief overview of phase transitions in active matter systems. There we have included scaling pictures associated with different kinetic mechanisms of growth. We have also discussed some structural aspects. In addition, methods of simulation and analysis are incorporated.

In Chapter 2 we consider systems in space dimension $d = 2$ that contain Vicsek-like aligning active particles and active Brownian particles. Via molecular dynamics simulations, we have quantified the dynamics of evolution towards steady states in both the cases for a low particle density $\rho = 0.05$ and a low temperature $T = 0.1$. We observe fractal-like 'solid' clusters that form due to the competition between two different time scales in the system. In Fig. 7.1(a) we have shown the plots of average mass versus time, in a log-log scale, for a Vicsek-like system, with alignment strength $f_A = 1$, as well as for a system of active Brownian particles (ABP), for propulsion force $f_p = 1$. The slower growth in the ABP case can be appreciated from the mentioned exponents of the power-law enhancements. The growth in the systems of Vicsek-like particles can be explained via the theory of ballistic aggregation of clusters, while we observe that the system of active Brownian particles evolves via the particle diffusion mechanism, referred to as the Lifshiftz-Slysov mechanism. In this study, our focus has been on drawing comparative pictures of cluster growths and morphologies in aligning and non-aligning active matter systems [1].

In Chapter 3 we have investigated the dynamics of velocity ordering in systems of Vicsek-like active particles with high particle density $\rho = 1$. We aim to identify the growth picture for different alignment strengths f_A. The vicsek order parameter, V_a, in Fig. 7.1(b), shows higher saturation values for larger f_A. We observe that the

enhancement in velocity ordering occurs via the reduction in the number of the vortex and anti-vortex pairs. We also look at the velocity-velocity correlations that demonstrate self-similar growth of the velocity field. The ordering dynamics here has similarity with the evolution picture in the dynamical XY model in $d = 2$ [2].
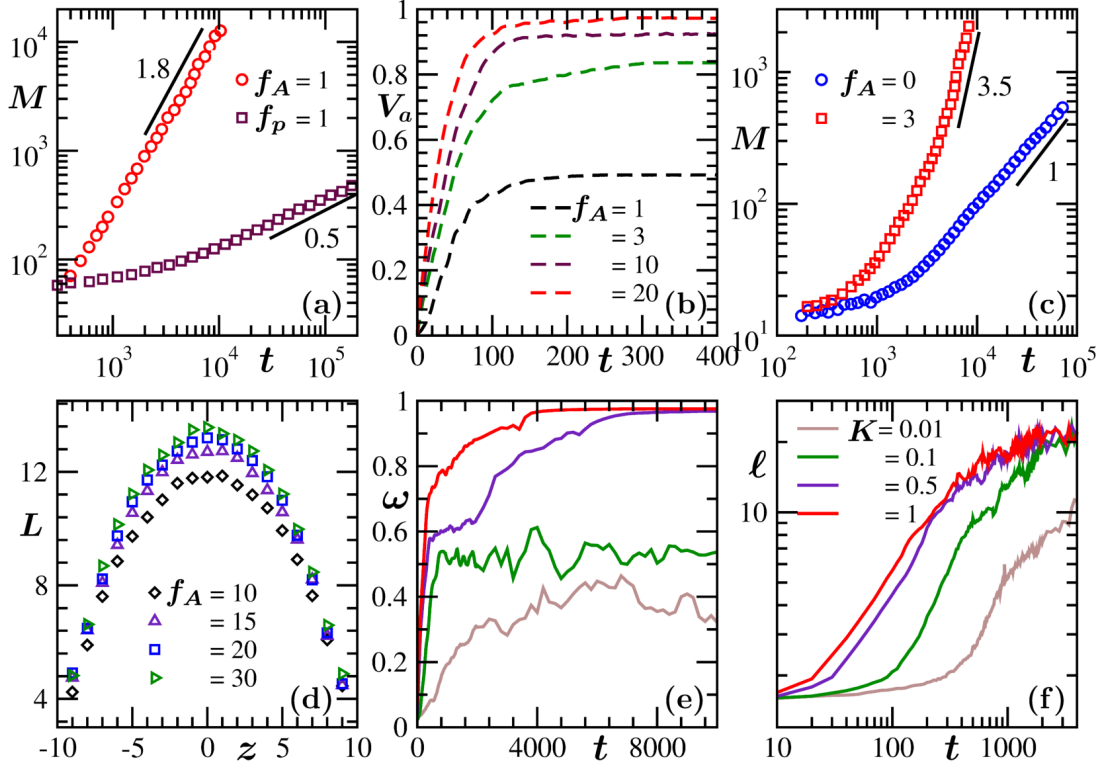
Figure 7.1: (a) Plots of average mass (M) versus time (t) for the systems consisting of Vicsek-like active particles (with alignment strength $f_A = 1$) as well as for systems of active Brownian particles (with propulsion force $f_p = 1$) are shown in a log-log scale. The solid lines represent power-laws with mentioned values of exponent. (b) The Vicsek order parameter V_a for two-dimensional systems of Vicsek-like active particles are shown with the evolution of time, for different f_A. These results are for overall particle density $\rho = 1$. (c) The growth of average mass of clusters is shown for Vicsek-like particles in an explicit solvent for alignment strength $f_A = 0$ and 3. (d) The average angular momentum L of active colloids, for different f_A, in a colloid-polymer mixture under spherical confinement, are plotted with the variation of z, the distance of a colloid from the center of the cavity along the long axis of the ellipsoidal cluster of polymers. These results are for cavity radius $R = 10$ and near-neutral wall scenario. (e) The order parameter ω, equivalent to the average magnitude of angular momentum of active particles, for a system of a binary mixture of active and passive particles on a spherical surface are shown for various alignment strengths K [labels are same as in (f)]. (f) The average domain lengths ℓ, versus time, are shown for the same systems as in (e), but here for a two-dimensional planar surface, for different K values.

Chapter 4 deals with the clustering dynamics in a system of Vicsek-like active particles that are immersed in an explicit solvent. Here we have performed a hybrid molecular dynamics and multi-particle collision dynamics simulation to identify the role of hydrodynamics in the growth of clusters. In Fig. 7.1(c) we compare the plots of average mass of the clusters versus time, in a double log scale, between active ($f_A = 3$) and passive ($f_A = 0$) cases. There exist power-law growths. Clearly growth exponent is much higher in the active case. We have found that the growth in passive systems occurs via the diffusive coalescence of clusters, known as Binder-Staffur (BS) mechanism. The growth in the active case, on the other hand, can be explained via a theory of ballistic aggregation, like in a previous chapter. When the hydrodynamic interactions are destroyed, the ordering in velocity fields breaks and the growths of clusters in both active and passive systems occur via the *simple* particle diffusion mechanism [3].

In Chapter 5 we investigate the structure and dynamics in a system consisting of active colloids and passive polymers that are kept in spherical confinement. Considering a smooth repulsive wall we have studied different wetting scenarios. For a near-neutral wall, in terms of the passive interaction, we have quantified the phase diagram of the system in the plane of packing fractions of colloids and polymers, for different active strength. For various state points inside the coexistence regions, we observe macroscopic rotations of the active colloids around the ellipsoidal cluster of passive polymers. In Fig. 7.1(d) we show the average angular momentum (L) of the colloids versus z, the distance from the center of the cavity along the long axis of the ellipsoid, for different alignment strengths f_A. Near the equatorial region ($z = 0$), L increases with the increase of f_A. The long axis of the ellipsoid fluctuates in steady states in a scaling manner. The poles of the axis on the spherical surface move diffusively and the diffusion constant decreases with the increase of alignment strength [4].

Chapter 6 contains a comparative study of demixing of certain active and passive particles that are constraint to move on spherical and planar surfaces. Here we have considered a somewhat different type of alignment interaction among active particles. The active particles form a rotating ring near the equatorial region of the sphere, while the passive particles form caps at the poles. The corresponding dynamics we quantify by defining an appropriate order parameter which is the average angular momentum (ω) of the active particles. In Fig. 7.1(e) we have shown ω with the evolution time for different alignment strengths K. The saturation value close to unity indicates the formation of 'perfect' ring for higher values of K. On planar surfaces, the phase separated clusters of active and passive particles stay in contact. In this case the motions of clusters of active

particles trigger the growth of clusters of passive particles. In Fig. 7.1(f) we have shown the domain growth within these systems for different K. Faster growth for higher K values are appreciable from the presented data [5].

Bibliography

[1] S. Paul, A. Bera, and S. K. Das, Soft Matter **17**, 645 (2021).

[2] A. Bera and S. K. Das, Manuscripts under preparation.

[3] A. Bera, S. Sahoo, S. Thakur, and S. K. Das, Phys. Rev. E **105**, 014606 (2022).

[4] A. Bera, K. Binder, S. A. Egorov, and S. K. Das, arXiv: 2112.00500 (2021).

[5] A. Bera and S. K. Das, Manuscript under preparation.

Re: Permission for using one image from your photography in my PhD thesis

Purohit <purohit@jncasr.ac.in>
Thu 6/16/2022 4:38 PM

To: Arabinda <arabinda@jncasr.ac.in>

Dear Arabinda,
You have my permission to use the image.
Thanks,

Get Outlook for Android

From: Arabinda <arabinda@jncasr.ac.in>
Sent: Thursday, June 16, 2022 4:34:11 PM
To: Purohit <purohit@jncasr.ac.in>
Subject: Permission for using one image from your photography in my PhD thesis

Dear Sumukh,
I am using the attached image from your photography in my PhD thesis. I request you to give permission for the same.

Thanking you,

Best regards,
Arabinda Bera
Research Scholar
JNCASR, Bangalore 560064, India

ROYAL SOCIETY
OF CHEMISTRY

(/)

Members' area (https://members.rsc.org/) | Donate (/support-us/)

Journals, books & databases

Licences, copyright & permissions

When you publish in a Royal Society of Chemistry journal, you keep the copyright of the manuscript. On this page you can learn more about our Licence to Publish and the rights you retain as an author. We also explain where you can deposit and share your article, and how to request permission to re-use other people's work.

The following details apply only to authors accepting the standard Licence to Publish. Authors who are interested in publishing open access should visit our open access pages for more information about our open access licences (/journals-books-databases/open-access/open-access-info/#choose) and deposition rights.

On this page

About our licence to publish
(/journals-books-databases/author-and-reviewer-hub/authors-information/licences-copyright-permissions/#about-licence)Rights retained by authors

(/journals-books-databases/author-and-reviewer-hub/authors-information/licences-copyright-permissions/#author-rights)Deposition & sharing rights

(/journals-books-databases/author-and-reviewer-hub/authors-information/licences-copyright-permissions/#deposition-sharing)Reusing Royal Society of Chemistry material (/journals-books-databases/author-and-reviewer-

hub/authors-information/licences-copyright-permissions/#reuserscmaterial)

About our licence to publish

In order to publish material the Royal Society of Chemistry must acquire the necessary legal rights from the author(s) of that material. In general, we must obtain from the original author(s) the right to publish the material in all formats, in all media (including specifically print and electronic), with the right to sublicense those rights.

For all articles published in our journals, we require the author to accept a 'licence to publish'. This licence is normally requested after their article is accepted for publication. By signing this licence the author (who is either the copyright owner or who is authorised to sign on behalf of the copyright owner, for example his/her employer) grants to the Royal Society of Chemistry "the exclusive right and licence throughout the world to edit, adapt, translate, reproduce and publish the manuscript in all formats, in all media and by all means (whether now existing or in future devised)".

The Royal Society of Chemistry thus acquires an exclusive licence to publish and all practical rights to the manuscript, except the copyright. The copyright of the manuscript remains with the copyright owner. The copyright owner also retains certain rights regarding the sharing and deposition (/journals-books-databases/author-and-reviewer-hub/authors- information/licences-copyright-permissions/#deposition-sharing) of their article and the re-use of the published material (/journals-books-databases/author-and-reviewer-hub/authors-information/licences-copyright- permissions/#reuserscmaterial). For short items in journals (news items, etc) we take a non-exclusive licence in the form of a brief 'terms and conditions for acceptance' document.

What is copyright? +

Assurances

In the licence to publish, the author provides the assurances that we need to publish the

material, including assurances that the work is original to the author, that the work has not been published already and that permissions have been obtained if previously published material has been included.

Download the Royal Society of Chemistry licence to publish. (/globalassets/05-journals-books-databases/journal-authors-reviewers/licenses-copyright-permissions/rsc-licence-to-publish-hybrid-article-signable.pdf)

If the manuscript includes material that belongs to someone else (for example, a figure or diagram), we require the author to obtain all permissions that may be needed from third parties. If you wish to reuse material that was not published originally by the Royal Society of Chemistry please see Re-use permission requests (/journals-books-databases/author-and-reviewer-hub/authors-information/licences-copyright-permissions/#reuserscmaterial).

Rights retained by authors

When the author accepts the exclusive licence to publish for a journal article, he/she retains certain rights that may be exercised without reference to the Royal Society of Chemistry.

Reproduce/republish portions of the article (including the abstract).

Photocopy the article and distribute such photocopies and distribute copies of the PDF of the article for personal or professional use only (the Royal Society of Chemistry makes this PDF available to the corresponding author of the article upon publication. Any such copies should not be offered for sale. Persons who receive or access the PDF mentioned above must be notified that this may not be made available further or distributed.).

Adapt the article and reproduce adaptations of the article for any purpose other than the commercial exploitation of a work similar to the original.

Reproduce, perform, transmit and otherwise communicate the article to the public in spoken presentations (including those that are accompanied by visual material such as slides, overheads and computer projections).

The author(s) must submit a written request to the Royal Society of Chemistry for any use other than those specified above.

All cases of republication/reproduction must be accompanied by an acknowledgement (/journals-books-databases/author-and-reviewer-hub/authors-information/licences-copyright-permissions/#acknowledgements) of first publication of the work by the Royal Society of Chemistry, the wording of which depends on the journal in which the article was published originally. The acknowledgement should also include a hyperlink to the article on the Royal Society

of Chemistry website.

The author also has some rights concerning the deposition of the whole article.

Deposition and sharing rights

The following details apply only to authors accepting the standard licence to publish. Authors who have accepted one of the open access licences to publish, or are thinking of doing so, should refer to the details for open access deposition rights (/journals-books-databases/open-access/open-access-info/#choose).

When the author accepts the licence to publish for a journal article, he/she retains certain rights concerning the deposition of the whole article. This table summarises how you may distribute the accepted manuscript and version of record of your article.

Sharing rights	Accepted manuscript	Version of record
Share with individuals on request, for personal use	✓	✓
Use for teaching or training materials	✓	✓
Use in submissions of grant applications, or academic requirements such as theses or dissertations*	✓	✓
Share with a closed group of research collaborators, for example via an intranet or privately via a scholarly communication network (/journals-books-databases/open-access/green-open-access/#share)	✓	✓
Share publicly via a scholarly communication network that has signed up to STM sharing principles	⧗	✕
Share publicly via a personal website, institutional repository (/journals-books-databases/open-access/green-open-access/#share) or other not-for-profit repository	⧗	✕
Share publicly via a scholarly communication network that has not signed up to STM sharing principles	✕	✕

*You may include your article in the electronic version of your thesis or dissertation as long as it is not made available as a separate document.

⌛ Accepted manuscripts may be distributed via repositories after an embargo period of 12 months

If you are a reader looking for the terms of use for information published by the Royal Society of Chemistry under our standard licence to publish please refer our terms of use (/journals-books-databases /librarians-information/products-prices/licensing-terms-and-conditions/#non-commercial-terms).

CHORUS

We are members of the CHORUS initiative, and therefore make the Accepted manuscript version of articles describing research funded by participating funders publicly available on our web site after an embargo period of 12 months. This is effective for research published from 1st March 2018 onwards. Unless otherwise noted on the article the Accepted manuscript is licensed under the terms of our standard license to publish and is subject to our standard reuse terms (/journals-books-databases/librarians-information /products-prices/licensing-terms-and-conditions/#non-commercial-terms).

Reusing Royal Society of Chemistry material

Reuse permissions requests

Material published by the Royal Society of Chemistry (RSC) and other publishers is subject to all applicable copyright, database protection and other rights. The graphic below outlines the steps to obtain permission to reuse RSC materials, where required:

I am the author of the RSC material I wish to reuse

I am NOT the author of the RSC material I wish to reuse

(/globalassets/05-journals-books-databases/journal-authors-reviewers/licenses-copyright-permissions
/flowcharts-for-permissions---i-am-the-author.pdf)

⬇ Download full-sized flowchart (/globalassets/05-journals-books-databases/journal-authors-
reviewers/licenses-copyright-permissions/flowcharts-for-permissions---i-am-the-author.pdf)
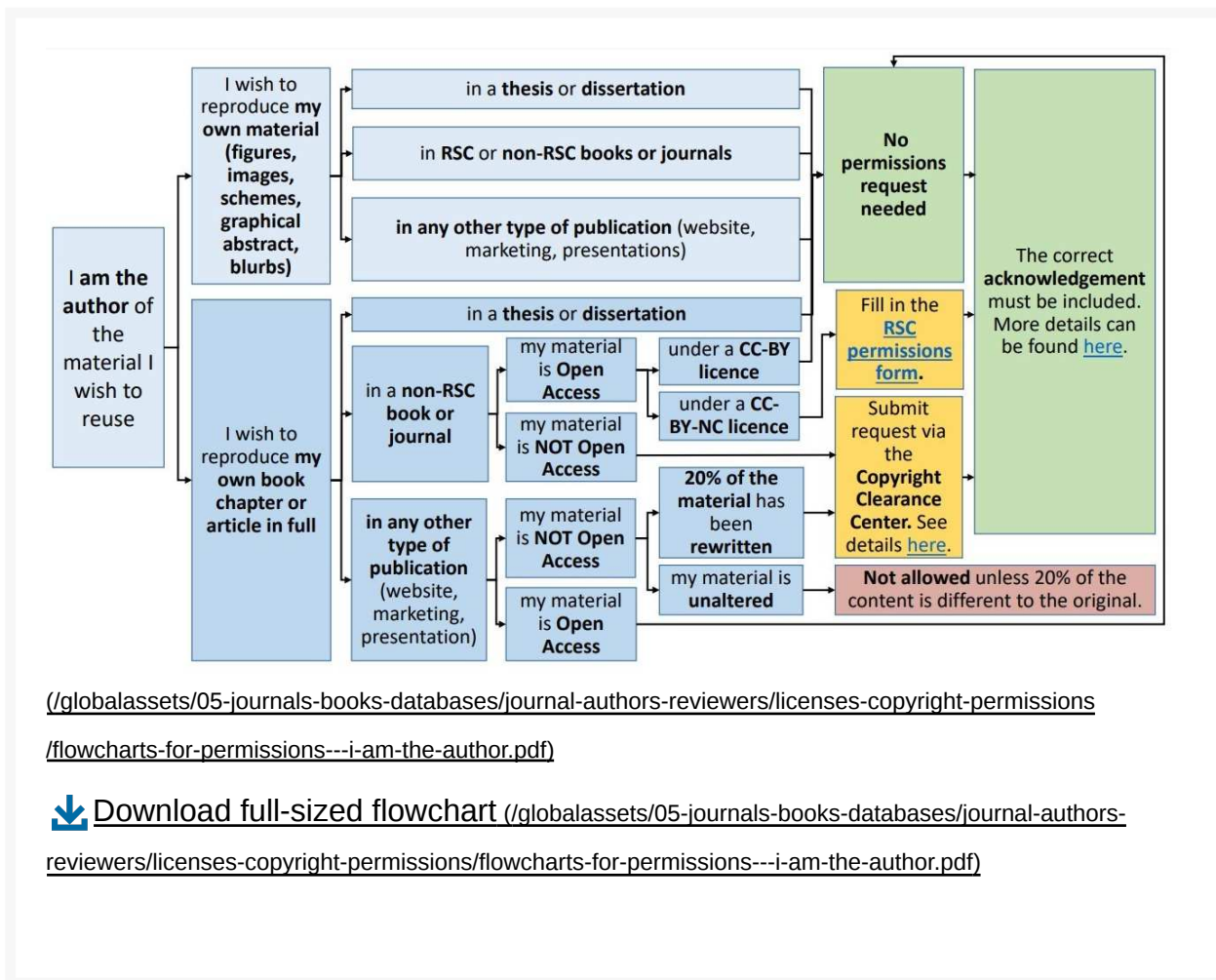
More details ━

Author reusing their own work published by the RSC

You do not need to request permission to reuse your own figures, diagrams, tables, or images that were originally published in an RSC publication. However, permission should be requested for use of the whole article or chapter except if reusing it in a thesis. If you are including an article or book chapter published by the RSC in your thesis please ensure that your co-authors are aware of this.

Reuse of material that was published originally by the RSC must be accompanied by the appropriate acknowledgement of the publication. The form of the acknowledgement is dependent on the journal in which it was published originally, as detailed in the 'Acknowledgements' section (/journals-books-databases/author-and-reviewer-hub/authors-information /licenses-copyright-permissions/#acknowledgements).

Authors reusing RSC material in another RSC publication

Authors contributing to RSC publications (journal articles, book or book chapters) do not need to formally request permission to reproduce material contained in another RSC publication. However, permission should be requested for use of a whole article or chapter. For all cases of reproduction the correct acknowledgement of the reproduced material should be given. The form of the acknowledgement is dependent on the journal in which it was published originally, as detailed in the 'Acknowledgements' section (/journals-books-databases/author-and-reviewer-hub/authors-information/licences-copyright-permissions /#acknowledgements).

Reusing RSC material in material for another publisher, including signatories to the STM Permissions Guidelines

Please submit a permissions request via the Copyright Clearance Center (/journals-books-databases/author-and-reviewer-hub/authors-information/licences-copyright-permissions/#copyrightclearancecenter) to reuse RSC material in material for another publisher. If you are an academic or you are reproducing Royal Society of Chemistry material in a publication to be published by an STM Publisher you will be granted the permission for free for up to three figures. The STM Publishers are those who have signed up to the STM Permissions Guidelines (https://www.stm-assoc.org/intellectual-property/permissions/permissions-guidelines/) and include publishers such as the American Chemical Society, Elsevier, Springer and Wiley. Please submit your request well ahead of publication of your material.

You should check that the material you wish to reproduce is not credited to a source other than the RSC before sending in any request. If the material is credited to another publisher, you are required to seek permission from them.

Reusing RSC material published under a CC-BY and CC-BY-NC licence

An Open Access article is one published under a CC-BY or a CC-BY-NC licence. To check if an article is Open Access, find the journal article from which you want to reproduce material on https://pubs.rsc.org/ (https://pubs.rsc.org/), go to the article landing page by clicking on the article's title, and check the 'Article information' on the right-hand side. An Open Access article would read 'This is an Open Access article'.

If the material for which you are requesting reproduction rights has been published under a **CC-BY** licence, you may reproduce the material, even commercially, without requesting formal permission as long as the material is fully acknowledged and a link is included back to the article on our website.

If the material for which you are requesting reproduction rights has been published under

a **CC-BY-NC** licence, you may reproduce the material in a non-commercial publication without requesting formal permission as long as the material is fully acknowledged and a link is included back to the article on our website. Permission must be requested using this RSC Permissions Request Form (/journals-books-databases/author-and-reviewer-hub/authors-information/licences-copyright-permissions/permissions-form/) for commercial reproduction.

Reusing material from other RSC publications

If you are reproducing material from an RSC website, education publication or science policy publication, please fill in the RSC Permissions Request Form (/journals-books-databases /author-and-reviewer-hub/authors-information/licences-copyright-permissions/permissions-form/).

Requests are usually for use of a figure or diagram, but they may also be for use of the entire article or chapter. Requests to use individual figures or diagrams are invariably granted. Permission for another publisher to print an entire RSC article or chapter may be granted in special circumstances.

The permission form should only be used to request permission to reproduce material from Chemistry World, Education in Chemistry, and other non-journal publications of the RSC. For these requests please complete and send the RSC Permissions Request Form (/journals-books-databases/author-and-reviewer-hub/authors-information/licences-copyright-permissions /permissions-form/) to our Contracts and Copyright team.

How to request permission from the RSC via the Copyright Clearance Center

Journals

Find the journal article from which you want to reproduce material and go to the article landing page by clicking on the article's title.

Click on 'Request permissions', which will open up a new window containing permissions information for the article. If required, click on 'Formally request permission' to go to the Copyright Clearance Center.

Please note that these pathways won't be available if the RSC material you wish to reuse is published under a CC-BY or CC-BY-NC licence. More information can be found here (/journals-books-databases/author-and-reviewer-hub/authors-information/licences-copyright-permissions /#reuserscmaterial)

Books

Refer to Copyright Clearance Center's Buyer Guide to submit a request to reuse material from a book. Queries regarding this service should be addressed to customercare@copyright.com.

Drop-down menus in the Copyright Clearance Center

Use the drop-down menus to select the reproduction options you require and provide any additional details needed. You will obtain the permission for free if both of both the following conditions apply:

- your request falls within the terms of the STM Permission Guidelines (in short, up to three figures or a single text extract of less than 400 words).
- you are reproducing the material in a publication published by another STM Publisher (i.e. publishers who have signed up to the STM Permission Guidelines, for example, American Chemical Society, Elsevier, Springer and Wiley), or you are reproducing the material in your thesis for submission to your educational institution

After 'Describe who will republish the content (person or entity)...' if you are:

- reproducing the figure in a thesis or dissertation, please specify 'Academic institution'
- reproducing the material in a publication published by a member of the STM Association, select 'Publisher, STM'

When your order has been accepted you will be sent an email providing the order confirmation and any licence details. If you need any support to submit your request, please refer to Copyright Clearance Center's Buyer Guide (http://www.copyright.com/wp-content/uploads/2015/03/Repub_Buyer_Guide.pdf). Queries regarding this service should be addressed to customercare@copyright.com.

Acknowledgements

The Royal Society of Chemistry publishes some journals in partnership with, or on behalf of, other organisations; these journals require a specific wording of the acknowledgement when work is reproduced from them. The text for the acknowledgement for these journals, and the standard wording to be used by all other journals are given below.

See acknowledgements $+$

Proof of permission

If you require a signed permissions form, please submit the <u>Permissions Request Form</u> <u>(PDF)</u> <u>(/globalassets/05-journals-books-databases/journal-authors-reviewers/licenses-copyright-permissions/ag-gc-permission-request-form-for-rsc-material.pdf)</u> instead of the form above. Our Contracts and Copyright team will organise an electronic signature and return the form to you.

Using third party material in Royal Society of Chemistry publications

We must ensure that the material we publish does not infringe the copyright of others. We require the author(s) to obtain, at the earliest opportunity, the relevant permissions that might be needed from third parties to include material that belongs to someone else.

Please contact the publisher/copyright owner of the third party material to check how they wish to receive permission requests. Please plan to submit your request well ahead of publication of your material.

The most common procedures for permission requests are outlined below.

- A number of publishers have opted out of receiving express permissions as long as they fall under the rules of the <u>STM Permission Guidelines</u> <u>(http://www.stm-assoc.org</u> <u>/copyright-legal-affairs/permissions/permissions-guidelines)</u>.
- If they do not fall into the category above, the majority of publishers now use the Copyright Clearance Center (CCC) to process their requests.
- Other publishers have their own permission request forms and/or specify what information they need to process any permission request.
- If the publisher/copyright owner does not have a specific procedure please complete and submit the <u>Permission Request Form for non-RSC materia</u> <u>(/globalassets/05-journals-books-databases/journal-authors-reviewers/licenses-copyright-permissions/ag-gc-permission-request-form-for-non-rsc-material.pdf)</u>l form, instead of the form above. Send the form to the permission administrator or editor of the relevant publication.
- If the copyright owner has opted to publish under a Creative Commons licence,

licensees are required to obtain permission to do any of the things with a work that the law reserves exclusively to a licensor and that the licence does not expressly allow. Licensees must credit the licensor, keep copyright notices intact on all copies of the work, and link to the license from copies of the work.

In all cases the following rights need to be obtained. Permission is required to include the specified material in the work described and in all subsequent editions of the work to be published by the Royal Society of Chemistry for distribution throughout the world, in all media including electronic and microfilm and to use the material in conjunction with computer-based electronic and information retrieval systems, to grant permissions for photocopying, reproductions and reprints, to translate the material and to publish the translation, and to authorise document delivery and abstracting and indexing services.

Please note that the Royal Society of Chemistry is also a signatory to the STM Permission Guidelines.

Reproducing material from a Gold open access article

If you wish to reproduce material (figures, tables etc.) from a Gold open access paper the following applies:

- If the figure caption states that the figure has been reproduced from another article you need to request permission from the publisher of that article.
- If the figure caption does <u>not</u> state that the figure has been reproduced from another article and the open access article has been published under a CC-BY licence you can reproduce the figure without formal permission as long as it is fully acknowledged.
- If the figure caption does <u>not</u> state that the figure has been reproduced from another article and the open access article has been published under a CC BY-NC licence you will have to request permission from the publisher of the open access article. Please note that you do not have to formally request permission to reproduce figures from one RSC publication in another RSC publication providing that you include the correct credit line.

Contact our
Contracts &
Copyright
Team
Email:
Send us an
email

Customer Services team

For general
publishing
and open
access
enquiries.
Office open:
9am - 5pm
Mon-Fri
Tel:
+44 (0) 1223
432176
Email:
Send us an
email

Share

Advertisement

Recently viewed

Copyright & permissions (/journals-books-databases/book-authors/copyright-permissions/)

Not a member?

Join us now (/membership-and-community/join/)

Journals

Networks

Contacts

f   y   in   ▶

© Royal Society of Chemistry 2022.
Registered charity number 207890.

Advertise (/advertise/) |

Legal (/help-legal/legal/) |

Privacy (/help-legal/legal/privacy/) |

Accessibility (/help-legal/legal/accessibility/)

Re: Permission for using our work in my PhD thesis

Subhajit Paul <subhajit.paul@icts.res.in>
Fri 6/17/2022 6:51 PM
To: Arabinda <arabinda@jncasr.ac.in>
Cc: Subir K Das <das@jncasr.ac.in>
Dear Arabinda,

 I agree with that. You can use them from the Soft Matter paper in your thesis.

Regards
Subhajit Paul.

On Fri, Jun 17, 2022, 18:21 Arabinda <arabinda@jncasr.ac.in> wrote:
> Dear Dr. Paul,
> I want to use our published article [Soft Matter **17**, 645 (2021)] in my PhD thesis. Can I
> have your permission for that?
>
> Thanking you,
>
> Regards,
> Arabinda Bera

PHYSICAL REVIEW JOURNALS (/)
Published by the American Physical Society

Journals (/about)   Authors (/authors)   Referees (/referees)   Collections (/collections)

Browse (/browse)   Search (/search)   Press (/press)   🔊 (/feeds)

December 2017

APS Copyright Policies and Frequently Asked Questions

- What is copyright?
- What does copyright protect?
- How is a copyright different from a patent or a trademark?
- What is the difference between copyright infringement and plagiarism?
- Why should I transfer copyright to APS?
- Why should I transfer copyright to APS before the article is accepted for publication by an APS journal?
- Does transferring copyright affect my patent rights?
- As the author of an APS-published article, may I post my article or a portion of my article on my own website?
- What happens if the author has posted an APS-published article on a free access e-print server or on the authors' or institutions' web pages and subsequently a fee is imposed for access to those sites?
- As the author of an APS-published article, may I post my article or a portion of my article on an e-print server?
- As the author of an APS-published article, can I post my article or a portion of my article on a web resource like wikipedia or quantiki?
- As the author (or the author's employer) of an APS-published article, may I use copies of part or all of my articles in the classroom?
- As the author of an APS-published article, may I use figures, tables, graphs, etc. in future publications?
- As the author of an APS-published article, may I include my article or a portion of my article in my thesis or dissertation?
- As the author of an APS-published article, may I give permission to a colleague or third party to republish all or part of the article in a print publication?
- As the author of an APS-published article, may I give permission to a colleague or third party to republish all or part of the APS-published version in an online journal, book, database compilation, etc.?

What is copyright? http://www.copyright.gov/ (http://www.copyright.gov/)

Copyright is a form of legal protection for original works of authorship. Copyright covers both published and unpublished works.

What does copyright protect?

Copyright, a form of intellectual property law, protects original works of authorship including literary, dramatic, musical, and artistic works, such as poetry, novels, movies, songs, computer software, and architecture. Copyright does not protect facts, ideas, systems, or methods of operation, although it may protect the way these things are expressed. See Circular 1, Copyright Basics, section "What Works Are Protected", see http://www.copyright.gov/circs/circ01.pdf (http://www.copyright.gov/circs/circ01.pdf)

How is a copyright different from a patent or a trademark?

Copyright protects original works of authorship, while a patent protects inventions or discoveries. Ideas and discoveries are not protected by the copyright law, although the way in which they are expressed may be. A trademark protects words, phrases, symbols, or designs identifying the source of the goods or services of one party and distinguishing them from those of others.

What is the difference between copyright infringement and plagiarism?

Copyright infringement occurs when an author's work is reused or republished without the permission of the copyright owner, whether or not author attribution accompanied the reuse.

Plagiarism occurs when an author's work has been reused or republished in such a manner as to make it appear as someone else's work, e.g., without quotation marks and citation of the original work.

Why should I transfer copyright to APS?

Like many other scientific publishers, the American Physical Society (APS) requires authors or their employers to provide transfer of copyright prior to publication. This permits APS to publish the article and to defend against improper use (or even theft) of the article. It also permits APS to publish the article online and to use the article in other forms or media, such as PROLA. By the APS transfer agreement, authors and their employers retain substantial rights in the work, as specified in the agreement https://journals.aps.org/authors/transfer-of-copyright-agreement (https://journals.aps.org/authors/transfer-of-copyright-agreement) and discussed in your copyright permission letter.

Why should I transfer copyright to APS before the article is accepted for publication by an APS journal?

Transferring copyright early in the process avoids the possibility of delaying publication if the transfer has to be obtained later in the process. As stated in the terms of the copyright transfer agreement, transfer does not take effect until the paper is accepted by an APS journal. The author retains the copyright until acceptance, and has the full freedom, for example, to withdraw the paper from consideration by an APS journal and submit it elsewhere.

Does transferring copyright affect my patent rights?

No. Copyright is separate from any patent rights, and the APS transfer agreement specifically states that patent rights are not affected. However, you should be aware that submitting a manuscript to a journal without first taking steps to protect your patent rights (e.g., filing for a patent) could endanger those rights. Consult your patent attorney.

As the author of an APS-published article, may I post my article or a portion of my article on my own website?

Yes, the author or the author's employer may use all or part of the APS published article, including the APS-prepared version (e.g., the PDF from the online journal) without revision or modification, on the author's or employer's website as long as a fee is not charged. If a fee is charged, then APS permission must be sought. In all cases, the appropriate bibliographic citation and notice of the APS copyright must be included.

What happens if the author has posted an APS-published article on a free access e-print server or on the authors' or institutions' web page and subsequently a fee is imposed for access to those sites?

When a fee is imposed, the author must either obtain permission from APS or withdraw the article from the e-print server or Institutional Repository.

As the author of an APS-published article, may I post my article or a portion of my article on an e-print server?

The author has the right to post and update the article on a free-access e-print server using files prepared and formatted by the author. Any such posting made or updated after acceptance of the article for publication by APS should include a link to the online APS journal article abstract. In all cases, the appropriate bibliographic citation and notice of the APS copyright must be included.

As the author of an APS-published article, can I post my article or a portion of my article on a web resource like wikipedia or quantiki?

Sites like wikipedia and quantiki are strict about permissions and require that authors hold copyright to articles that they post there. In order to allow authors to comply with this requirement, APS permits authors to hold copyright to a "derived work" based on an article published in an APS journal as long as the work contains at least 10% new material not covered by APS's copyright and does not contain more than 50% of the text (including equations) of the original article. The APS will extend the author of a "derived work" the right to all papers published in APS journals.

As the author (or the author's employer) of an APS-published article, may I use copies of part or all of my article in the classroom?

Yes, the author or his/her employer may use all or part of the APS-prepared version for educational purposes without requesting permission from the APS as long as the appropriate bibliographic citation is included.

As the author of an APS-published article, may I use figures, tables, graphs, etc. in future publications?

Yes, as the author you have the right to use figures, tables, graphs, etc. in subsequent publications using files prepared and formatted by you or the APS-prepared versions. The appropriate bibliographic citation must be included.

As the author of an APS-published article, may I include my article or a portion of my article in my thesis or dissertation?

Yes, the author has the right to use the article or a portion of the article in a thesis or dissertation without requesting permission from APS, provided the bibliographic citation and the APS copyright credit line are given on the appropriate pages.

As the author of an APS-published article, may I give permission to a colleague or third party to republish all or part of the article in a print publication?

Yes, as the author you may grant permission to third parties to republish print versions of the article provided the APS-published version (e.g., the PDF from the online journal, or a copy of the article from the print journal) is not used for this purpose. The article may not be published in another journal, and the third party may not charge a fee. The appropriate bibliographic citation and notice of the APS copyright must be included.

As the author of an APS-published article, may I give permission to a colleague or third party to republish all or part of the APS-published version in an online journal, book, database compilation, etc.?

No, an author may not grant permission in this case. To request permission to republish APS-copyrighted material, please refer to the "Reuse & Permissions" link that can be found on each APS article page.

As the author of an APS-published article, may I provide a PDF of my paper to a colleague or third party?

The author is permitted to provide, for research purposes and as long as a fee is not charged, a PDF copy of his/her article using either the APS-prepared version or the author prepared version.

As a third party (not an author), may I republish an article or portion of an article published by APS?

Yes, APS will grant permission to republish articles or portions of articles (e.g., tables, graphs, excerpts) published by APS. Depending on the reuse and medium APS has the right to grant permission subject to APS terms and conditions and a fee may be assessed.

As a third party, may I use articles published by APS for lecture and classroom purposes?

Yes, you may use photocopied articles published by APS for lecture and classroom purposes without asking permission from APS as long as you remain an Authorized User of the APS online research per your institution's site license. Also, there is no limitation on the use of APS articles using links to the material accessible through institutional subscriptions.

How do I request permission to republish APS-copyrighted material?

APS uses Aptara's SciPris™ platform to manage rights and permission requests. APS will continue to support the STM guidelines for all copyright needs. To request permission to republish APS-copyrighted material, please refer to the "Reuse & Permissions" link that can be found on each APS article page.

Once directed to the SciPris™ platform, the following information is required:

1. The format in which the material will be republished, e.g., print, online, CD-ROM, and/or other format
2. How much of the article you want to republish, e.g., all or portion of article; if a portion describe the specific material, e.g., figure numbers, excerpt
3. How the material will be used, e.g., in a book, journal, proceeding, thesis, etc.
4. The title of the article/thesis/chapter etc., and the name of the publication in which your work will appear
5. The name of the publisher
6. Indicate whether or not a fee will be charged for the publication

Upon submission, a letter of permission will be generated, specifying all guidelines and regulations to follow.

Blanket permissions are not granted. Please note all requests are subject to APS terms and conditions (/info/terms.html) and a fee may be assessed.

If your questions have not been addressed and you need further assistance, please email customercare@aps.org (mailto:customercare@aps.org).

Further information

For further information about copyright in general, please refer to the Library of Congress FAQ at https://www.copyright.gov/help/faq/ (https://www.copyright.gov/help/faq/)

Journals published by the American Physical Society can be found at https://journals.aps.org/ (https://journals.aps.org/).

FAQ Version: December 12, 2017

Sign up to receive regular email alerts from *Physical Review Journals*

Sign up   (https://info.aps.org/journals-emails)

AUTHORS

General Information (/authors)

Submit a Manuscript (https://authors.aps.org/Submissions/)

Publication Rights (/pub_rights.html)

Open Access (/open_access.html)

Tips for Authors (/authors/tips-authors-physical-review-physical-review-letters)

Professional Conduct (/authors/professional-conduct-ethics)

REFEREES

General Information (/referees)

Submit a Report (http://referees.aps.org/)

Update Your Information (http://referees.aps.org/)

Referee FAQ (/referees/faq.html)

Outstanding Referees (/OutstandingReferees)

LIBRARIANS

General Information (https://librarians.aps.org/)

Subscriptions (https://librarians.aps.org/subscriptions)

Online License Agreement (https://librarians.aps.org/sitelicense.pdf)

Usage Statistics (http://counter.aps.org/)

Your Account (https://librarians.aps.org/account)

STUDENTS

Physics (https://physics.aps.org)

PhysicsCentral (http://www.physicscentral.com/)

Student Membership (https://www.aps.org/membership/student.cfm)

APS MEMBERS

Subscriptions (https://www.aps.org/membership/aps-publications.cfm)

Article Packs (https://journals.aps.org/article-packs)

Membership (https://www.aps.org/membership/index.cfm)

FAQ (https://www.aps.org/membership/faq.cfm)

APS News (https://www.aps.org/publications/apsnews/index.cfm)

Meetings & Events (https://www.aps.org/meetings/index.cfm)

Privacy (https://www.aps.org/about/webpolicies.cfm#privacy)   Policies (/policies)   Contact Information (/contact.html)

Feedback (mailto:feedback@aps.org)